Technical University of Crete

School of Electronics and Computers Engineering

Diploma thesis

‘Global Optimization analysis of dynamic optical data for the *in-vivo* diagnosis of epithelial neoplasia’

Giakoumakis Theodoros-Marios

Committee Members:

Associate Professor Balas Constantinos *(Supervisor)*

Professor Kalaitzakis Constantinos

Assistant Professor Chalkiadakis Georgios

Chania, 2013

Technical University of Crete

School of Electronics and Computers Engineering

Diploma Thesis

"Global Optimization analysis of dynamic optical data for the *in-vivo* diagnosis of epithelial neoplasia"

Giakoumakis Theodoros – Marios

Supervisor: Assoc. Professor Costas Balas

Abstract

In vivo, dynamic, contrast-enhanced optical imaging is a novel, non-invasive, method for the identification of epithelial tissue abnormalities. It was first used in the case of the cervical neoplastic epithelium. A mathematical model simulating the pharmacokinetics of the biomarker has been developed. Eight structural and functional biological parameters, correlating well with neoplasia progress, have been identified and with global sensitivity analysis were reduced to a set of four most identifiable. In the current thesis, ***global optimization analysis*** has been performed for the purpose of investigating whether the model parameters can be estimated, within adequate accuracy, by fitting of outputs of the model to dynamic optical signals. The capability to predict uniquely the full and the reduced set of the proposed parameters has been assessed by a parallel working software, that was created in order to automatically compare nine, equally constrained, state-of-the-art global optimization algorithms. Statistical analysis concluded that the unidentified experimental optical data converge adequately. This occurs more predominantly when the reduced set of the four most identifiable parameters is used, in agreement with global sensitivity analysis results. In particular, the most optimally performing algorithm is currently the differential evolution algorithm, offering parameter estimation statistical accuracy up to 99% in under 2.5 minutes per trial and for the reduced set. On such grounds, it can be reasonably argued that the solution of parameter estimation problem is substantially unique. Finally, fitting of experimental data to the outputs of the model allow the prediction of the identifiable tissue parameters, thus enabling for the first time *in silico* biopsy of neoplasia growth.

Acknowledgements

This diploma thesis took understanding of complicated mathematical processes such as modelling of biological procedures and global optimization. Despite the difficulty of the theories and the practical challenges involved, the subject of the thesis was rather interesting and meaningful. Not often is given the chance to participate in studies for diagnostic tools of great scientific importance and practical application.

Firstly, I would like to thank my supervising professor Costas Balas, Associate Professor to School of Electronics and Computer Engineering (ECE) of Technical University of Crete (TUC), for granting me this unique opportunity of involving myself with such a subject and for his invaluable guidance through the study. I would also like to thank Professor Costantinos Kalaitzakis and Assistant Professor Giorgios Chalkiadakis, for their participation in my three-man examining committee. Specials thanks need to be directed to ph.D. candidate Giorgos Papoutsoglou for his priceless guidance, aid and patience throughout my thesis. Moreover, many thanks should be also directed to all members of the group of Optoelectronics of Electronics Laboratory members, Thanasis Tsapras, Giorgos Epitropou, Dimitris Hliou and Vasilis Kavvadias for their encouragement, patience and for creating a great and fun working environment within the lab.

Finally, I would like to thank my family and friends who with their support, love and encouragement all these years regardless of the difficulties present, helped me throughout all these years.

Table of Contents

Table of Figures

Introduction

1.1 Cervical Cancer

Cervical cancer is the second most common and fifth deadliest type of cancer affecting women globally [1] and poses a more serious threat in the developing world where 80% of the incidents occurring [2] counting 225.000 deaths for the year 2010 alone. High rates of incidents occur mostly in Central and northern regions of South America, sub-Saharan Africa and Cambodia (Figure 1). This is mostly due to the lack of effective screening methods for detection of pre-cancerous conditions and of effective treatment of those conditions before they progress to invasive cancer. During the last half century there has been recorded a cervical cancer deaths decrease of nearly 74%, mainly due to *Papanikolaou*[1], who improved the diagnosis process through the Pap smear screening. Leading cause of this type of cancer is the Human Papillomavirus (HPV) with 85% of cervical cancer globally caused by 4 strains of the virus. HPV infections of genital organs, such as the cervix, are primarily transmitted via sexual activity [3], and unlike a commonly sexually transmitted infection it cannot be prevented by the use of condom since the areas around the genitals including the inner thigh are exposed to the infected person's skin [4]. The cervical cancer type with the most incidences is squamous cell carcinoma. Other known subtypes, distinguished based on histology of the infected cells, are adenocarcinoma, adenosquamous carcinoma, small cell carcinoma, neuroendocrine tumor, glassy cell carcinoma and villoglandular adenocarcinoma [5, 6]. *In situ*[1] cervical cancer, characterized as stage 0 by the International Federation of Gynecology and Obstetrics (FIGO), is treatable though it could lead to terminal conditions once reaching stage IV. This treatable pre-invasive stage is called cervical intraepithelial neoplasia (CIN) and is distinguished in two subcategories based on the level of progress. These categories are Low Grade Squamous Intraepithelial Lesion (LSIL) and High Grade (HSIL). LSIL characterizes grade I or less severe stages of the progress of the infection, while HSIL characterizes more sever stages such as grades I, II Micro-invasive and Invasive.

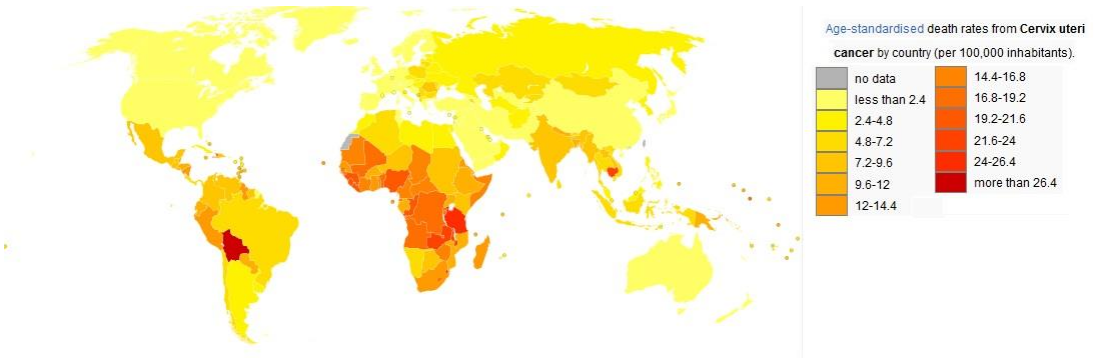

Figure 0-1. Age-standardized death rates from Cervix Uteri Cancer by country

[1] In oncology *in situ* cancer means that malignant cells are present as a tumor but has not metastasized, or invaded, beyond the original site where the tumor was discovered

1.2 Diagnosis and Biopsy

Screening for cervical cancer can be achieved through several tests such as the Pap smear (cytology), VIA, VILI and HPV. Of all these, only the Pap smear is applicable in large populations, reducing cervical cancer and mortality incidents globally [7]. For women with abnormal screening results colposcopy examination is performed, followed by biopsy sampling [8]. Colposcopy examination is used in determining the region of tissue with most severe dysplasia in order to be sample for biopsy [9, 10]. Colposcopy is critical, since its accuracy in identifying and sampling the, disease true positive, region is what determines the reliability of the diagnosis. It is based on visually observing the tissue through the colposcope (low magnification microscope) for the optical signal triggered after the application of acetic acid solution as a contrast agent, a phenomenon known as acetowhitening. Traditional colposcopy practice suffers from quality and subjectivity as it is highly based upon the visual prowess and training of the examiner. Therefore, colposcopy suffers from low sensitivity, high biopsy sampling error rate and disagreement in identification of cervical lesions [9, 10, 11].

1.3 Acetowhitening Phenomenon

Acetowhitening phenomenon is manifasting in abnormal cells after infusion of acetic acid solution in the tissue. Reasearches have shown that the dynamic characteristics of the optical signal recorded during the pheomenon are directly related with both the perchentage of neoplastic cells of the tissue as well as their abnormal metabolic activities. This correlation of the backscattered light and the population of infected cells grants the capability of identifying the neoplasia stage (CIN I, II, III).

Glucolysis, taking place in the cytosol of cells,is a metabolic pathway where a glycose molecule is dissolved into pyruvate acid (1.1) and is the fundamental energy source for a cell.

$$C_6H_{12}O_6 \rightarrow CH_3COCOO^- + H^+ \quad (1.1)$$

Neoplastic cells reproduce with faster than normal rate, thus demand more volumes of oxygen. This lack of oxygen forces pyruvate acid to disolves into lactic acid (1.2), which is emitted in the extracellular space.

$$CH_3COCOOH \rightarrow 2C_3H_6O_3 \quad (1.2)$$

In order for a given, neoplastic or not,cell to maintain its functionality, it needs to have the value of the pH from 7 to 7.5, which is considered normal pH. This leads to acidic extracellular space around neoplastic cells, allowing slow accumulation of weak acids in the intracellular space, which are constantly ionized. The cellular membrane is impregnable to charged particles thus entrapping the ions within the cells (“ion trapping”).

When infusing acetic acid in the tissue, it is instantly ionized producing salt and a hydrogen cation (1.3).

$$CH_3COOH \leftrightarrow CH_3COO^- + H^+ \quad (1.3)$$

Ionization of the acitic acid is a duplex chemical reaction, thus governed by Le Châtelier 's principle (Equilibrium Law):

"If a chemical system at equilibrium experiences a change in concentration, temperature, volume or partial pressure the equilibrium shifts to counteract the imposed change and a new equilibrium is established."

Obeying this principle, acidic acid is passively diffused unionized inside neoplastic cells, where pH regulation mechanisms of the cell kick in. As a result, there is high concentration of hydrogen cations, which transubstantiate the proteins inside the cellular core, altering the scattering characteristics of the core. This is a reversible procedure and within few moments the tissue regains its original characteristics once intracellular pH levels return to normal.

1.4 Dynamic Spectral Imaging System

Figure 1-2. Dynamic Spectral Imaging System

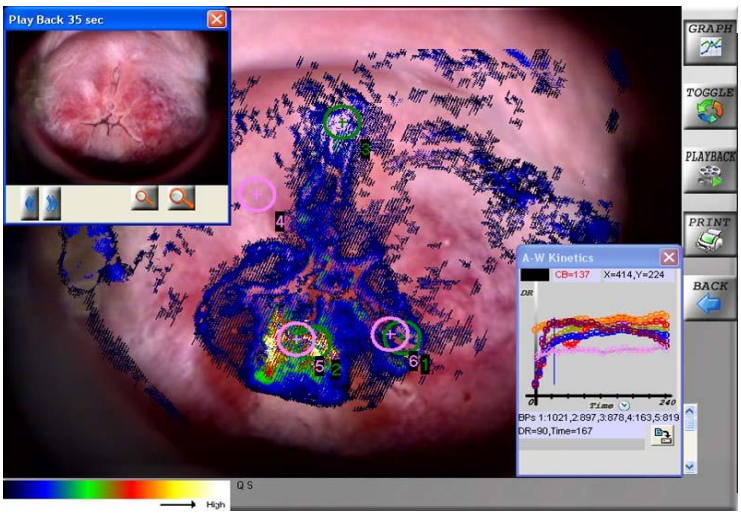

Figure 1-1. Pseudo-color mapping of the cervix

Researches made with purpose of introduction of more accurate screening methods, led to the creation of DySIS, which records with the aid of a CCD camera the acetowhitening phenomena in a time span of 250 seconds and projecting the results in a pseudo-color mapping of the cervix. Through this map it is easy to verify neoplasia existence, asses the threat level, identify the dysplastic area and guide treatment.

1.5 Chapters summary

In this study, a method for accurately identifying the values of structural and functional biological parameters, proven to be related with neoplasia, is presented by implementing global optimization analysis on dynamic optical signals. For this purpose a comparison of global optimization algorithms is performed. A study like that is of dire importance, for it

allows the creation of pseudo-chromatic maps of these biological parameters, creating an extremely useful and valuable diagnostic tool.

In Chapter 2, an introduction to the biology of the cervix and more specifically the epithelium covering the cervix. This simple introduction allows better understanding on the significance of identification of those parameters by understanding the organic tissue studied and the transformation it undergoes during precancerous stages.

In Chapter 3, the model the basic principles governing the mathematical are presented. Thus the level of difficulty of the inverse problem is better depicted, as the differential equations and the non-linear relations of the parameters are discussed.

In Chapter 4, the main concern of this study is analyzed by stating the inverse problem at hand, which is the identification of the values of the biological parameters by using measurements of dynamic optical signals. It is evident that the solution of the inverse is meaningful if for each optimization algorithm the problem converges adequately and the values of the biological parameters are identified with accuracy and precision. Also a brief description of the global optimization algorithms included in the study is given. The algorithms compared are Controlled Random Search (CRS), Shuffled Complex Evolution (SCE), Differential Evolution (DE), Particle Swarm Optimization (PSO), gblSolve, Simplex Simulated Annealing (SIMPSA), Thermodynamically Simulated Annealing, Stochastic Ranking Evolutionary Strategy (SRES) and Mixed Integer Distributed Ant Colony Optimization (MIDACO). The system fits a test signal and returns a set of parameters.

In Chapter 5, the procedure followed in order of assessing the experimental results and ranking the algorithms to infer the optimal one is explained. In order for the comparison to be reliable, a certain set of ground rules followed by all algorithms is suggested. Moreover, a brief description is given of a simple, automated and paralleled software, which was developed during this study. This software is able of running the algorithms provided and produce statistical results over the outputs of the algorithms, providing ease over the comparison of the algorithms and assuring they submit to the common rules. Finally a few metrics are introduced for evaluation of the algorithmic results.

In Chapter 6, the overall results are presented, stating observations over them as well as claims drown by the analysis. The results are evaluated by the metrics introduced.

In Chapter 7, conclusions over the study are presented. Algorithmic behavior is also evaluated by claims made after comparison in the literature. The algorithms were basically judged by dynamic optical signal fitting accuracy, biological parameter value estimation accuracy and time consumed for the estimation and as a result DE algorithm was proven to be optimal for the inverse problem at hand. Moreover, in the chapter a reference to future work that could be done to further the study and achieve better performance is made.

2. Biology: introduction to the Cervix

2.1 General features of a cell [13]

The cell is the basic, structural and functional unit of all living organisms. Cells can exist individually as living organisms, such as bacteria, or group and form tissues and organs as parts of a greater organism, such as animal life forms.

In the human body there is a large variety of different cells like brain cells, skin cells etc. Each kind has unique functional and structural characteristics according to their greater purpose, as well as some identifiable similarities.

A cell is surrounded by membrane, named plasma cell membrane, which differentiates and protects it from its environment. All transactions of any substances in and out of the cell are regulated by the membrane. A cell's DNA as well as RNA used in protein manufacture can be either distributed within the cell (prokaryotic cell) or gathered in a distinguished spherical area named nucleus (eukaryotic), which is surrounded and delimited by the nuclear membrane. The latter type is the dominant cell type found in fauna, of which human organism is also a member. The rest part of the intracellular space, is the cytoplasm and out of all the organelles contained within three types are the most noticeable, the ribosomes, the mitochondria and the lysosomes. The ribosomes number in thousands inside a single cell and in there is continued the manufacture of the proteins once the first stage within the nucleus is complete. That is the second stage, beginning when mRNA reaches the ribosome after exiting the endoplasmic reticulum. Mitochondria is an important organelle inside which three of the most fundamental functions for the cell take place. Firstly, it is in there where chemical reactions that produce energy, such as glycolysis mentioned in *1.3,* occur. Moreover, it maintains water and other material on normal levels and lastly it recycles and decomposes proteins, fats and carbohydrates, whereas it is lysosomes that "digest" these materials and transport what has failed to be digested to the cellular membrane and from there in the extracellular space. Lastly, near the nucleus lies the Golgi apparatus where protein manufacture undergoes most of the time its final stage forming the final form of a protein.

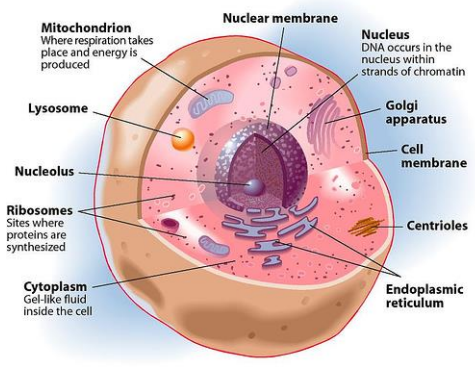

Figure 2-1. Simplistic intracellular representation

2.2 The epithelia [14]

Inner body cavities as well as many organs are covered by a layer of cells known as the epithelia. Glands and even the epidermis consist the epithelia. A major epithelial function is forming a protective barrier and therefore epithelial cells are contiguous and joined together by special junctions. In general, intercellular space between epithelial cells is limited. Depending of the functionality they serve epithelial tissue can be impermeable barrier (*eg*. skin) or have the ability to absorb substances (*eg*. epithelium lining the intestine). Some have secretory functions (*eg*. glands) while others actively participate in metabolism (*eg* endothelial cells lining blood vessels). All of the epithelia is attached to the underlying tissue through a basement membrane and is generally not identifiable by the light microscope due to its thin nature. Also, all epithelia have a free surface, to which there is not attached any cellular or extracellular formed elements.

One way to classify the epithelium is the number of cellular layers. A single layer epithelium is called ***simple***, whereas arrangement of two or more layers is called ***stratified*** epithelium. Another classification is the shape of cells. When the cells have assumed a flattened shape, it is called ***squamous***; cells of same height, width and depths is called ***cuboidal*** whereas if the height exceeds their width, it is called ***columnar***. In stratified epithelia where cells are of different shapes the classification is based upon the outermost layer (ie the free surface).

This thesis is focused on epithelial neoplasia mainly occurring in the cervix of the uterus, where epithelial tissue is either simple columnar epithelia or stratified squamous, depending on the cervix region they cover [16].

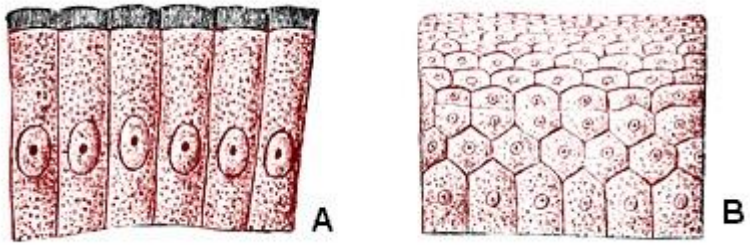

Figure 2-2 (A)Simple columnar epithelia (B)Stratified Squamous

2.3 Tight Junctions

Tight junctions are junctions that connect adjacent cells and control the paracellular substance exchanges. The tight junction pores are dynamic ion channels. Studies have shown that during neoplasia the tight junctions are reduced, thus allowing the creation of gaps in the epithelium, and allowing greater infusion of ions and molecules.

2.4 The Cervix of the Uterus [15]

The uterus, the fallopian tubes and the ovaries consist the female reproductive system. The tissue upon which the uterus lies is called cervix connecting it with the vagina. It is cylinder-shaped with radius approximately 2.5 cm and is covered by smooth, moist tissue, which consist the epithelium of the cervix. It consists of two regional parts, the endocervix and the ectocervix. The endocervix or endocervical canal, is a tunnel through the cervix, from an opening in the center of the ectocervix,known as external os, into the uterus, whereas the ectocervix is the lower cervical region, which is seen from inside of the vagina during a gynecologic examination. The external os allows passage between the uterus and the vagina. The overlapping region between the endo- and ectocervix is called the transformation zone. Stratified squamous epithelium is found on the ectocervix, whereas on the endocervix there is simple columnar epithelium [16].

2.5 Structural cervical epithilial differences based on CIN grade [17]

Accurate cytological diagnosis is based on the distinction of cancer to normal cells by light microscopy. This distinction is made on grounds of fundamental structural differences between neoplastic and normal cells.

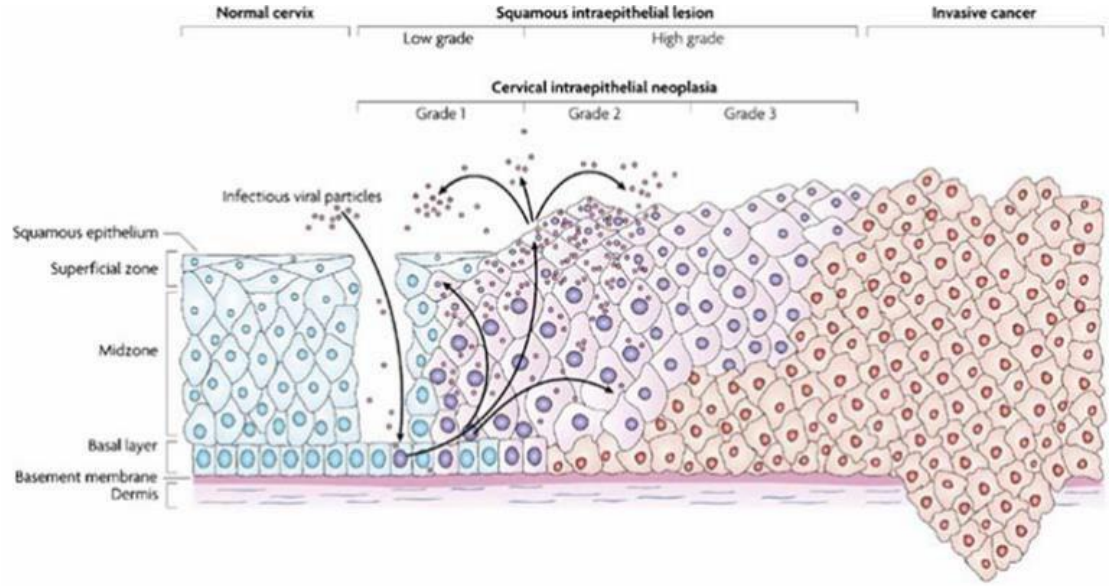

Figure 5-3 Epithelium in evolving grades of neoplasia

As stated in 2.3 the cervical epithelia observed during screening procedures is the stratified squamous epithelium on the ectocervix which consists of, standard-shaped per layer, cells. All cancerous and precancerous cells alter their size and shape since their normal state, varying in size and shape according to the stage of cancer cellular life circle. In normal tissue each cell, based on the layer it participates, has a certain form and size. When neoplasia begins, regardless of the cellular layer, the form and size of infected cells begins to assume a certain shape and volume. This results in generating homogenous epithelium as CIN stages progress. Nucleus size is also significantly different; a lesion named anisonucleosis, and at the same time the nucleus shape is varying than in normal state. In HSIL there can also exist

cells with multiple nucleus. Moreover, coarse granular chromatin[2] is unevenly distributed throughout the nucleus and is often increased. The amount and distribution of chromatin varies due to the abnormal cell division. Hyperchromasia is observed on neoplastic cells due to common reflecting increased chromatin and/or rapid cell turnover[3]. These differences are caused by errors in mitosis (cell division), which normally is an ability only the basal layers of the epithelium have. Pap test is based on the distinction between normal, precancerous and cancerous epithelium. The distinction between stages of CIN is made upon the population size of neoplastic cells. Epithelia cellular homogeneity can be observed throughout the epithelium (CIN III) or may differ from the basal layer to the free surface.

[2] Chromatin is the combination of DNA and proteins which consists the contents of the cellular nucleus.

[3] Cell turnover is a term referring to the replacement of old cells with newly generated ones.

3. Biological Model

3.1 Compartmental modeling

3.1.1 Basic Principles

Models, in general, are used to describe functions of the real world. In mathematical modeling that description is translated into mathematics. The most commonly used method to describe of chemical reaction products and nutritious substances in based on compartmentation. The tissue is divided into sequential compartments and the substance fluxes are translated in mathematical equations. A compartment in biological systems, such as the one discussed in this thesis, is considered a common block of cells with the same structural and functional characteristics. Many compartments can coexist in the same region of a living organism.

Figure 3-6 Single Compartment model

3.1.2 Single Compartmental modeling of tissues [18]

The simplest application of compartmental modeling is in observing a single compartment. For the purposes of this thesis and based on prior studies, a single compartment will be considered the equivalent of a single cellular layer. The concentration of the solution, C, infused inside a compartment through time, can be described by a single differential equation

$$\frac{dC}{dt} = \frac{Input(t) - (CL * C)}{V} \qquad (3.1)$$

Where:

CL: is the rate of infused solution elimination divided by plasma concentration, giving a volume of plasma from which the solution is completely removed per unit of time,

V: is the volume of the compartment.

3.1.3 Multi Compartmental modeling of tissues [20]

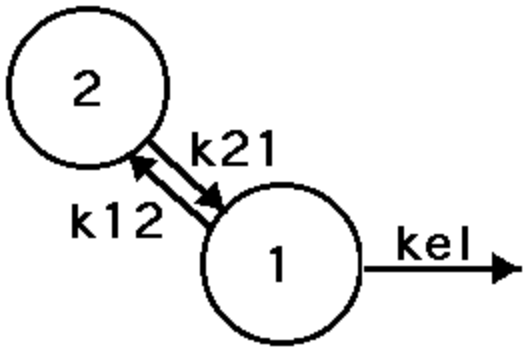

Figure 3-7 Two Compartment Pharmacokinetics Model

In multi compartmental modeling many distinct compartments are used to describe different structural or functional regions of tissue and the connections between the compartments is represented [19]. The arrows connecting each compartment denote the mobility orientation and the amount of substance moved is denoted usually as *k(i, j)* or *L(i, j),* where *i* is the compartment of origin and *j* the target compartment. The function of a single compartment is described by a balance of the mass of the form:

$$\frac{dQ_i}{dt} = \sum R_{ij} - \sum R_{ji} \quad (3.2)$$

Where, $\sum R_{ij}$ is the sum of the mass flux rates from compartment *i* to compartment *j*.

The transaction is possible either by a chemical reaction or by natural transport. As a result of sequential positioning the amount of a substance entering a given compartment is less than the one that entered the previous compartment and more than the one following. Differential equations are used to describe a change of state in the model over a time span.

A model is considered linear, when all values of the parameters of the equations are either constant or time functions. A model is considered on the other hand as non-linear, when at least a single transport factor is a size function of at least one compartment.

The capability of describing a system as a compartmental model depends on its characteristics and is valid only if the substances consisting different compartments and the exchanges occurring are clearly discrete.

The transaction time rates need to be constant throughout the simulation, for consistency to be maintained. Any alteration of the substance being studied that occurs inside a compartment is considered instant compared to the time needed for the transaction.

3.2 Biological Model of Neoplastic Cervical Epithelium

The mathematical model developed in [12] is based in multi compartmental modeling method and is provides an accurate description of the biological procedures during the infusion of acetic acid in the epithelium of the cervix. Each compartment represents a cellular level. The number of compartments depends on the stage of CIN. In cases of CIN I there is a low number and in cases of CIN II or CIN III the number rises. Each compartment is divided into two smaller compartments, one for the intracellular space (IS) and one for the extracellular space (ES).

The developed model simulates the AA motion from the first neoplastic IS to its surrounding ES and vice versa for each dysplastic cellular layer and from there to the next level.

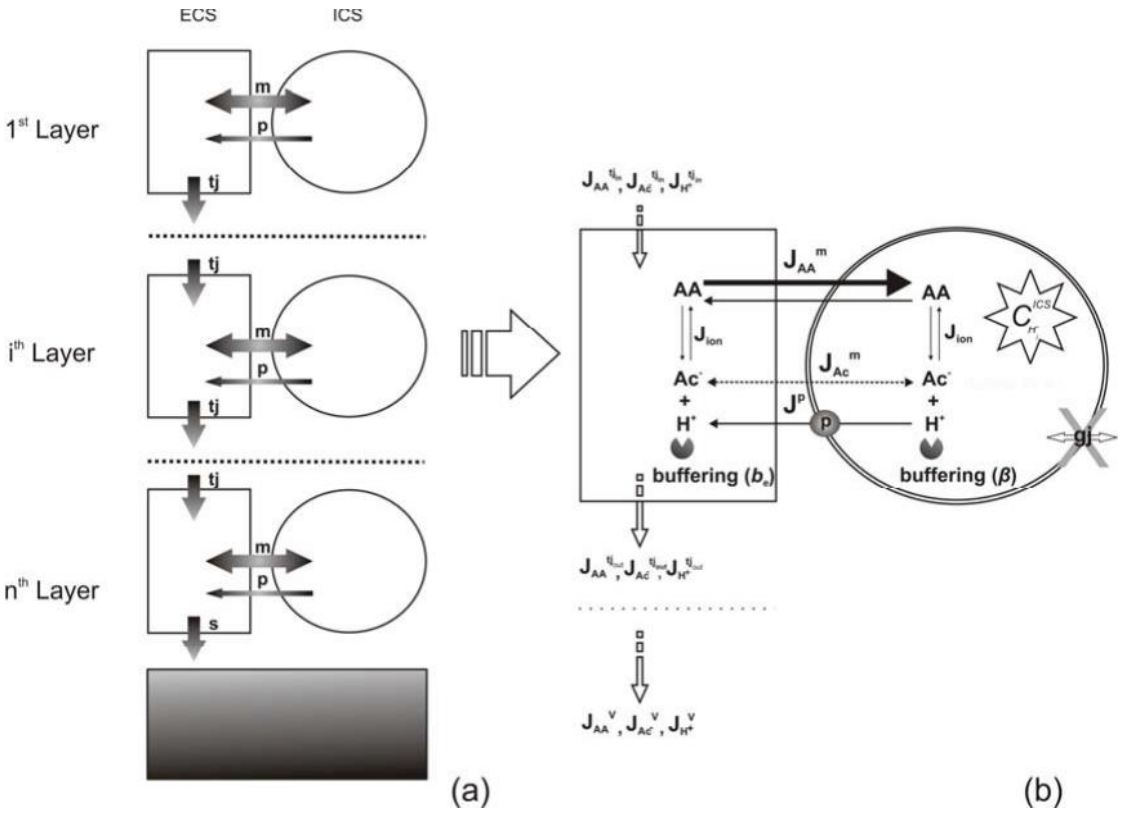

Figure 8-3 (a)Epithelial compartments and transport fluxes (b)The two-compartment cell model and transport fluxes

In Figure 3-3 (a) is shown the flow diagram of the biomarker[4] through multiple compartments, clearly depicting the transport fluxes in and out of each compartment. Exchange of mass of the biomarker is permitted by passive infusion through the cellular membrane (m) and by active ion flux (p). Intercellular communication is achieved by passive electroosmotic infusion, through the membrane of the tight junctions that exist between each compartment and its adjacent upper and lower cellular levels.

In Figure 3-3 (b) the communication of intra- with extracellular space is more clearly represented. Acetic acid, anions of acetic acid (Ac^-) and cations of hydrogen (H^+) enter the

[4] A *biomarker*, or biological marker, generally refers to a measured characteristic which may be used as an indicator of some biological state or condition

extracellular space from the upper cellular level through the tight junctions ($J_{AA_i}^{tjin}$,$J_{AC_i}^{tjin}$,$J_{H_i}^{tjin}$). The acetic acid (AA) is ionized (J_{ion}) depending on the extracellular pH (pH_{ES}) and the extracellular buffering capability (β_{ES}). As a result of the AA ionization pH_{ES} drops and the hydrogen buffering mechanisms are activated. Molecules of acetic acid are passively diffused through the cellular membrane towards IS. The molecules that entered the cell undergo the same reactions resulting on the same results, drop of intracellular pH value (pH_{IS}) and activation of the hydrogen buffering mechanisms of the cell (β_{IS}). Differences between pH_{IS} and pH_{ES} create a weak conductivity field that allows infusion of Ac^- ($J_{AC_i}^{m}$). Once the intracellular hydrogen concentration ($C_{H_i}^{IS}$) rises, the proton pumps of the cell (J^p) are activated actively defusing H^+ out of the cell. Anions of acetic acid and cations of hydrogen still remaining within the cell are joined together again into neutral acetic acid. After this process concludes its cycle, residual molecules and ions in the extracellular space are diffused through the tight junctions ($J_{AA_i}^{tjout}$,$J_{AC_i}^{tjout}$,$J_{H_i}^{tjout}$) into the next compartment beginning a new cycle of the biochemical process, which was just described.

3.3 Mathematical Model of Neoplastic Cervical Epithelium [12]

3.3.1 Introduction to the differential equations of the model

Epithelial dysplastic layers

$$n = \sum_{i=1}^{4} \frac{90}{h_i} \quad (3.3)$$

The total *number of epithelial layers*, N, for each CIN grade is estimated by (3.3) where n is the total number of layers and h_i is the cell height for each epithelial section. The constant value 90 is calculated by dividing the proven cervical epithelial depth (360μm) by the number of different epithelial section, after making the assumption that each of the four different epithelial sections (basal, parabasal, intermediate and superficial) span equally sized areas.

Acetic acid ionization (J_{ion})

AA ionizes following (1.3) chemical equation and is subjugated to k_1 and k_2, forward and backward dissociation rates, respectively. According to the mass action law, the rate which AA is ionized is

$$J_{ion} = -k_1 C_{AA}(t) + k_2 C_{AC^-}(t)\, C_{H^+}(t) \quad (3.4)$$

where *C(t)* is the concentration of the biomarker at a given time. Based on the acute nature of AA it is considered as being constantly at chemical equilibrium. As a result, for $J_{ion} = 0$, at which steady state is assumed *the AA dissociation constant* K_a subjugates to the following function:

$$K_a = \frac{k_1}{k_2} = \frac{C_{AC^-}(t) C_{H^+}(t)}{C_{AA}(t)} \quad (3.5)$$

Concentration change rates by acetic acid passive diffusion through the cellular_membrane and tight junctions (J_{AA}^{m} , J_{AA}^{tjm})

The model assumes that AA kinetics is constantly in equilibrium. Based on that, solid state (ss) of passive diffusion between two adjacent compartments is governed by Fick's Law resulting in the function:

$$J_{AA}^{pm_{1\to 2}} = -\frac{Dk_S}{d} C_{AA}^{1} \overset{ss}{=} P_{AA}^{pm} (C_{AA}^{1} - C_{AA}^{2}) \Leftrightarrow$$

$$-C_{AA}^{1} = \rho_1 P_{AA}^{pm} (C_{AA}^{1} - C_{AA}^{2}) \qquad (3.6)$$

where *D* is the AA diffusion factor, k_S the AA factor in aquatic environment, d the length of the pores, P_{AA}^{pm} the membrane permeability and ρ_1 the ratio of area to volume. The rates of concentration changes in (3.6) are given by the equations:

$$\dot{C}_{AA_i}^{IS} = -\rho_{IS} J_{AA_i}^{m} = -\rho_{IS} P_{AA}^{m} \left(C_{AA_i}^{ES} - C_{AA_i}^{IS}\right) \qquad (3.7)$$

$$\dot{C}_{AA_i}^{ES} = -\rho_{ES} J_{AA_i}^{m} = -\rho_{ES} P_{AA}^{m} \left(C_{AA_i}^{IS} - C_{AA_i}^{ES}\right) \qquad (3.8)$$

where ρ_{IS} ,ρ_{ES} are the area/volume ratios of the intracellular and extracellular space and P_{AA}^{m} is the diffusion coefficient of AA through the cellular membrane. In cases of small pores, as is those of the tight junctions (4.9 to 7$\hat{A}$), and due to the relative size of AA molecules (3$\hat{A}$) diffusion is considered as hindered diffusion. According to the Renkin's Law the permeability of the hindered diffusion is described as:

$$P_{AA}^{H} = \frac{N\pi r^2 D_{AA}^{bulk} F(a/r)}{d * \frac{1-\frac{a}{r^2}}{1-\frac{a_W}{r^2}}} \qquad (3.9)$$

where P_{AA}^{H} is the hindered diffusion of AA, N the number of pores, D_{AA}^{bulk} the bulk solution diffusion factor of AA, d the length of the pore, a_w the molecular diameter of water and a factor between AA and the walls of the tight junctions, $F(a/r) \approx 1-2.1044(a/r)+2.089(a/r)^3-0.948(a/r)^5$. For a given cellular level *i*, the rate of AA concentration in ES from the previous level towards the next is:

$$\dot{C}_{AAtj_i}^{ES} = \rho_{ES}(J_{AA_i}^{tj_{in}} - J_{AA_i}^{tj_{out}}) = -\rho_{ES} P_{AA}^{H} \left(C_{AA_{i-1}}^{ES} - 2C_{AA_i}^{ES} + C_{AA_{i+1}}^{ES}\right) \qquad (3.10).$$

Concentration change rates of ionic diffusions ($J_{Ac^-}^{tj}$, $J_{H^+}^{tj}$)

Ions are infused also due to electrical fields appearing due to the pH difference. Assuming that the electrical field that has been generated in between the two sides of the cellular membrane is stable, the Goldman-Hodgkin-Katz assumes the form:

$$J_S^{I\to II} = \frac{z_S F D V}{RT} P_S C_S^{I} - \frac{C_S^{II} e^{\frac{z_S F D V}{RT}}}{1 - e^{\frac{z_S F D V}{RT}}} \Leftrightarrow \dot{C}_S^{II} = \rho J_S^{I\to II} \qquad (3.11)$$

where z is the valence, F the Faraday's constant, R gas constant, T the temperature, index S denotes the diffusing ion (H^+ or Ac^-), ρ is the volume/area ration of the diffusing compartment and C^I, C^{II} are respectively the concentrations of compartment I and II (positive flux from I to II).

Despite the cations over anions discrimination in tight junction pores, a common channel resistance policy is adopted for the developed model and Ac^- diffusion is considered hindered based on the molecular dimensions. Using (3.9) the ions concentration change rates of IS and ES at any given layer is:

$$\dot{C}^{ES}_{S_{tj_i}} = \rho_{tj}(J^{tj_{in}}_{S_i} - J^{tj_{out}}_{S_i}) = -\rho_{tj}\frac{z_S F D V_{tj}}{RT} P^H_S \left(\frac{C^{i-1}_S - C^i_S e^{\frac{z_S F D V_{tj}}{RT}}}{1 - e^{\frac{z_S F D V_{tj}}{RT}}} - \frac{C^i_S - C^{i+1}_S e^{\frac{z_S F D V_{tj}}{RT}}}{1 - e^{\frac{z_S F D V_{tj}}{RT}}}\right) \quad (3.12).$$

Assuming similar formulation is applied in passive ion diffusion through the cellular membrane, the rates of Ac^- in IS and ES due to electrodiffusion of the membrane is:

$$\dot{C}^{IS}_{Ac^-} = -\rho_{IS} J^m_{Ac^-} = -\rho_{IS}\frac{(z_{Ac^-})FDV_m}{RT} P^m_{Ac^-} \frac{C^{ES}_{Ac^-} - C^{IS}_{Ac^-} e^{\frac{(z_{Ac^-})FDV_m}{RT}}}{1 - e^{\frac{(z_{Ac^-})FDV_m}{RT}}} \quad (3.13)$$

$$\dot{C}^{ES}_{AA_i} = -\rho_{ES} J^m_{Ac^-} = \rho_{ES}\frac{(z_{Ac^-})FDV_m}{RT} P^m_{Ac^-} \frac{C^{IS}_{Ac^-} - C^{ES}_{Ac^-} e^{\frac{(z_{Ac^-})FDV_m}{RT}}}{1 - e^{\frac{(z_{Ac^-})FDV_m}{RT}}} \quad (3.14)$$

The fraction of unionized AA ($C^{IS}_{AA_T}$) is given by the formula:

$$a = C^{IS}_{H^+_i} / (C^{IS}_{H^+_i} + K_a) \quad (3.15)$$

Thus in (3.12) the number of variables can be reduced by the use of:

$$C^{IS}_{Ac^-} = (1 - a) C^{IS}_{AA^T} \quad (3.16)$$

Active proton and vasculature flux ($J^P_{H^+}, J^V_{AA}, J^V_{Ac^-}, J^V_{H^+}$)

Acetic acid extrusion from the cells and stroma diffusion are unidirectional, proportional to the concentration of the native diffusing solute and to its perfusion rate through the membrane.

$$J = kC_S \quad (3.17)$$

is used to describe the fluxes in the most simplistic circumstances, where k is a proportionality constant (cm/sec) and C_S is the concentration of transported solute. The concentration change rates by a generic pump $\dot{C}_{H^+_p}$ and stroma diffusion $\dot{C}^{ES}_{S_V}$ are described by:

$$\dot{C}_{H^+_p} = \rho_p J^p_{H^+} = k_p C^{IS}_{H^+} \quad (3.18)$$

$$\dot{C}^{ES}_{S_V} = \rho_V J^V_S = k_V C^{ES}_S \quad (3.19)$$

where k_p, k_V are the proportionality constants, ρ_p and ρ_V are the area/volume ratio of pump and stroma respectively and *S* the diffusing AA, Ac^- and H^+.

Differential equation system of the model

As described in Chapter 1.3, the AW dynamics are proportional to the pH_{IS} dynamics. This lead to the model equations to be developed, with the purpose of providing pH_{IS} as output.

These dynamic characteristics ($\dot{C}^{IS}_{H^+_p}$), as well as the total AA concentration ($\dot{C}^{IS}_{AA^+_p}$), are described by the following differential system:

$$\dot{C}^{IS}_{H^+_p} = -\ln 10^{C^{IS}_{H^+_p}} \rho_{IS}\left((1-a_i)J^m_{AA_i} - a_i J^m_{Ac^-_i}\right) - J^p_{H^+} \quad (3.20)$$

$$\dot{C}^{IS}_{AA^T_i} = \rho_{IS} J^m_{AA_i} + \rho_{IS} J^m_{Ac^-_i} \quad (3.21)$$

where $\ln 10^{C^{IS}_{H^+_p}}$ is a factor describing the conversion of pH to H^+, ρ_{IS} is the cell area/volume ration (A_{cell}/V_{cell}) and β is the intracellular buffering power of a solution. ($\beta = dC^{IS}_{H^+_i}/dpH_{IS}$).

The equivalent system for the ES is:

$$\dot{C}^{ES}_{AA_i} = \rho_{tj}\left(J^{tj_{in}}_{AA_i} - J^{tj_{out}}_{AA_i}\right) + \rho_{ES} J^m_{AA_i} + J_{ion} \quad (3.22)$$

$$\dot{C}^{ES}_{Ac^-_i} = \rho_{tj}\left(J^{tj_{in}}_{Ac^-_i} - J^{tj_{out}}_{Ac^-_i}\right) + \rho_{ES} J^m_{Ac^-_i} - J_{ion} \quad (3.23)$$

$$b_{ES}\dot{C}^{ES}_{H^+_i} = \rho_{tj}\left(J^{tj_{in}}_{H^+_i} - J^{tj_{out}}_{H^+_i}\right) + \rho_{ES} J^m_{H^+_i} - J_{ion} \quad (3.24)$$

where ρ_{ES} and ρ_{tj} are the area/volume ratio of the ES and the tight junctions respectively, b_{ES} is a proportionality constant defined by the ratio of the ionized/non-consumed protons in the ES. Regarding the last layer, $\rho_{tj}J^{tj_{out}}_{AA_i}$, $\rho_{tj}J^{tj_{out}}_{Ac^-_i}$, $\rho_{tj}J^{tj_{out}}_{H^+_i}$ are substituted by the terms $k_V J^V_{AA_i}$, $k_V J^V_{Ac^-_i}$, $k_V J^V_{H^+_i}$ respectively.

Approximation of the model

The differential system, as described above, results in high computational cost. It is desirable to reduce computational cost without sacrificing accuracy. A stricter observation of the parameters of the model reveals two kinds of kinetics during the AW phenomenon, the slow and fast kinetics procedures. In order to simplify the model the Rapid Equilibrium Approximation method was applied, resulting in expunging J_{ion} from the differential equations and reduced the number by one. By setting

$$X_i = C_{AA_i}^{ES} + C_{Ac_i^-}^{ES} \qquad (3.25)$$

$$Y_i = C_{H_i^+}^{ES} - C_{Ac_i^-}^{ES} \qquad (3.26)$$

And by differentiating (3.25) and (3.26), the result is the sum of (3.22) and (3.23) for the first and the subtraction of (3.24) from (3.23):

$$\dot{X}_i = \rho_{tj}\left(J_{AA_i}^{tj_{in}} - J_{AA_i}^{tj_{out}}\right) + \rho_{ES}J_{AA_i}^{m} + \rho_{tj}\left(J_{Ac_i^-}^{tj_{in}} - J_{Ac_i^-}^{tj_{out}}\right) + \rho_{ES}J_{Ac_i^-}^{m} \qquad (3.27)$$

$$\dot{Y}_i = \rho_{tj}\left(J_{H_i^+}^{tj_{in}} - J_{H_i^+}^{tj_{out}}\right) + J_{H_i^+}^{p} + \rho_{tj}\left(J_{Ac_i^-}^{tj_{in}} - J_{Ac_i^-}^{tj_{out}}\right) - \rho_{ES}J_{Ac_i^-}^{m} \qquad (3.28)$$

Parameters of the model

Table 1 Parameters of the model

Parameters	Unit	Description
pH_{ES}		pH of extracellular space
pH_{IS}		pH of intracellular space
IS volume	μm^3	Volume of extracellular space
ES volume	μm^3	Volume of intracellular space
Cell area (A_{cell})	μm^2	Area of cellular membrane
TJ area (A_{tj})	μm^2	Area of membrane of tight junctions
P_{AA}^{m}	μm/s	Permeability rate of membrane by AA
P_{Ac}^{m}	pm/s	Permeability rate of membrane by Ac^-
P_{AA}^{tj}	μm/s	Permeability rate of tight junctions by AA
P_{Ac}^{tj}	μm/s	Permeability rate of tight junctions by Ac^-
P_{H}^{tj}	μm/s	Permeability rate of tight junctions by H^+
Intracellular buffering (β)	mM	Consumption rate of H^+ in ES
Pumping rate (k_p)	μM/s	H^+ rejection rate from cytoplasm
ΔV_m, ΔV_{tj}	mV	Voltage of electric field formed between the edges of cellular membrane and tight junctions respectively
AA ionization constant at 37°C (K_a)		Ionization factor of AA
F	C/mol	Faraday constant
R	J/mol/K	Constant of gas
T	K	Temperature
Z_{Ac}		Valence of Ac
Z_H		Valence of H

Final form of the differential system [21]

The following differential equation system is created for each neoplastic layer:

$$\dot{C}_{TA_i}^{IS} = a^{-1}(J_{AA_i}^{m} + J_{Ac^-}^{m}) \quad (3.29)$$

$$\dot{C}_{H_i^+}^{IS} = -\ln 10^{C_{H^+}^{IS}}\, \alpha\beta_{IS}\left(q_i^{IS} J_{AA_i}^{m} - w_i^{IS} J_{Ac_i^-}^{m} - J_{H_i^+}^{p}\right) \quad (3.30)$$

$$\dot{C}_{TA_i}^{ES} = b^{-1} J_{AA_i}^{m} + b^{-1} J_{Ac^-}^{m} + a^{-1}\varepsilon J_{AA_i}^{tj} + b^{-1}\varepsilon J_{Ac^-}^{tj} \quad (3.31)$$

$$\dot{C}_{H_i^+}^{ES} = -\ln 10^{C_{H_i^+}^{IS}}\, \beta_{ES}^{-1}[q_i^{ES}(b^{-1} J_{AA_i}^{m} + a^{-1}\varepsilon J_{AA_i}^{tj}) - w_i^{ES}\left(b^{-1} J_{Ac_i^-}^{m} + a^{-1}\varepsilon J_{Ac_i^-}^{tj}\right) + b^{-1} J_{H^+}^{p} + a^{-1}\varepsilon J_{H^+}^{tj}] \quad (3.32)$$

where the dot ($\cdot$) denotes the time derivative, *TA* is the total AA concentration, in both ionized and unionized form, *i* is the ith neoplastic layer (*i=1,2,…,N*), *q* and *w* account for the dynamic ionization constants of AA, including its self-burning effect. The developed differential equation system is solved numerically with the aid of a mixed-integer, nonlinear algorithm. It should be noted that the reservoir layer equations (3.31) and (3.32) are abolished and for the last layer the outgoing paracellular flux is replaced by the $K_V C$ term, where K_V is the permeability at the boundary between the epithelium and the stroma and C corresponds to the concentration of either AA, Ac^- or H^+.

3.3.2 Global Sensitivity analysis, parameter identifiability and estimability [21]

As mention before pH_{IS} over time is produced as output of the model. That is graphically depicted as a curve of intracellular H^+ versus time. Information on all structural and functional biological parameters, that determine the AA pharmacokinetics through the epithelial and are related to neoplasia, is contained in the model predictions. Under an idealized, *in silico*, environment Global Sensitivity Analysis (GSA), parameter identifiability and parameter estimability has been performed. GSA provides an estimate of model's output sensitivity to the variations of the input parameter. The GSA outcomes was used as input for both parameter identifiability and parameter estimability. A given parameter is considered as identifiable when its respective sensitivity function is neither null nor collinear with the sensitivity function of another parameter. In parameter estimability analysis the level of interactions and/or correlations between the identifiable parameter sets was defined. Based on these studies the parameters were ranked with the purpose of reducing the dimensionality of the inverse problem that is described in Chapter 4. The parameters that display high sensitivity, no collinearities and minimum interdependency with other parameters are considered as the key determinants of the bio-optical dynamic characteristics, whereas parameters that are not fulfilling these criteria can be considered as non-identifiable and kept constant at around their nominal values.

Finally, the value ranges of the set of neoplasia related biological parameters, as measured experimentally are shown in Table 2.

Table 2 Value Range of biological parameters

Parameters	Description	Lowest value	Highest value
N	dysplastic cellular layers number	1	10
b	ES linear dimension	$4* 10^{-7}$	$8* 10^{-7}$
pH_{ES}	pH value of ES	3	13.8
E	tight junctions' porosity factor	6	7
β_{ES}	ES buffering efficiency	0.035	0.05
$\mathbf{pH_{IS}}$	pH value of IS	7	7.4
β_{IS}	IS buffering efficiency	0.01	0.018
$\mathbf{K_V}$	Permeability of tissue boundary	$1* 10^{-7}$	$10* 10^{-7}$

These eight parameters are considered the full set, whereas the first four parameters of Table 2 are considered the half-set, as they were deemed most identifiable after the analyses where completed. These parameters are all structural and functional parameters that have identified to directly correlate with existence and progress of cancer.

N: this parameter is the number of dysplastic cellular layers. As stated in Chapter 2, as cancer progress in stages, the number of dysplastic cellular layers increase.

b: area of the extracellular space. Cancerous cells are mole loosely connected thus the distance between them increases. That affects the extracellular space directly by proportional increase as cancer progresses.

pH_{ES}: the value of pH in the extracellular space. Studies have shown that cancerous cells are surrounded by acidic environment. This functional parameter has lower than normal value depending on the existence or not of cancer.

ε: this factor depicts the ability of the tight junctions between cells to allow movement of ions.

β_{ES}: this parameter depicts the ability of the extracellular space to consume ions. This ability is a structural parameter that actively affects the pH value of the extracellular space.

pH_{IS}: the value of pH in the intracellular space. All cells, cancerous or not, tend to maintain the intracellular pH value at neutral levels. Thus ions are ejected on the extracellular space raising its acidity.

β_{IS}: a parameter depicting the ability of the intracellular space to consume ions, dependent of the pH regulation mechanisms used by pH.

K_V: a factor of permeability of the cellular membrane that is directly linked with the structural and functional characteristics of the cell.

4 Inverse problem

An *inverse problem* is a term used to describe a problem in which it is attempted to convert the observed measurements into information about a physical problem or system. The specific problem tackled in this thesis, attempts to extract information of some biological parameters by fitting of dynamic optical data, in form of curves depicting concentration of hydrogen within the cytoplasm of the epithelium of the cervix. In this attempt, the mathematical model that simulates the acetic acid pharmacokinetics through the epithelium of the cervix consists a priceless asset. The end goal is acquisition of the ability to assert the values of the biological parameters, both structural and functional, with only knowledge the observed dynamic optical data obtained during screening diagnosis for cervical cancer, thus enabling for the first time *in silico,* non-invasive and immediate biopsy of neoplasia growth.

4.1 Control theory

Control theory consists an interdisciplinary branch of engineering and mathematics that deals with the behavior of dynamical systems.

Experimental process

From medical examinations with DCE-OI, clinical experimental dynamic optical data are obtained by recording measurements of diffuse reflectance of the backscattered light through time, which reflect the pharmacokinetics of AA through the epithelial tissue during the AW phenomenon.

In silico process

From the deterministic, *in silico*, mathematical method described in Chapter 2, which simulates the experimental process, the normalized concentration of H^+ versus time is obtained for a given set of biological parameters.

Efforts are made for adequate fitting of the *in silico* computed output to the experimental acquired data. Achieving this fitting the known parameters that produce the output of the mathematical model can be assigned to the parameters of the experimental process with adequate accuracy that is investigated in this thesis.

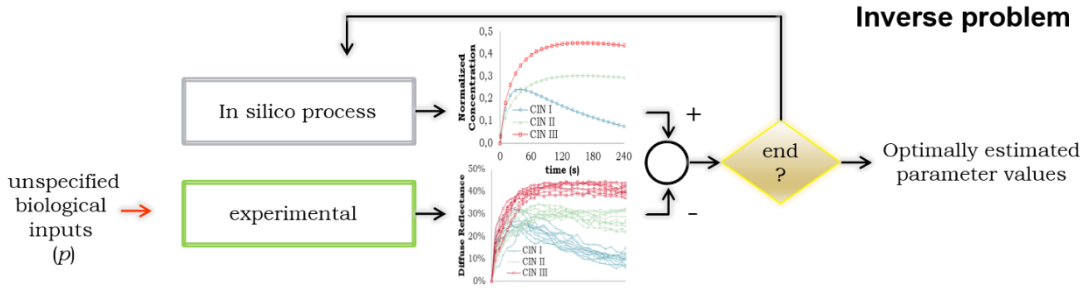

Figure 4-1 System of inverse problem investigated

The solution of this is the minimization of the non-linear objective function of this system:

$$J = ||y^{exp}(p,t) - y^{M}(p^{trial},t)|| \qquad (4.1)$$

which is subjected to: $f\left(\frac{dx}{dt}, x, p^{trial}, u\right)$

$$t_0=0$$

$$x(t_0)=x_0$$

$$t \in [0,240]$$

$$p_L \leq p^{trial} \leq p_U$$

$$u=u_0,$$

where f is the dynamic description of the model, x are the differential state variables, p^{trial} is latest set of p values used for an estimation, u is the initial amount of acetic acid and p_L, p_U are the lower and upper bounds of the values of the parameters respectively.

In the ideal case the global minimum is unique and has the form (in an analogous

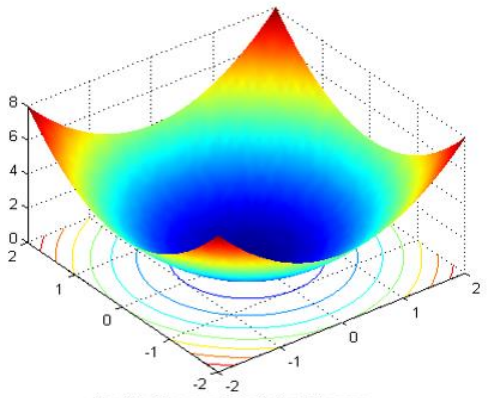

the ideal case of global minimum

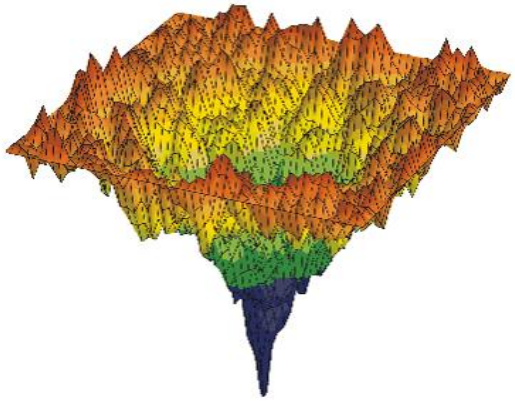
global minimum at the case of reality

Figure 4-2 Ideal global minimum for three parameter Figure 4-3 Realistic global minimum for three parameters

problem of three parameters) depicted in Figure 4-2

The system described in Figure 4-1 is not ideal though. More specifically, there are many local minima throughout the dimensional space defined by the system. In case of failing to locate the global minimum, an accepted estimation of the solution would be the value that is found closest to the global minima. A more realistic representation for the problem at hand would be the one presented in Figure 4-3.

4.2 Fitting constrictions

The system described in every fitting estimation assigns real values to the parameters, one of each is discrete and not continuous (parameter N that describes cellular layers is an integer). It is not deterministic thus cannot be solved in polynomial time. Finally the system is non-linear as the differential equations described in *Chapter 3.3.1* do not represent a linear combination of the variables. Thus the system is a real valued mixed integer non-linear system NP-complete problem, thus the fitting is difficult to be achieved and is of outmost importance to maintain the non-linearity that it includes. In order for the fitting to be achieved and the parameter values described in *Table 2* to be assigned to the experimental data, global optimization algorithms are conscripted.

4.3 Global Optimization

Global optimization (GO) is a branch of applied mathematics and numerical analysis dealing with the optimization of a single or a set of functions, according to some criteria and constrains.

Global optimization algorithms classification [22]

Global optimization algorithms classification can be made by the "nature" of the algorithms, meaning the method they use to estimate a new point during an iteration. There are two main categories:

1. *Deterministic algorithms*. Given the initial inputs these algorithms will always produce the same outputs in the same time interval.
2. *Stochastic algorithms*. These algorithms rely on probabilistic approaches, thus having weak theoretical guarantees of converge to global optima compared to the deterministic ones, but in high dimensionality problems they can locate the vicinity of global solutions with relative efficiency. They can be divide in five groups:
    a. *Adaptive stochastic methods.*
    b. *Clustering methods (multistart methods).*
    c. *Evolutionary computation* also known as *biologically inspired methods* or *population-based stochastic methods.*
    d. *Simulated annealing.*
    e. *Meta-heuristics,* based on biological or physical phenomena, eg ant colony movement.

The algorithms can be classified into two general categories based on the way they search across the dimensions. Those are:

1. *Population based algorithms*. The algorithm handles a random ensemble of points inside the feasible input space Ω and by iterative substitution of the population members with better ones, searches the dimensional space until a termination constrain is met.
2. *Point-to-point algorithms.* These algorithms begin from a single point and substitutes with a better estimation on the occurring iterations until a termination constrain is met.

A brief reference of each algorithm utilized in this study follows, focusing on the general idea behind each algorithm and a description of the mechanics behind each iteration.

4.4 Algorithms

4.4.1 Deterministic Algorithms

Deterministic methods can provide a level of assurance that the global optimum will be located, due to the deterministic method they follow searching the d-dimensional space[5]. Although global optimality can be even guaranteed in certain problems, deterministic algorithms cannot guarantee solution to be found with certainty in finite time [23]. The deterministic algorithm gblSolve has been included in the study as a recent method with good reported results for several challenging problems.

4.4.1.2 gblSolve algorithm [24, 25]

Introduction

glbSolve algorithm, also reffered to as DIRECT, is an algorithm presented in [25] as a modification of the existing algorithm presented in [24]. It is based on the idea of carrying out simultaneous searches using all possible Lipschitz constant values from zero to infinity, thus achieving operating on both the global and local level. By doing so a speed up in algorithmic convergence is achieved compared to standard Lipschitzian methods. It is guaranteed to converge to the global optimal function value if the objective function f is continuous or at least continuous in the neighborhood of a global optimum. The algorithm is based on the idea of iteratively dividing the d-dimensional space in smaller parts and compare one to the other.

Iterative description

In the first step the algorithm transforms the d-dimensional space into a hypercube. The center-point of this cube is then evaluated and the space is divided in smaller hyperrectangles, whose center points are also sampled. A set of *potentially optimal* rectangles is then identified and the same procedure follows for each rectangle.

[5] d-dimensional space refers to the dimensional feasible space where the solution of the inverse problem lies, defined by d number of parameters.

Flow Diagram

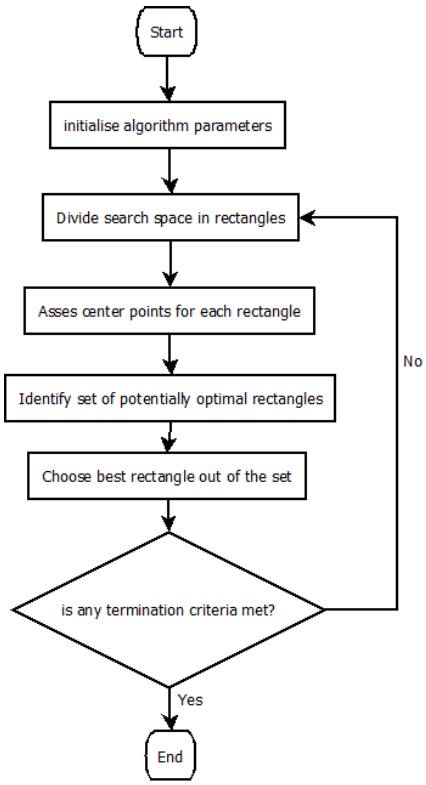

Figure 4-2 flow chart of gblSolve algorithm

4.4.2 Stochastic Algorithms

4.4.2.1 Controlled Random Search (CRS) - with Competing Heuristics [26, 27, 28, 29]

Introduction

Controlled Random Search (CRS) , is a random search procedure effective in identification of the global optima in both constrained and unconstrained multi-extrema functions. It was firstly implemented by W.L.Price in 1976 and in this study the version presented in [27] and [28] by Josef Tvrdik is included. It is a direct, random method, used for either constrained or unconstrained functions and regardless whether the variables are continuous. The algorithm is designed with more gravity to a full search of the d-dimensional space, rather than speed of fitting. Thus it is often used for further fitting of results of other faster converging GO algorithms.

New estimations for the global optima in query during each iteration is made based on heuristics mechanisms, a non-deterministic rule that produces a new estimated point *y* inside the feasible search space. In this study four heuristics mechanisms were used starting with equal probability for each to be used during an iteration. The probabilities change based on the estimation success rate of each heuristics. More specifically if a heuristic mechanism makes an estimation that is equally or better evaluated than the worst member of the population that exists in the iteration the algorithm is currently on, a higher probability value is assigned to that heuristic.

Heuristics methods

Three out of the four heuristics are creating a new trial point *y* from the subset S. Subset S is d+1 chosen points from the initial population of estimations and d is the number of dimensions, ie parameters. The trial point is given by:

$$y = g + U(g - x_H) \qquad (4.1)$$

Where $x_H = \underset{x \in S}{\operatorname{argmax}} f(x)$ and g the "centroid" of the d points remaining in the subset S. The factor U is a random variable uniformly distributed in the [s, a-s], where a>0 and s are input parameters of each heuristic mechanism, 0<2<a/2. All the d+1 points of the subset are randomly chosen from the P for the heuristics named REFL1 and REFL25. With factor a, the distance between each point from the "centroid" is defined and s the amount of reduction of a, in case the value of the function for the new estimation is worse than the existing worse estimation in the population. For the third heuristic, REFLB, for the creation of each subset S, d points from the initial population P are chosen, as well as the optimal point currently in the population. The forth mechanism is based in differential evolution mechanics, described in Chapter 4.4.2.2.

Iterative description

At the start of the algorithm if a population of points is not given a random one is initialized. Each point is evaluated by the function in order to define the one with the worst evaluation, the highest value on a minimization problem, and the one with the best evaluation. Next a heuristic method is randomly chosen by the roulette function. The roulette function is named thusly due to the mechanics being the same with the "Russian roulette" game. The first and second heuristics methods choose any d+1 distinct members of the initial population P for the creation of a subset S. The "centroid" g of the d+1 points is calculated and a new trial estimation is generated. The third heuristic chooses randomly d distinct members of P as well. The "centroid" g is again calculated and a new trial estimation point is generated. The forth heuristic is randomly choosing four members of P. Vectors r_1, r_2 and r_3 are defined according with the first three random points. For instance if the first point is 4, the forth vector of parameters of the initial population is chosen and assigned to r_1. The new trial point y, by use of the forth point found, is generated like the other three vectors r_1, r_2 and r_3. A temporary trial point is created by

$$v = r_1 + F(r_2 + r_3) \quad (4.2)$$

$$F = \begin{cases} \max\left(F_{min}, \left|\frac{f_{max}}{f_{min}}\right|\right), \text{if } |f_{max}/f_{min}| < 1 \\ \max\left(F_{min}, \left|\frac{F_{max}}{F_{min}}\right|\right), \text{ otherwise} \end{cases} \quad (4.3)$$

where f_{min} and f_{max} are the function evaluations of the best and worst members respectively. The new trial estimation produced by any of the four heuristics (one per iteration is used) is evaluated by the function, once it is verified that it obeys the constrictions, meaning if the parameters that were estimated are within the acceptable bounds. If it does not, the process described so far starting by the roulette function is repeated. Once the new estimation is evaluated then it is compared to the worst member. If it is better then the new point replaces the worst point in the population and the rate of success of the heuristic, that produced the point, is raised. If it is worse than the worst member then the process is repeated again from the roulette function downwards. After every successful creation of a new estimation and once its addition or not in the population is finished, the termination criteria are evaluation in order to halt the algorithm once any of them is met.

Constrains and general conclusions

By comparing new estimation to the worst member of the population the algorithm assumes that the solution is within the bounds of the initial population, therefore if a starting population is not large enough and the solution is out of the population bounds, the algorithm will fail. If additional constrains exist, an even greater amount of population is needed to be provided to the algorithm. With comparison of each new estimation to the worst member, a reasonable compromise between searching and fitting is made. The algorithm is simple and objective. Its most intriguing characteristic is that regardless of the amount of dimensions of the space many new trial points are generated fast and as long as

the size of the initial population does not rise exponentially not much memory allocation is needed.

Flow Diagram

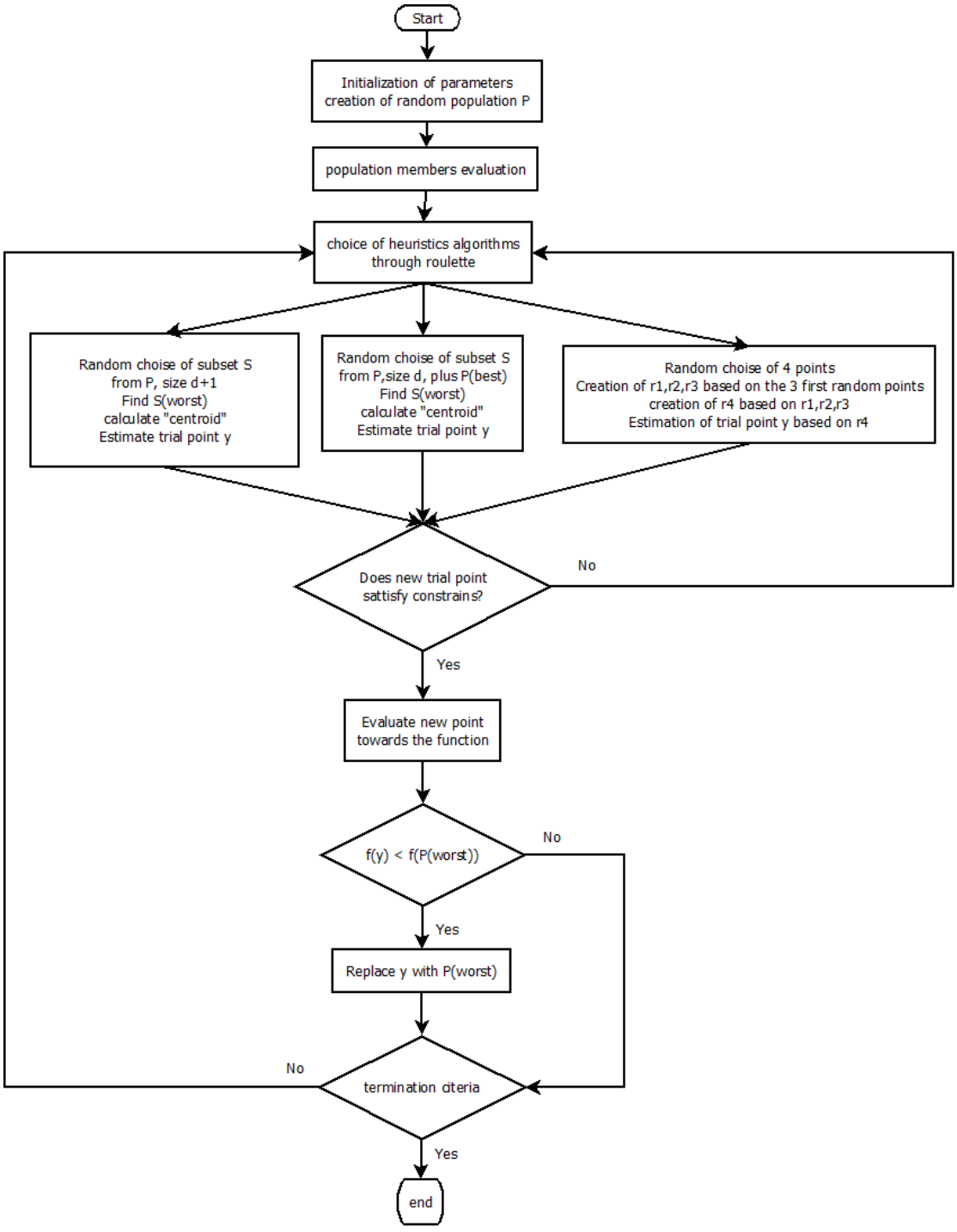

Figure 4-3 CRS flow chart

4.4.2.2 Differential Evolution [26, 30, 31]

Differential Evolution was introduced in [31] as a reliable, flexible and easy to use global optimization algorithm. It belongs to the class of evolutionary methods, while integrating essential elements from the adaptive random search methods, eg CRS described in 4.4.2.1.

Iterative Description

At the start of the algorithm, and if not provided, minimum and maximum nominal value for each dimension is set and a random initial population P is created. Each member of the population is evaluated by the objective function and the best member is identified. During an iteration of the algorithm each and every member of the population is targeted arrow to go under two stages, stage of **mutation** and the stage of **crossover**.

In the stage of mutation three randomly chosen members of the population are chosen and a new vector, v, of parameters is created from the parameters of these points using the (4.2) equation. In the case of DE, unlike in CRS, F is a constant factor provided to the algorithm from the interval [0, 2]. A trial vector, u, is created by the following method

$$u_{j,i,G+1} = \begin{cases} v_{j,i,G+1}, & if\ rand_{j,i} \leq CR\ or\ j = I_{rand} \\ u_{j,i,G+1}, & if\ rand_{j,i} > CR\ and\ j \neq I_{rand} \end{cases} \quad (4.4)$$

where i=1,2,…,N member of population currently targeted, j=1,2,…,d parameter currently observed, $rand_{j,i} \sim U[0,1]$, I_{rand} a random integer of the interval [1,2,…,d], CR is a probability threshold called crossover factor.

Once the trial vector is completed, it is evaluated towards constrains set upon the algorithm, such as the value of the parameters being within the desired bounds. If no constrain is evaluated it proceeds to the next step, otherwise it is discarded. On the next step, the accepted trial vectors are evaluated towards the objective function and compared towards their respective targeted vectors. The ones with the best out of the two evaluations will be accepted back in the population. Once the termination criteria are assessed, if none is met the algorithm begins the iteration from the start.

Flow Diagram

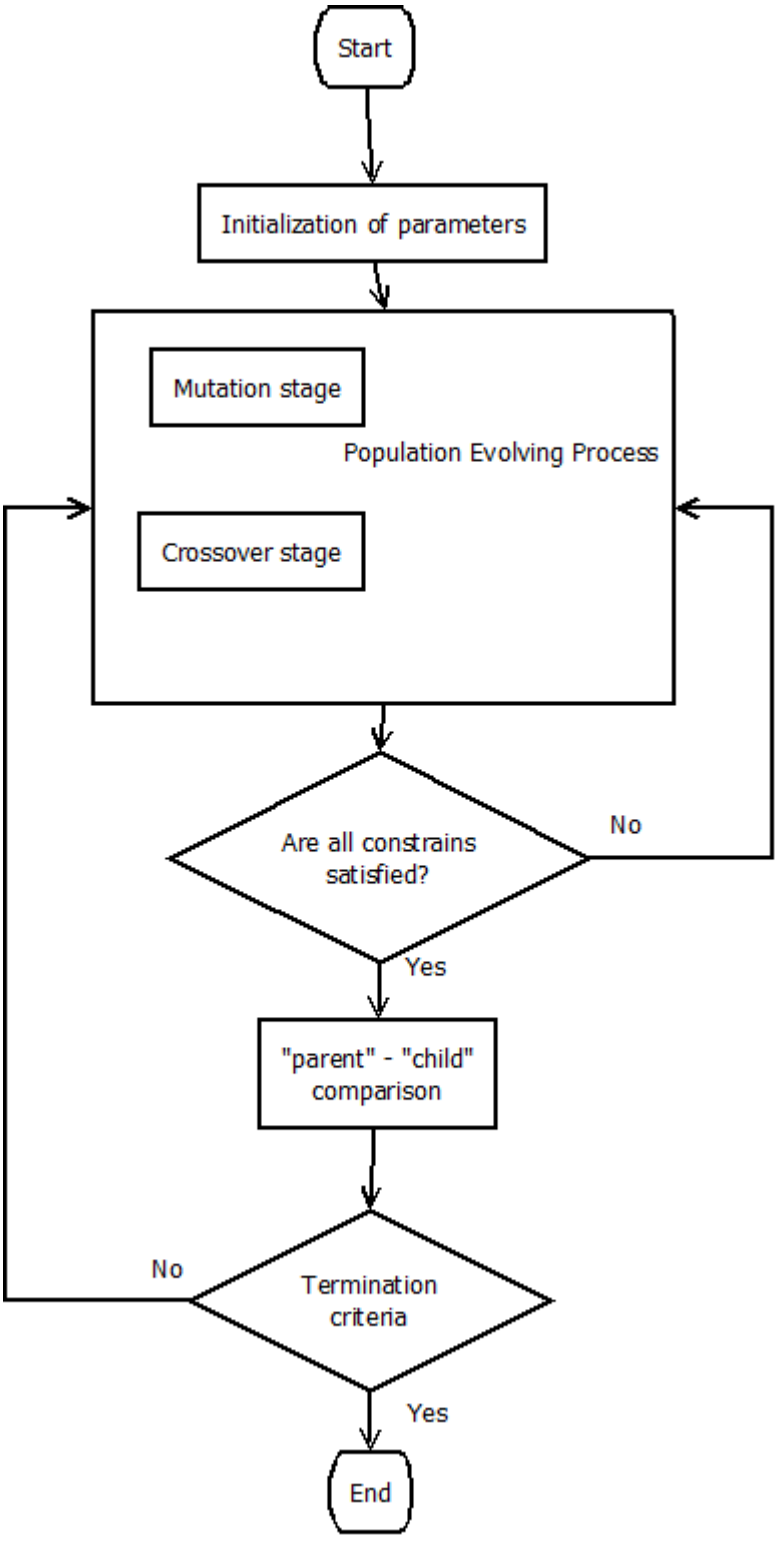

Figure 4-12 DE Flow DIagram

4.4.2.3 Shuffled Complex Evolution (SCE) [26, 32]

Introduction

The SCE algorithm is an attempt to synthesize four proven successful ideas of GO:

1. *Combination of random and deterministic approaches.* By use of deterministic strategies, SCE efficiently guides uses information provided, whereas by including random points aid towards the flexibility and robustness of the algorithm. The provision of a large enough population in the algorithm initialization will aid in ascertaining that the population contains information regarding the number, place and size of regions with high interest.
2. *Systematic Evolution of an ensemble of points stretching throughout the d-dimensional space, with the purpose of global optimization.* Systematic evolution aids in the ascertainment, that the search is guided by the structure of the objective function and is relatively robust.
3. *Competitive Evolution.* Application of this strategy has proven useful in the improvement of convergence towards a global extrema.
4. *Complex shuffling.*

The tree first ideas were based on preexisting approaches that were proven successful in the past (Holland 1975, Price 1978, Manetsch 1990, Wang 1991) and the last one was presented in [32].

Iterative Description

At the start of the algorithm, and if not provided, a random initial population P is created. Once each member of the population is evaluated by the objective function, it is ranked in ascending order. In the first stage of a given iteration, the population is divided in a user defined number of complexes, p, of equal size, which will be separately processed. If for instance P was divided into two complexes, for the first one the subset population would consist of the p(k-1)+1 ranked members and the second of the p(k-1)+2, where k=1,2,...,m and m is the size of the subset population. Each complex is the process according to the Competitive Complex Evolution algorithm (CCE). Once CCE finishes, the complexes are united into a new, single population and each member is again ranked in ascending order based on the objective function evaluation, the termination criteria are assessed for completion and if not, the algorithm proceeds to the next iteration.

The CCE algorithm

CCE algorithm does a finite amount of iterations in order to add a user defined number of new members to the population in a user defined of evolutions.

At the start of CCE a subset of n members of the complex being processed is randomly chosen from a trapezoid distribution. This distribution is defined so that the best evaluated member of the complex has more probability to be chosen and the worst member has the least probability. Once the subset is created, its worst member is identified and the "centroid" of the subset is calculated excluding the identified member. A reflection step is made, where trial estimation is made by reflecting the worst member towards the calculated "centroid". If the trial point is not within constrains a random point is generated

within constrains and the algorithm proceeds to its next new member calculation. If the trial point is within constrains, it is compared with the worst member of the population. If better it replaces it, if not a contraction step is made, where a new trial point is generated by calculating the center between the “centroid” and the worst member. Once again the trial point is compared with the worst member and replaces it if better, otherwise a random point is estimated and replaces the worst member. Once all these steps are complete the algorithm proceeds to calculate a new estimation to replace the new worst member. Once the user defined amount of new points are added to the population the evolution of the complex is complete and a new round of evolution begins, until the user defined evolution steps are reached.

Flow Diagram

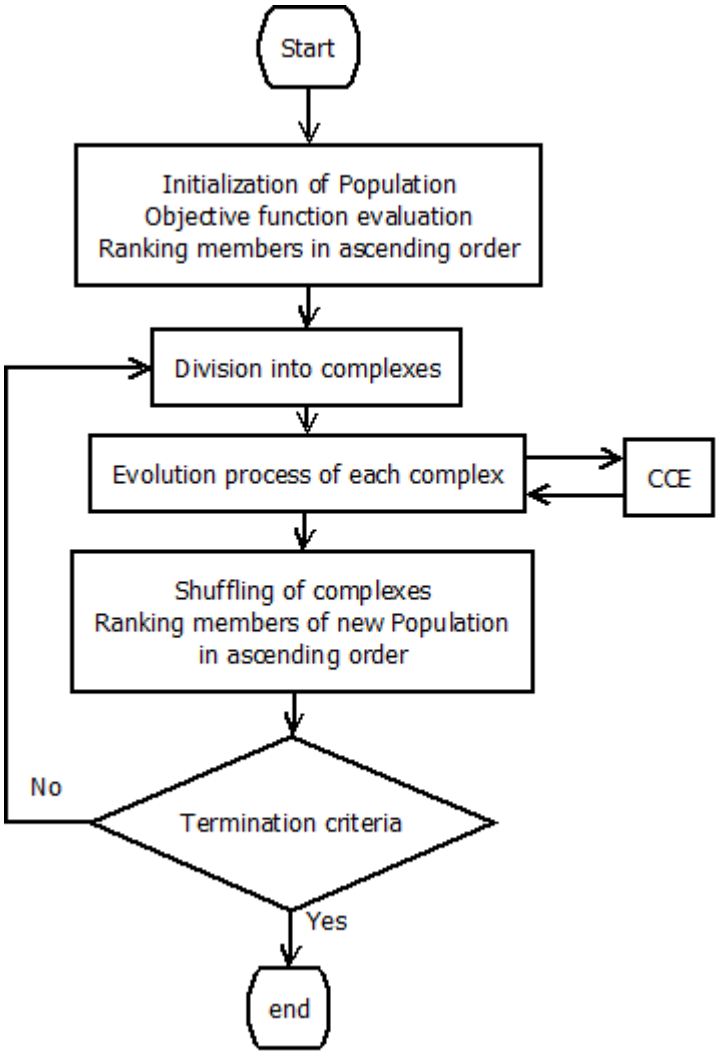

Figure 4-13 SCE flow diagram

Flow Diagram

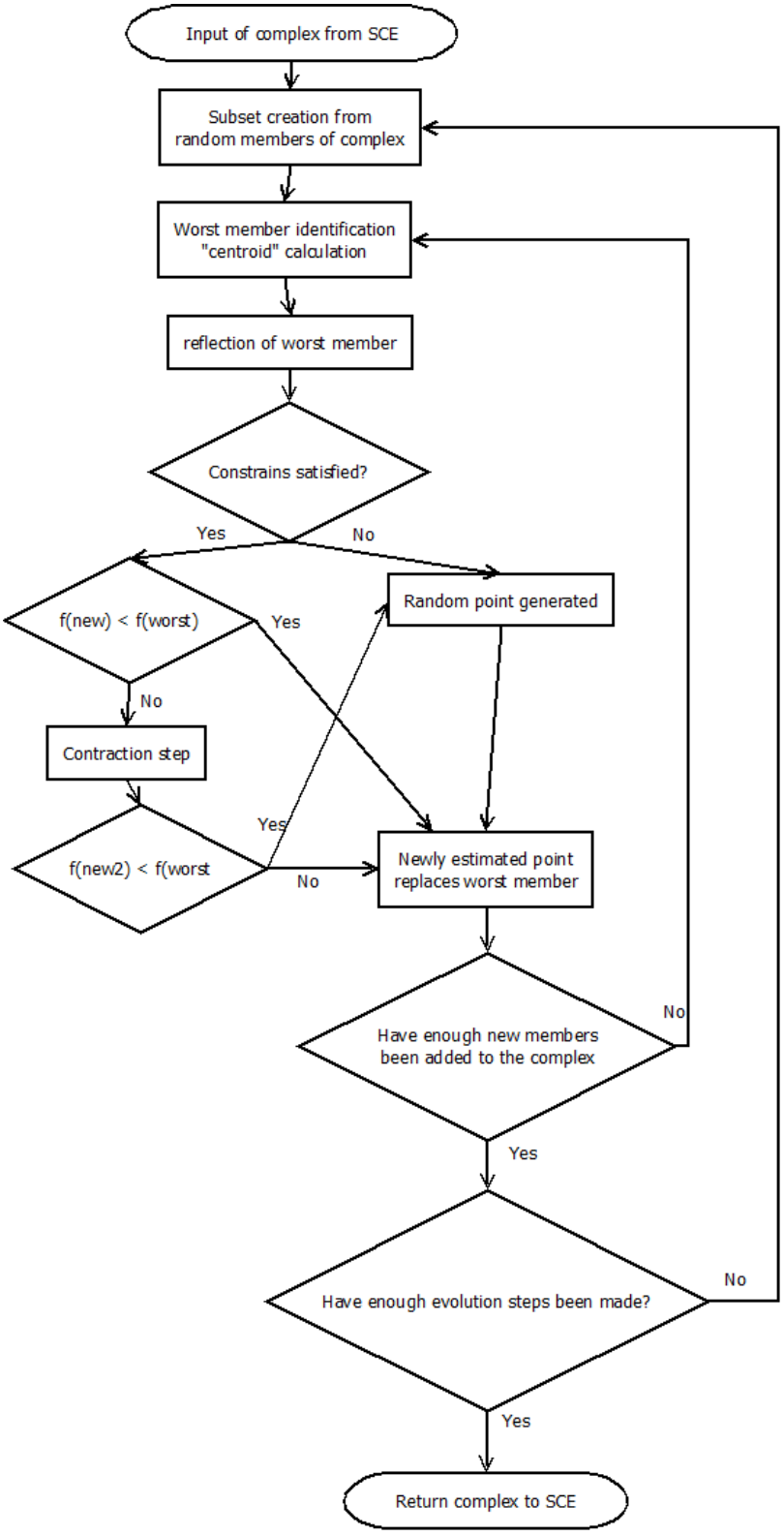

Figure 4-14 CCE flow diagram

4.4.2.4 Stochastic Ranking Evolution Strategy (SRES) [22, 33]

Introduction

SRES algorithm is an ES algorithm that involves a penalty term into the objective function, to penalize constraint violation, a method commonly used to deal with constrained optimization problems in order to be transformed into unconstrained ones. It also involves stochastic ranking of the members of the population in order to identify a set of best members.

Iterative Description

At the start of the algorithm, and if not provided, a random initial population P is created, referred to as λ in literature. The algorithm proceeds in stochastically ranking the members of the population by means of a bubble-sort-like procedure. This procedure ranks λ individuals by comparing adjacent individuals in at least λ sweeps and halts when no change in the rank ordering occurs within a complete sweep. The rank is done by use of the evaluation of each member by both objective function and a penalty function employed by SRES. Once the ranking is complete the μ best members out of the P are selected as parents for the next generation. The selected members are mutated according to a log-normal, self-adaptive rule presented in 1995 (H.-P.Schwefel). Each member produces P/μ offspring on average. If an offspring is not within constrains another mutation of the objective variable that is out of bounds will be retried a maximum of ten times, otherwise the variable of the parent will be preserved. Once a new generation is created, the algorithm restarts its iterative steps, begging by stochastically ranking the new generation, until a termination criteria is met.

Flow diagram

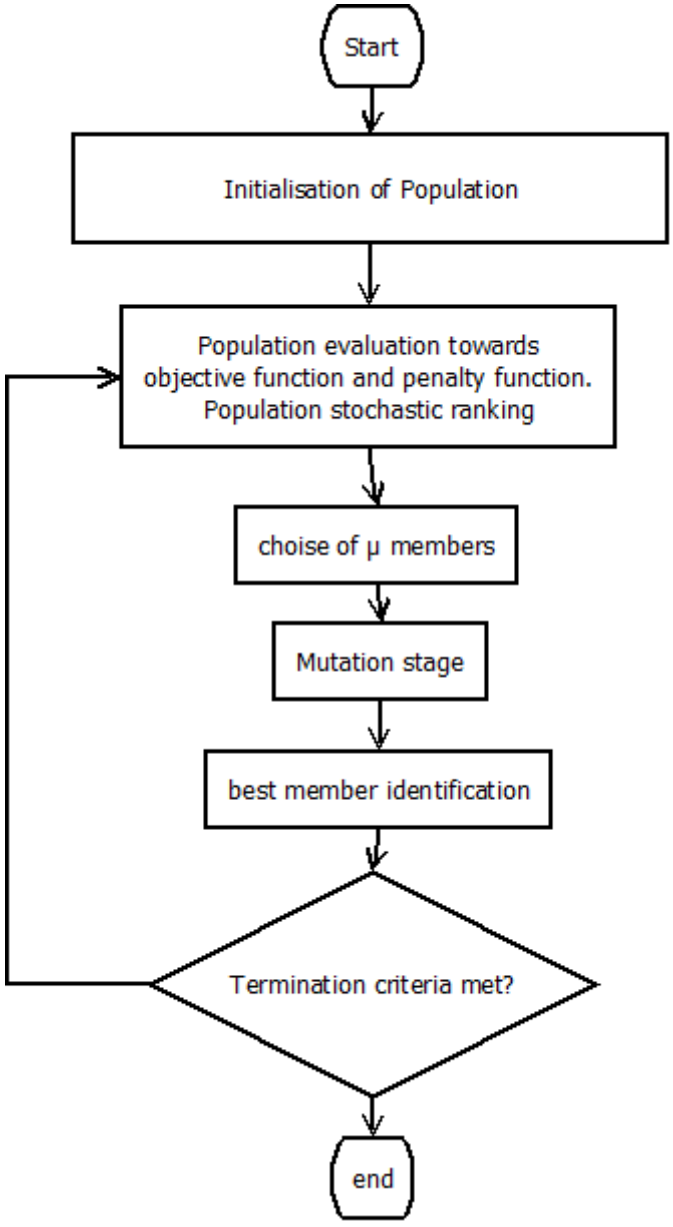

Figure 4-15 SRES Flow diagram

4.4.3 Simulated Annealing (SA)

Simulated Annealing (SA) algorithms are a combination of hill climbing algorithms and random search. They were named after the metallurgy process which in some level they simulate. Annealing in metallurgy is the process used to harder metals and glass, by heating in excess temperatures and then gradually cool in order to settle in a crystallized low energy state. The general idea of SA is to generate a random move and to accept it with a probability less than 1. This probability reduces exponentially depending how low evaluated is by the objective function and is proportionate to the current temperature *T* of the algorithm, an iteratively reduced factor that assumes for the algorithm the role of temperature in metallurgy. [34]

4.4.3.1 Simplex Simulated Annealing (SIMPSA) [35, 36]

Introduction

SIMPSA algorithm combines the deterministic non-linear simplex algorithm as proposed by Press and Teukolsky (1991) and the stochastic simulated annealing algorithm (NESA/Metropolis; Cardoso et al., 1994).

Iterative description

The SIMPSA version included in the study starts from a single-member Population, a starting point. The algorithmic parameters not defined are calculated, with most important of them being the initial Temperature. An initial simplex is created by generating, neighboring to the starting point, trial point, one for every dimension of the problem at hand. The members of the vertex are evaluated towards the objective function. The best member is stored and the simplex is reflected from the high point. Once the reflection is complete, new feasible solutions are calculated across the dimensions, by making a step towards each dimension and accept into a temporal population points that either have better function evaluation than the current best or they pass the Metropolis criterion.

$$probability\ threshold = e^{\frac{f_{best} - f_{trial}}{T_{current}}} \quad (4.4)$$

Once a step has been made towards every direction the step size is adjusted then a new cycle across the dimensions is made. Once a finite number of cycles are complete, the temperature is reduced and the algorithm begins anew from creating a simplex based on the best estimation so far.

Flow diagram

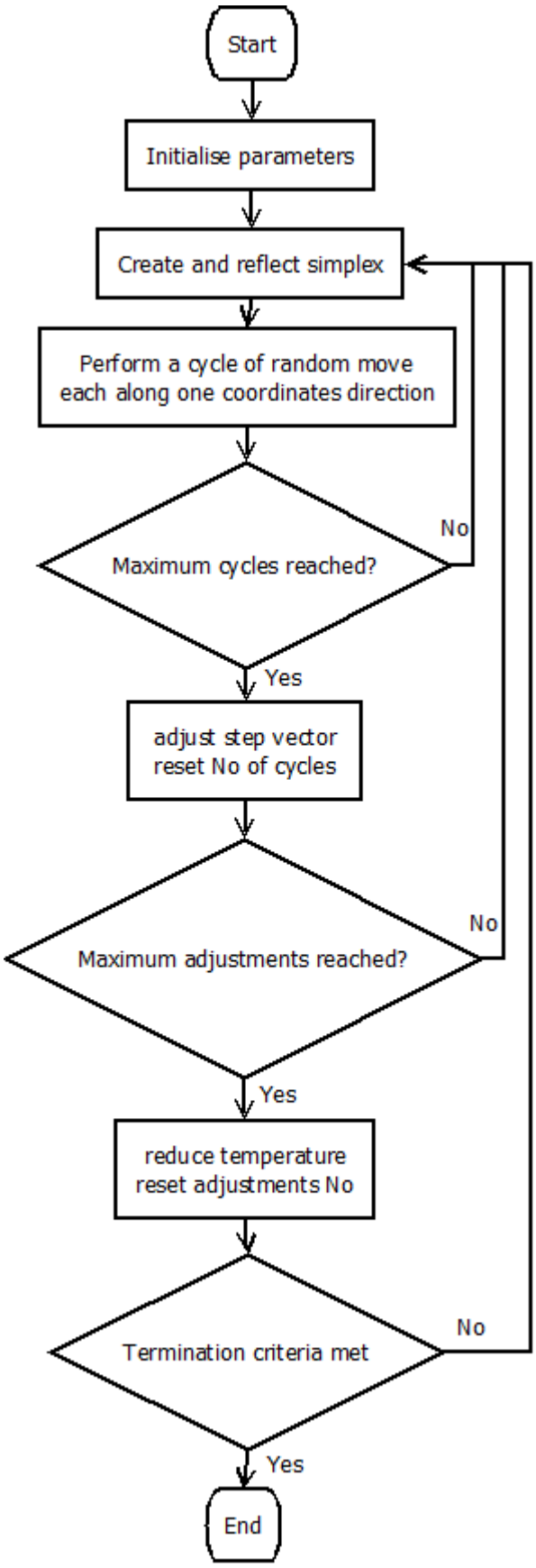

Figure 4-16 SIMPSA flow diagram

4.4.3.2 Thermodynamically Adaptive Simulated Annealing (tdASA)

Introduction

Thermodynamically adaptive simulated annealing is a script developed for the purpose of this study based on a script distributed for free in Mathworks.com, named Global Optimum Determination by Linking and Interchanging Kindred Evaluators (GODLIKE). Metropolis criterion was firstly incorporated but after experimental analysis it was concluded that for the problem at hand no benefit to the algorithm came as far as convergence is concerned, whereas time complexity was added without any benefit.

Iterative description

At the beginning of every iteration by the use of the Bolzmann generating scheme the entire population is perturbed

$$newPoint = parentPoint + \sqrt{T} * randn(1, dimensions) \quad (4.5)$$

with randn() random numbers from standard normal distribution and T the current temperature. Each individual arrow is examined whether it is within constrains. If it is not a random point is generated. The individual is then evaluated by the objective function and compared with the parent individual holding the same position in the population. If it is better it is instantly accepted, otherwise it will be accepted according to the probabilistic rule

$$rnd < e^{\frac{(f_{old} - f_{new})}{T}} \quad (4.6)$$

Then the algorithms proceed to reduce the temperature by constant factor, user provided, decide whether any termination criteria is met. If so halts the process otherwise proceeds to a new iteration.

Flow Diagram

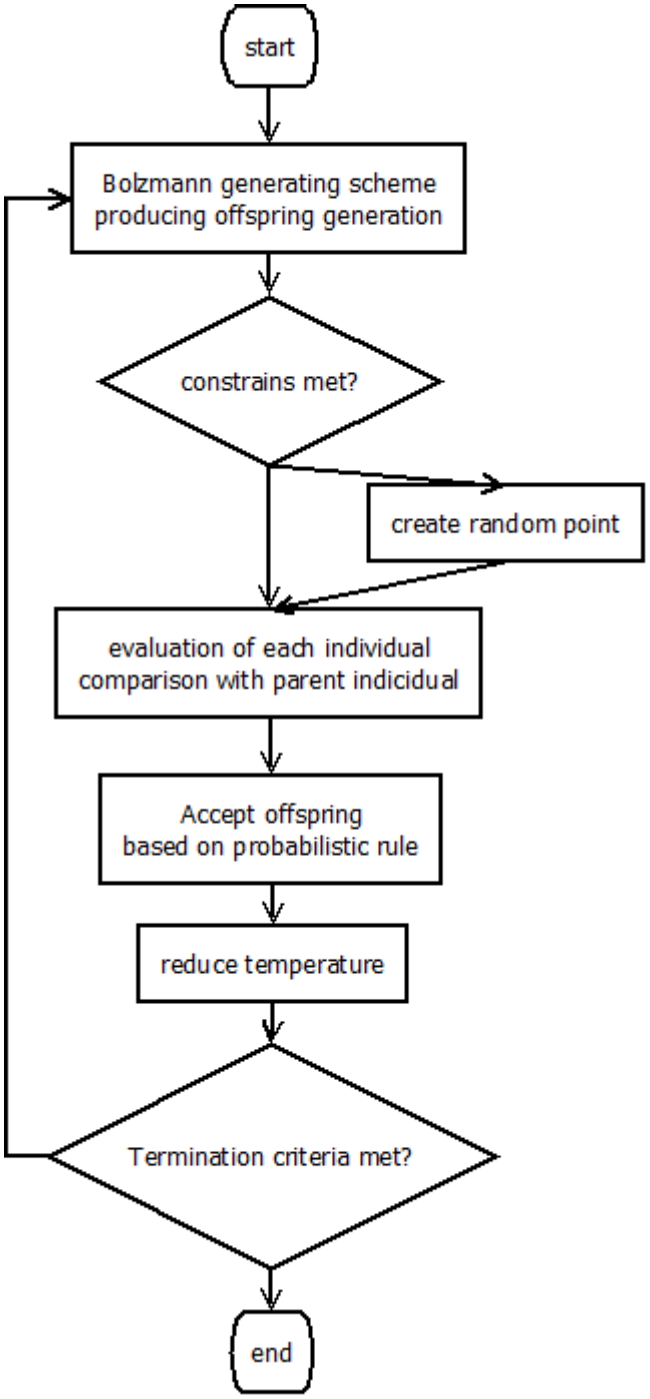

Figure 4-17 TdASA Flow Diagram

4.4.4 Meta Heuristic Algorithms

Meta heuristics algorithms are based on biological or physical phenomena mainly used in combinatorial optimization.

4.4.4.1 Mixed Integer Distributed Ant Colony Optimization (MIDACO) [37, 38]

Introduction

MIDACO algorithm included in this study is a copyrighted algorithm, distributed freely only for academic purposes. It is a GO algorithm for black-box MINLP problems based on the ant colony optimization metaheuristic for continuous search domains proposed by Socha and Dorigo(2008).

In real life, ants start to explore are around their nests randomly in search for food. Once an ant manages to locate a food source it returns to the nest laying pheromones upon its path, that after a while begin to evaporate. These pheromones attract more ants that follow down this path. The closer the source to the nest the more pheromones in the path.

MIDACO replaces the pheromone table, conventionally used in ant colony algorithms, with a probability density function (PDF), with the Gaussian function acting most commonly as a PDF. The PDF used in MIDACO is a weighted sum of several one-dimensional Gaussian functions for every dimension of the original search space.

Iterative description

The algorithm starts from a single-member Population, a starting point which is considered the initial nest. Based on the amount of ants specified by the user an equal amount of new points is created. Estimations (ants) are randomly made around the nest regarding the pheromones at the current time. The estimations are evaluated by the objective function and the information provided is stored in a solution archive. Once all ants have been constructed, the pheromones are updated and the algorithm proceeds in running the local solver MISQP. If no termination criteria is met then a new generation of ants is created anew and the algorithm starts another iteration.

Flow Diagram

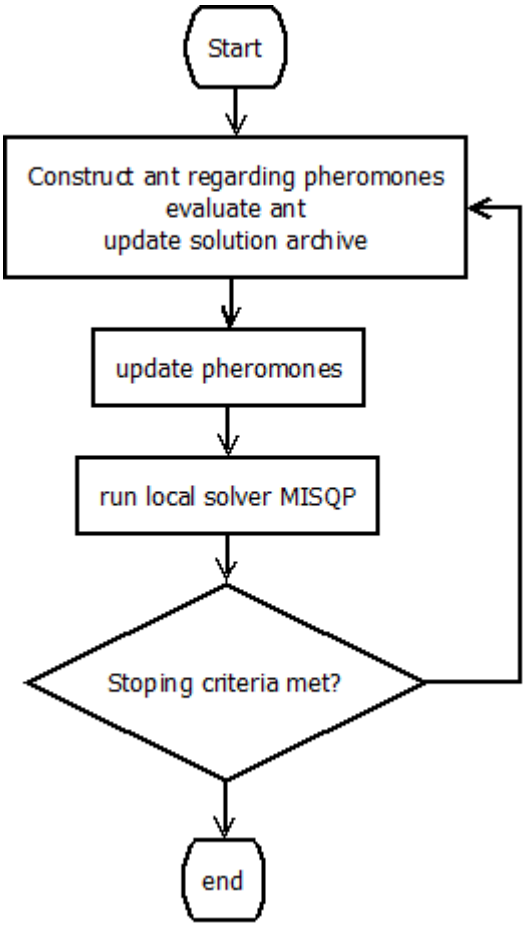

Figure 4-18 MIDACO flow diagram

4.4.4.2 Particle Swarm Optimization (PSO) [41]

Introduction

PSO is based upon a general belief that social sharing of information among the individuals of a populations, may provide an evolutionary advantage. A simulator of social behavior used to visualize the movement of bird's flock is PSO's precursor. Each individual has *adaptable velocity* according to which it moves in the search space and *memory* if its best position visited.

Iterative description

At the start of the algorithm, and if not provided, a random initial population P is created. The members of the P are evaluated by the objective function and the best member of the population is identified. A velocity is assigned to each member according to the member's best previous position and the best position in the P so far regardless of iteration. Then the members are moved according to the calculated velocity, while making certain that no constrains are violated, and the new positions are evaluated once more. If any termination criteria is met the algorithm halts otherwise a new iteration begins anew by calculating each members new velocity.

Flow diagram

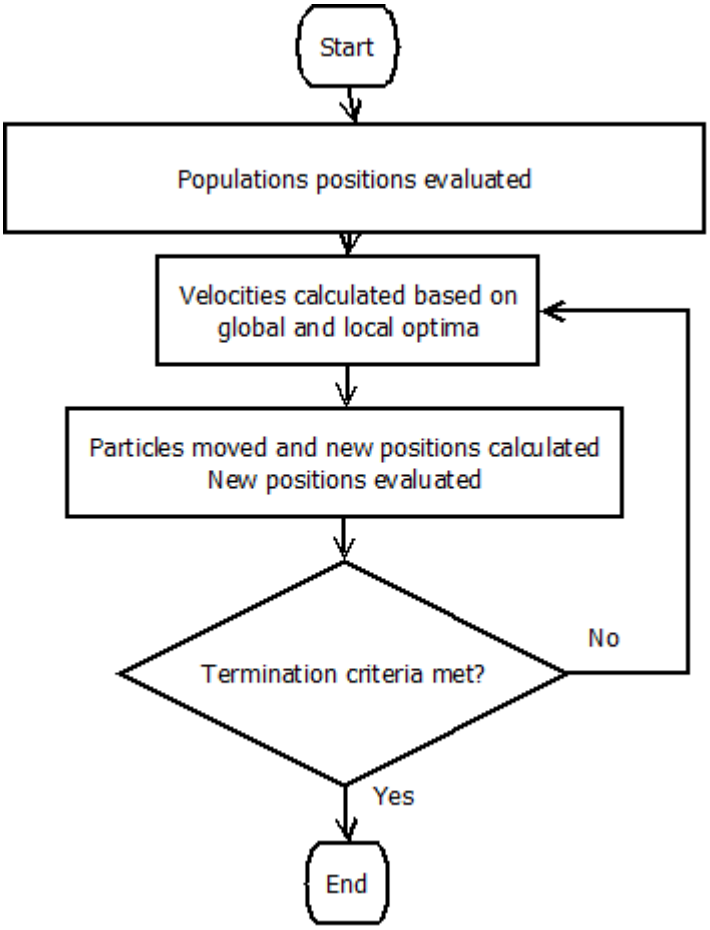

Figure 4-19 PSO flow diagram

5 Statistical Analysis

Before beginning statistically comparing the 9 algorithms mentioned in Chapter 4, a certain rules of fairness were set. Firstly, all trials for each algorithm would run in the same computational environment. For that reason an i7 8-thread CPU running at 2.66GHz per core was used with 8GB RAM memory under Matlab 2012a environment.

Moreover in order to achieve consistency over the statistical analysis of the 9 algorithms used, a set of common parameters in all of the algorithms was provided, as much as a common mechanism behind the assignment of values to those parameters.

5.1 Common termination criteria

Each algorithm would come to a halt once at least one of three criteria was met. These criteria were:

1. If fitting of the curve was achieved. A curve is considered to be fitted if the Euclidian distance of the experimental data from the mathematically produced data was at maximum 0.001cm.
2. If the appointed maximum running time was reached or exceeded. The running time concerns one trial of a given algorithm for each experiment.
3. If the population of the algorithm degenerates that much that the mean distance of the members from the geometrical mean of the population falls under a user provided threshold.

5.2 Common set of parameters provided to the algorithm

- bu, upper bounds of the variable parameters of the mathematical bio-model that produces an estimated solution
- bl, lower bounds of the variable parameters of the mathematical bio-model that produces an estimated solution
- max time, maximum time limit that each algorithm is allowed to spend searching for the global optimum for one run of the algorithm
- Pop, initial sample multiple/single estimation via which the algorithm can start computing its iterations. The sample size (single or multiple) depends on the mechanics of each algorithm, as same require a single point in the search domain via which to expand , where others require a multiple sample to evolve and inquire. Moreover the size of the sample is analogous to the number of parameters we seek to converge (reduced sample for half-set, increased sample for full-set)
- peps, an algorithm terminating parameter that determines the lower threshold under which the mean of all dimensions of the problem normalized mean absolute deviation of the estimated population of solutions in each algorithm is considered to have degenerated. Meaning that if the solutions tend to gather in a small area around a certain solution then it is better to terminate the algorithm earlier. Basically this algorithm parameter acts as a primal detection of local optima entrapment of the algorithm.

- VTR, it is the rough estimation of the global minima of our function that informs the algorithms that any solution produced lower than the value 'VTR' can consider as successful global minima identification.

5.3 Unique per algorithm search parameters

Each algorithm has a set of parameters that define its individual functional and structural mechanics. These parameters depending on the algorithm are directly involved with the searching procedure. It is of great importance these parameters to be assigned with optimal values, as the fine tuning of these parameters directly affect the performance of the algorithms. Again for the sake of statistical consistency these parameters are assigned common values for all experiments.

5.3.1 CRS

Unique user supplied parameters of the CRS algorithm version used are:

- the limit value δ for the reset of probabilities q_i to initial values, in order to reset the probability of choosing tendency of a heuristic
- the weight $w_0 > 0$ that satisfies the equation $q_i = \frac{W_i + w_o}{\sum_{j=1}^{h}(W_j + w_o)}$, where W_i is the sum of w_i in previous search and h is the number of heuristics used (in our case 4)

In [27] the initial values of the algorithm parameters are recommended having as default for non-linear regression problems $w_0 = 0.5$ and δ=0.04.

Thus, in our experiments we used $w_0 = 0.5$ and δ=0.1. We used higher reset probability of choosing tendency of the heuristics due to the high unsuccessful searches rate in an attempt to rebalance the search strategies faster, since the probability of the heuristics lessens with high rate.

5.3.2 SCE

Unique user supplied parameters of the SCE algorithm version used are:

- ngs, the number of complexes used in the search
- and a, the number of generations for each complex before the communities are forced to mix and shuffled

Through statistical experimentation and trials of the algorithm over a certain set of curves for various combinations of the two algorithm parameters we have concluded that for our specific inverse problem the recommended values are a=2 and ngs=4 or ngs=8, according with the biological parameters of the model, that we wish to estimate.

5.3.3 DE

Unique user supplied parameters of the DE algorithm version used are:

- I_bnd_const, flag for existing boundary constrains
  - 1: bounds as bound constrains
  - 0: no bound constrains
- I_strategy, choice of DE strategy/version to be followed
  - 1 → DE/rand/1
  - 2 → DE/local-to-best/1
  - 3 → DE/best/1 with jitter
  - 4 → DE/rand/1 with per-vector-dither
  - 5 → DE/rand/1 with per-generation-dither
  - 6 → DE/rand/1 either-or-algorithm
- F_weight, mutation scale factor from interval [0, 2] (referenced as F in literature)
- F_CR, crossover probability constant from interval [0, 1]. (referenced as CR in literature)

I_bnd_const is determined as 1 due to the inverse problem specifications. The DE version used in our experiments provides the choice of 6 different versions of DE through the I_strategy parameter to which we have assigned the value 1 for the classical approach of DE.

As described in literature the F_weight parameter, which provides the mutation scale factor for the DE, is agreed that it is should be optimally chosen from the [0.4, 1] interval as other values are only occasionally effective. It is also noted that the higher the value of F_weight the more premature convergence of the population and its degeneration. As far as F_CR is concerned, it is stated that the higher the value the faster the convergence to the global optimum value inquired, with 0.1 a good first choice followed by 0.9 and 1 with fast convergence when the solution is dependent from the mathematical model parameters.

As is suggested in [42], the values of F_weight and F_CR that correspond to our inverse problem are within the interval F_weight = [0.9, 1] and F_CR = [0.7, 0.9].

Through some practical experimentation following the pattern of SCE experimentations, it was concluded that suitable values for F_weight and F_CR are 1 and 0.8 respectively.

5.3.4 PSO

Unique user supplied parameters of the PSO algorithm version used are:

- cognitive_ACC, a positive constant called cognitive parameter
- social_ACC, a positive constant called social parameter

that satisfy the equations:

$$u_{id}^{n+1} = \chi\left(w * u_{id}^{n} + c_1 * r_1^n * (p_{id}^n - x_{id}^n) + c_2 * r_2^n * \left(p_{gd}^n - x_{id}^n\right)\right)$$

$$x_{id}^{n+1} = x_{id}^{n} + u_{id}^{n+1}$$

where w is the inertia weight;c1,c2 are the cognitive and social parameter respectively and χ is a constriction factor of the velocity.

As claimed in [41] these parameters are not critical but may result in faster convergence and avoidance of local minima entrapment of the algorithm. In [3] the suggestions are vague as it is proposed as default values 2 for both parameters but it is also argued that through experimental results the value 0.5 is indicated, ending with the conclusion that larger cognitive parameter than a social parameter is better, though their sum should be equal or lower than 4 as a constrain. In latter studies [44], is suggested as preferable values 2.8 for the cognitive and 1.3 for the social parameter and thus we utilize these values for our research.

5.3.5 SIMPSA

Unique user supplied parameters of the Simplex-SA algorithm version used are:

- Cool_rate, the rate with which the initial temperature will be reduced
- Min_cooling_factor, parameter that defines the minimum reduction of temperature
- Initial_acceptance_ratio, ratio of number of accepted estimations at a given algorithm iteration to number of total estimations at a given algorithm iteration.

As far as cool_rate is concerned [36], it is argued that values lower than 1 produce slow convergence whereas larger values than 1 produce convergence to poor local optima, stating that for unconstrained function, such as ours, value 10 was used and produced satisfactory results. In [45] is stated that the typical values of min_cooling_factor lie in the interval [0.8, 0.99]. Moreover, the initial_acceptance_ratio is suggested [36] that it should be such that maintains the ratio of accepted estimations to rejected estimations equal or close to 1.

Given such information from the literature and with empirical, statistical experimentation while observing the way in which these values affect the algorithm we resulted at using as values 0.9 for min_cooling_factor, 0.95 for initial_acceptance_ratio and 10 for cool_rate.

5.3.6 tdASA

Unique user supplied parameters of the thermo-dynamic-ASA algorithm version used are:

- ❖ c, the cooling rate with which the algorithm "temperature" is reduced in every iteration with values within the interval (0, 1).

After statistical experimentation for a value in which speed and convergence quality could be combined, we resulted in assigning the value 0.5 in the parameter c. Due to the simplicity of the Matlab script of the algorithm c value greatly affects the speed and the quality of the algorithm convergence. Thus further investigation would be extremely valuable not only in the value assigned in parameter 'c' but to the mechanics behind the reduction of the temperature in every algorithm iteration so as to increase the algorithms robustness and tolerance over the 'c' value.

5.3.7 gblSolve

Unique user supplied parameters of the DIRECT algorithm version used (gblSolve version) are:

- epsilon, is a global/local weight parameter.

As noted in [25] and by the authors of the gblSolve Matlab script utilized in our experiments [24] the suggested epsilon value is 10^{-4}, which is supplied as the default value in the case of absence of user defined value.

5.3.8 MIDACO

Unique user supplied parameters of the MIDACO algorithm version used are:

- SEED, initial seed for internal pseudo random number generator,
- QSTART, parameter that allows the user to specify the quality of the initial estimation,
- AUTOSTOP, parameter that activates an internal stopping criteria of the algorithm,
- ORACLE, parameter used by the penalty function of the algorithm,
- ANTS, amount of estimations within a single algorithm iteration,
- KERNEL, amount of best estimations in a given iteration to be saved in a solution estimations archive within the algorithm,
- CHARACTER, activation option for specific set of MIDACO internal parameters specially tuned according to problems at hand, based on the problem dimensions n and n_{int} , where n is the number of optimization variables in total and n_{int} is the number of integer optimization variables:
    - 1→ problem is an Integer Problem (IP) ($n_{int} = n$)
    - 2→problem is an Non Linear Problem (NLP) ($n_{int} = 0$)
    - 3→problem is an Mixed Integer Non Linear Problem (MINLP)

From the literature [37][38][39][40], we concluded in the following values for these parameters:

SEED=0, QSTART=0, AUTOSTOP=10, ORACLE=0, ANTS=136, KERNEL=12, CHARACTER=3.

SEED is the initial seed for internal pseudo random number generator within the MIDACO algorithm. All algorithms tested have the default settings for Matlab random number generator which is the Mersenne Twister with seed=0 and as such we assign the SEED parameter the value 0.

QSTART parameter attributes the quality of the algorithm starting estimation. The higher the value the better quality of the starting estimation and the closer to that ewstimated solution the algorithm searches for the global optima. Our statistical analysis is using random initial estimations for each algorithm, thus we assigned the QSTART parameter with value 0, which equals with absence of quality evaluation of the starting point.

AUTOSTOP parameter is basically a weight that the higher its value the more the priority of the algorithm from convergence quality is shifted to computational speed, by internally stopping the MIDACO algorithm after “AUTOSTOP” consecutive unsuccessful improvements towards the local optima. As given in [12] values within the interval [1,49] are consider fast but with a low chance of global optimality. Knowingly of this disadvantage due to the algorithm specifications and after some experimentation with the value we chose to assign the value 10 to the parameter in order to make MIDACO a competitive algorithm compared to the rest used, speedwise.

ORACLE is a parameter used to the penalty function within MIDACO relevant only with constrained problems and thus we assigned the value 0.

ANTS and KERNEL must be used combined, and are intended to make MIDACO more efficient on specific problems, assigning the number of estimations done by the algorithm per iteration and the number of optimal estimations at a given iteration respectively. After little statistical experimentation and for the sake of the algorithms speed competitiveness with the rest set of algorithms we concluded in the use of values of 136 and 12 respectively, though further investigation on the MIDACO algorithm parameter fine-tuning should be valuable.

CHARACTER is de facto assigned the value of 3 as our problem consist a MINLP problem.

5.3.9 SRES

Unique user supplied parameters of the SRES algorithm version used are:

- lamda, is the number of offspring generated in every generation with value within the interval [100,200]
- mu, number of parents with ratio of mu/lamda→1:7,
- pf, is the pressure of fitness with values within the interval [0,0.5]
- varphi, expected rate of convergence
- G, maximum number of generations
- Mm, parameter stating the optima in search
    - ‘min’ for minimization of the fitness function
    - ‘max’ for maximization of the fitness function

Taking into consideration the successful use of a certain parameter set of SRES algorithm in [22] plus the author’s comments of the free licensed Matlab script of the SRES algorithm and after a sampled statistical experimental testing, we attributed the values of lamda=150, mu=20,pf=0.45, varphi=1 and G=500 though as in MIDACO further investigation on the SRES algorithm parameter fine-tuning should be valuable. It is notable to say that in [13] was observed the higher the varphi and the pf values the better the convergence towards a global optima. Finally, mm parameter is de facto assigned the value ‘min’ according to optimizing function, which we are investigating for global minima.

Table 3 Algorithmical Unique Parameters

Algorithm					
CRS	$w_0 = 0.5$	*δ=0.1*			
SCE	*ngs = (dimension of problem) = 4 or 8*	*a = 2*			
DE	*I_bnd_const =1*	*I_strategy = 1*	*F_weight = 1*	*F_CR =0.8*	
PSO	*cognitive_ACC =2.8*	*social_ACC =1.3*			
gblSolve	*epsilon =* 10^{-4}				
SIMPSA	*COOL_RATE =10*	*min_cooling_factor = 0.9*	*initial_acceptance_ratio =0.95*		
tdASA	*C = 0.5*				
SRES	*lamda =150*	*mu =20*	*pf =0.45*	*varphi =1*	*G =500*
MIDACO	*SEED = 0*	*QSTART = 0*	*AUTOSTOP = 10*	*ORACLE = 0*	*ANTS = 136*
	KERNEL = 12	*CHARACTER = 3*			

5.4 Test Bench

The experimental data obtained by DCE-OI defined the output space the mathematical model needs to be able to cover. An instance of this space created by the experimental data is shown in Figure 5.1

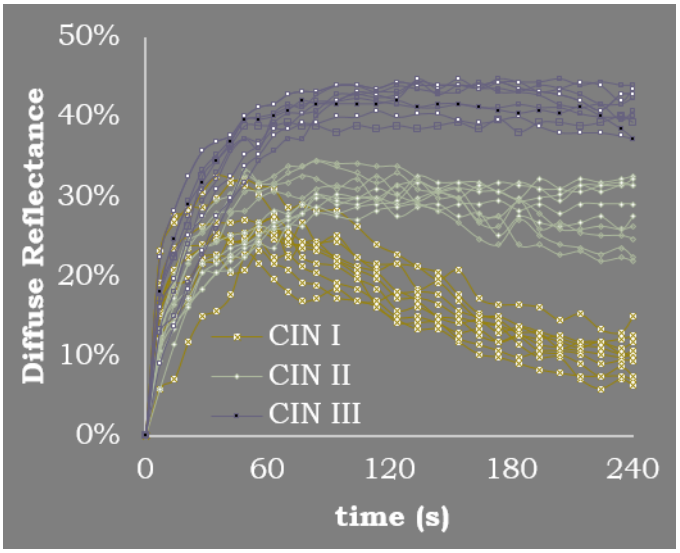

Figure 5-20 Experimental Data

A test bench needed to be established by which all algorithms could be tried out under common restrictions and inputs In order to be certain that the analysis performed would cover the entire feasible output space. With that purpose thirty test problems ie a set of thirty pseudo-experimental (PE) curves, for both the full set of eight and the half set of four parameters, were created by the means of the following procedure:

❖ Ten curves per set were created by manual selection from confirmed experimental data of different CIN stages:

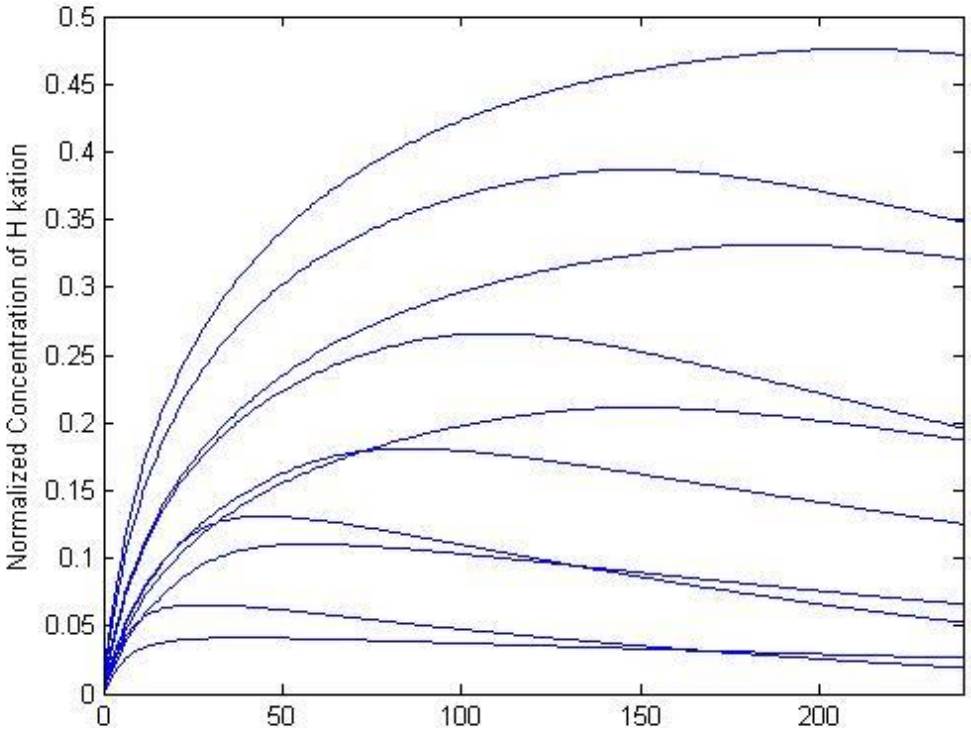

Figure 5-21 Ten manually selected PE for half set

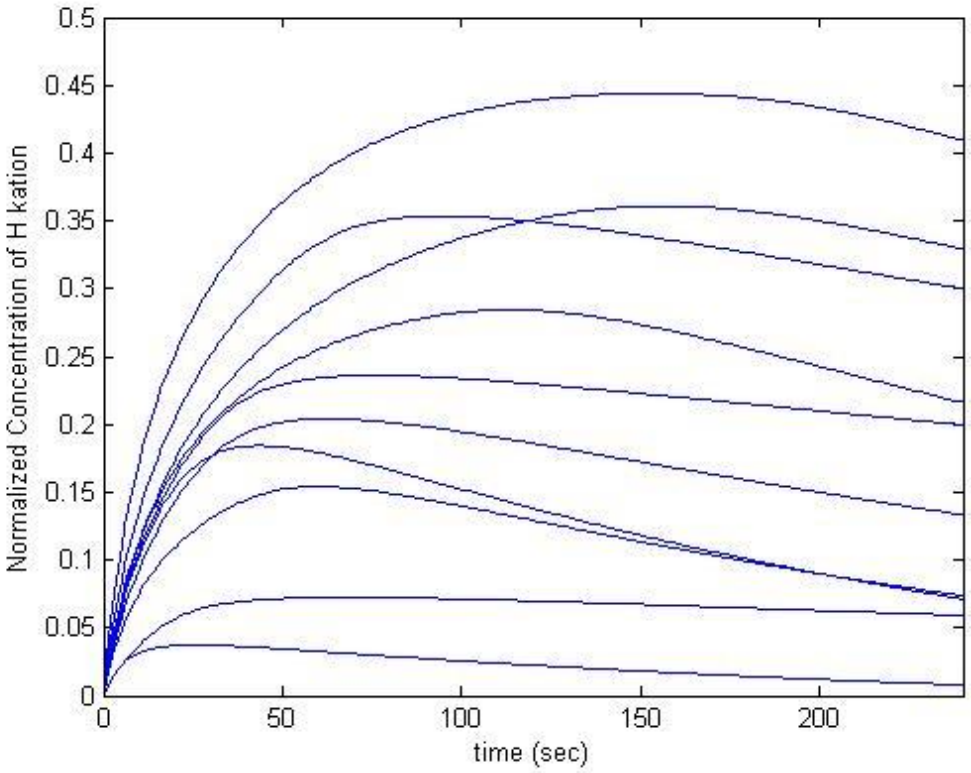

Figure 5-22 Ten manually selected PE for full set

❖ Ten curves were chosen by dividing the feasible search domain of each parameter into ten subintervals of equal length and then systematically, step-wise, sampling from the lower to the higher values

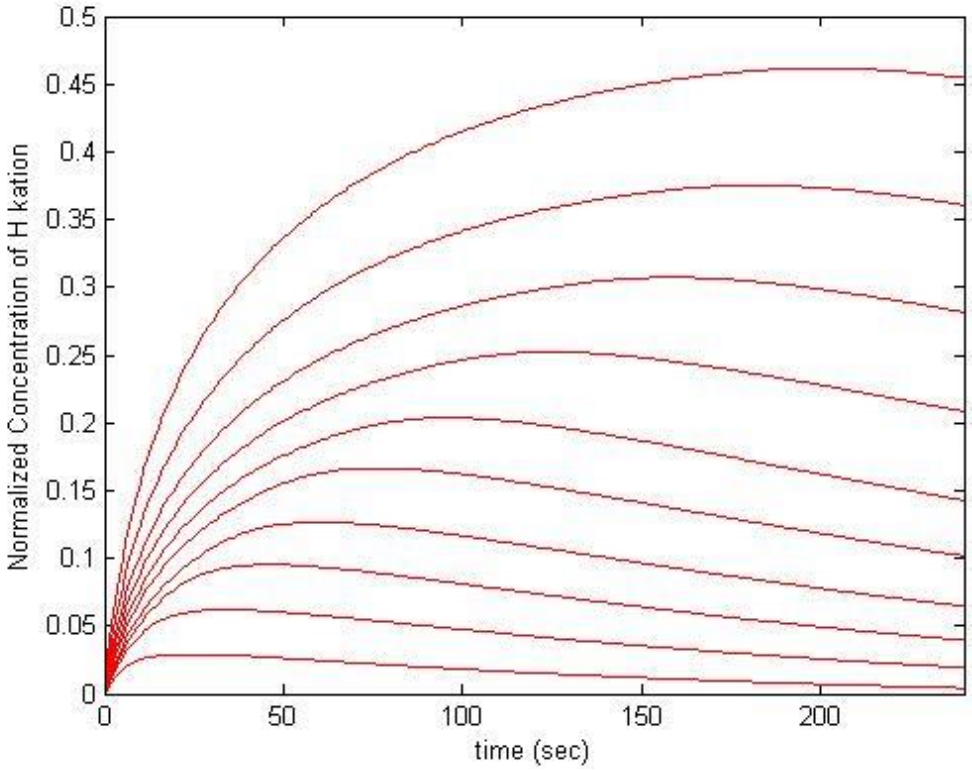

Figure 5-23 Ten systematically sampled PE for half set

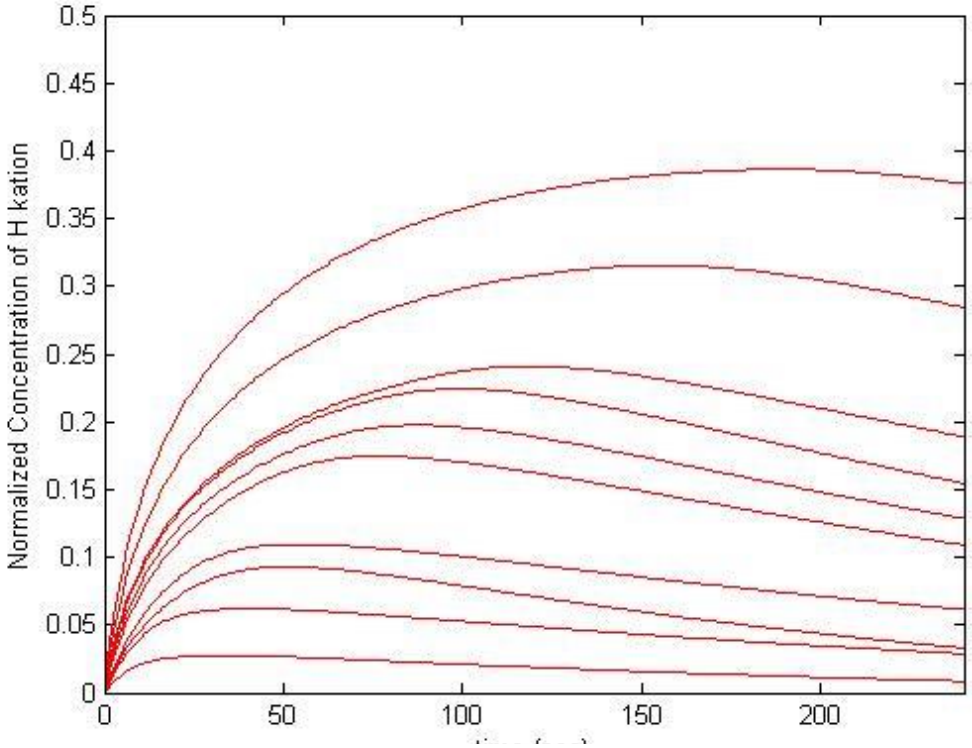

Figure 24-5 Ten systematically sampled PE for half set

❖ Ten randomly selected PE

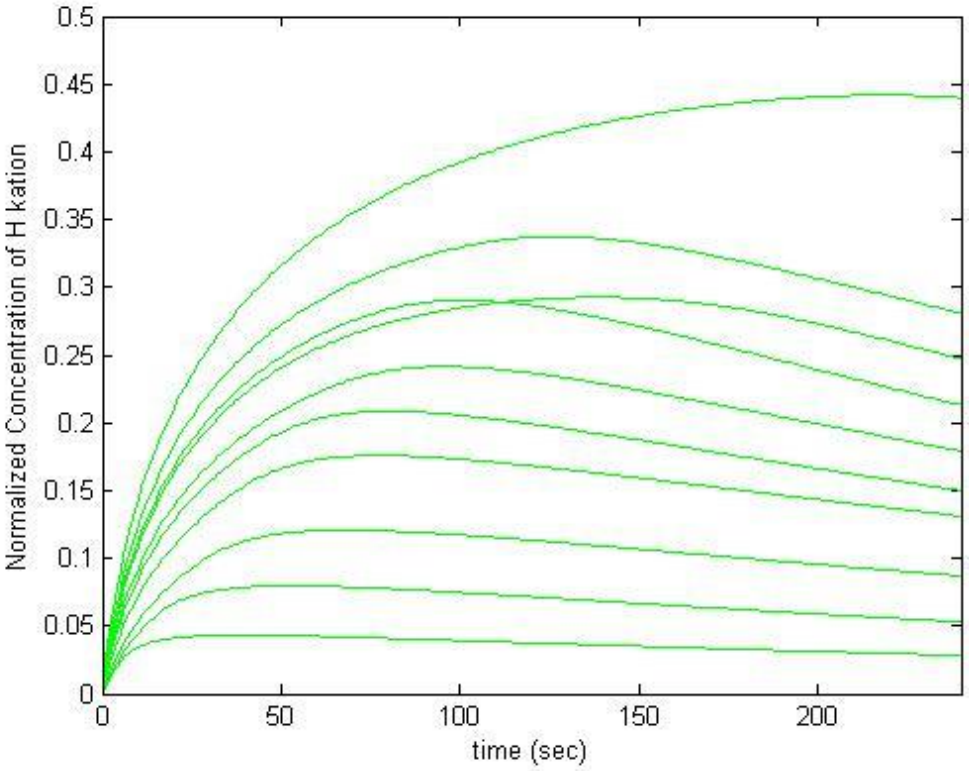

Figure 5-25 Ten randomly selected PE for half set

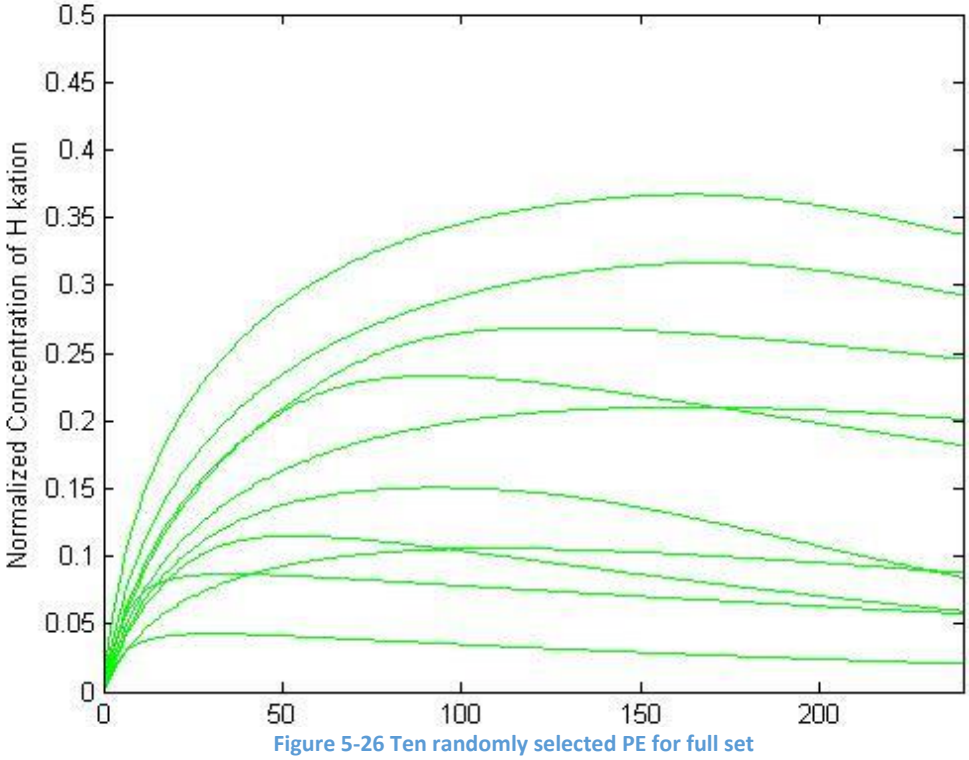

Figure 5-26 Ten randomly selected PE for full set

Thus for each parameter set we have the above test bench of 30 test problems.

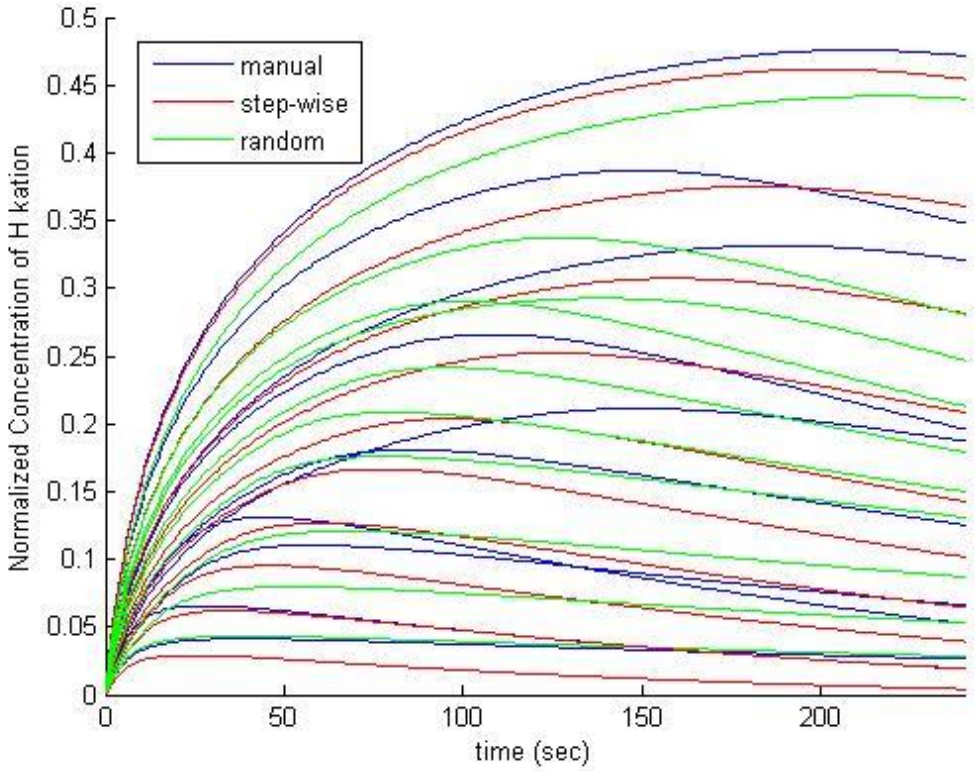

Figure 5-8 Test bench of half set

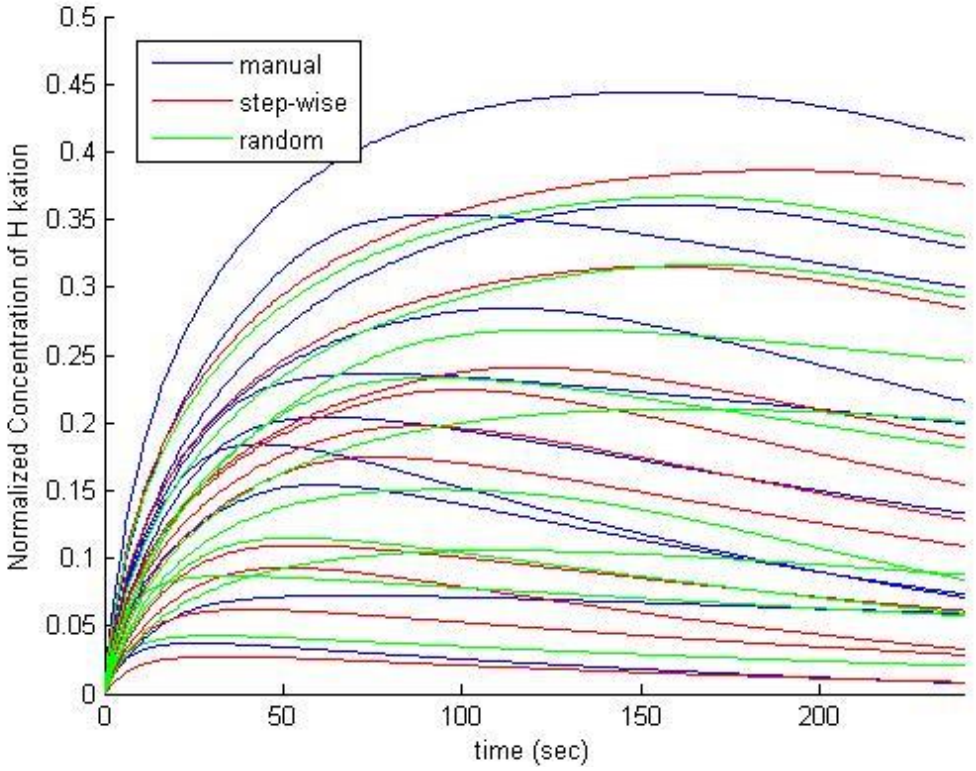

Figure 5-9 Test bench of full set

5.5 Global Optimization Comparison Software

Each PE curve was fitted 30 times with the nine global optimization algorithms described in Chapter 4. Meaning 30x30x9=8100 runs in total were performed. With the purpose of those runs being efficiently conducted a global optimization algorithm comparison software was developed in order for consecutive algorithmic trials to be automatically run the experiments. Moreover, through the software collection of the raw data was automatic, and in some cases parallel, allowing instant processing of the results and immediate production of statistical figures and histograms.

Inputs

This software is initialized by a simple menu in the beginning and then runs automatically until all outputs are produced. The user first is prompted to choose for which of the subsets the experimentations will run, thus is able to activate the proper test bench. Then the desired runs per algorithm are defined (ie 30). Then a choice is made of which of the biomodel scripts to run (matlab, reference table, fortran). The differences of these scripts and how they affect the process is described in Chapter 5.7. Once all these choices are made, the algorithms that will participate in the comparison are chosen. The termination criteria, as well as the rest of the parameters, are initialized by default, regardless whether they are unique or common per algorithm.

It needs to be noted that at the current version of the software the CPU cores to be used, the objective function in the form of a Matlab script, as well as the PE data and the known solution of these data, need to be manually provided by the user within the script.

Outputs

As outputs, the software provides a visual representation of all the trials for each algorithm and for each PE in the form of a JPEG file. Moreover, the raw data collected during the experiments are processed and for each PE a set of figures of fitting and parameter convergence versus time of all algorithms is produced. More specifically, for each PE 5 JPEG files for the half set and 9 for the full set are produced, each visualizing in a single figure for all algorithms the curve fitting through time or the parameter convergence through time. Thus the ability to asses better the speed of each algorithm is provided. Moreover the data are statistically processed by calculating a certain set of metrics which are used to create statistic histograms, barplots and boxplots for visual representation of the results. Finally an MS EXCEL file is produced containg for each PE the results of each trial for all algorithms as well as the metrics given by the trials.

5.6 Metrics

For each of the 30 PE curves a series of metrics are calculated. The most noticeable of which are:

- The relative error (*err*), a metric that gives an indication of how good a measurement is relative to the size of the thing that is being measured. It is calculated by the relation:

$$\text{relative error} = \frac{\text{absolute error}}{\text{value of the thing measured}} \qquad (5.1)$$

where

$$\text{absoluter error} = |\text{estimation of value} - \text{real value}| \qquad (5.2)$$

- The standard deviation(σ_p) of the estimated values of the parameters, shows how much variation or dispersion from the average exists.
- The coefficient of variation (*CoV*), is a normalized measure of dispersion of a probability distribution or frequency distribution. It is also known as unitized risk or relative standard deviation (RSD).
- The NRMSD of the parameters is calculated, separately for each of the 8 algorithms

$$\text{NRMSD}(\mathrm{p})_{\mathrm{k}}^{\mathrm{PE}} = \frac{\text{RMSD}(\mathrm{p})_{\mathrm{k}}^{\mathrm{PE}}}{\mathrm{p_{max}} - \mathrm{p_{min}}} = \frac{\sqrt{\sum_{\mathrm{i=1}}^{\mathrm{so}} \left(\mathrm{p_{i,k}^{PE}} - \hat{\mathrm{p}}_{\mathrm{k}}^{\mathrm{PE}}\right)}}{30(\mathrm{p_{max}} - \mathrm{p_{min}})} \qquad (5.3)$$

where *k* is the identification number of the algorithm (k=1,…,9), *i* the simulation, *p* and $\hat{\mathrm{p}}$ are the estimated and expected parameter values respectively and $\mathrm{p_{max}}$, $\mathrm{p_{min}}$ denote the maximum and minimum parameter values.

5.7 Time complexity

The mathematical model simulating the AW phenomena needs to calculate from 4 up to 40 differential equations. This large differential system was proactively proven time consuming even for the CPU used. More specifically, the mathematical model in matlab script takes approximately 0.9sec to produce a solution for the full set and 0.6sec for the half set. This time consumption is of extreme importance, if it is considered the fact that every algorithm needs to solve the differential equation at from once per iteration to the size of the entire population per iteration. For that reason each trial for each algorithm needed maximum 2 hours for the full set and 1.5 hours for the half set. For the purpose the algorithms are compared that time is not applicable. The results of this comparison were presented in [45].

In an attempt to reduce time complexity a reference table was made as a minor database of estimation points. More specifically, by systematically, step-wise, sampling from the lower to the higher values of all parameters and each sample given as input to the model, a reference table of PE with known parameters was made. Due to the time complexity of creation of the reference table, this solution was applied at first only for the half set before a better solution was found. Each parameter was sampled with the following steps

- Parameter N: as it is discrete all values from 1 to 10 were used
- Parameter b: $0.08 * 10^{-7}$
- Parameter pH_{ES}: 0.02
- Parameter ε: 0.3

This solution provided a 3000% speed increase (0.02 sec per model output) permitting trial runs for 15 minutes in both the half and the full set. The reference table was rejected as a solution due to the transformation of continuous values to discrete. This transformations led to untrustworthy results despite the time complexity reduction.

The second solution that was actually applied was the download of the script of the biomodel from Matlab (a high level programming language) to Fortran (a low level programming language). Fortran is a low level programming language similar to C that is often used for problems of mathematics and physics. More specifically the version of Fortran 90 was used with a free distribution of DLSODE differential equation solver scripted in Fortran 77.

This led to the creation of a even faster biomodel identical to the Matlab scripted that offered approximately 6666% speed increase, producing an output in just 0.009sec on average, while no transformations of the output space needed to be made thus maintaining the reliability the deterministic biomodel offers. By implementing this solution, each algorithm needed just 2.5 minutes per trial.

5.8 Algorithmic Accuracy, Precision and Hypothesis Testing

Accuracy

In numerical analysis, accuracy is the nearness of a calculation to the true value and precision is the resolution of the representation. Before statistically comparing the algorithms, a metric of accuracy needed to be established as a measurement of the performance for each algorithm. The average NRMSD of the parameters was chosen as that metric. Accuracy for each PE fit for each algorithm, as the parameters do not influence equally the output of the model, is calculated as a weighted average of the NRMSDs of the estimated parameters:

$$Accuracy_k^{PE} = \sum_{i=1}^{n}\{w_i * NRMSD(p_i)_k^{PE}\} \qquad (5.4)$$

where i=1,…,n is the parameter identification number and w_i is the weight of each parameter. As w_i the mean first order sensitivity value of parameter i can be used. The first order sensitivity value was utilized because it quantitatively depicts which is the amount of output variance that is attributed to each individual parameter. In this study, the value assigned to the weight was 1, having all parameters equally affect the performance of the algorithm. As this is the first application of global optimization algorithms on this specific problem with the purpose of fitting the experimental data and identifying the set of the parameters, we are equally interested in the error of estimation of all parameters. Moreover, these parameters consist both structural and functional, biological parameters of the epithelium of the cervix, thus it is required accuracy on all of them.

According to the Central Limit Theorem the arithmetic mean of a sufficiently large number of individual samples of independent random variables, each with a well-defined expected value and well-defined variance, will approximately follow the normal distribution. Empirically, a sufficient number of these individuals is 30. Therefore, 30 attempts for fitting were made per PE and for each algorithm a new metric was produced, namely the mean accuracy.

Based on the initial assumption that the test bench of PEs created represents sufficiently most of the output space of the model, the mean accuracy of each algorithm was calculated as the mean of the accuracy of estimation for each PE for the specific algorithm.

$$\mu_k = \frac{1}{30}\sum_{PE=1}^{30} Accuracy_k^{PE} \qquad (5.5)$$

Precision and Hypothesis testing

What needs to be noted is that precision in the conventional meaning for the fields of science, engineering, industry and statistics, was not calculated in the study for three reasons. First of all precision in numerical analysis, of which global optimization is part, is used for the actual numerical precision of the results. Matlab and FORTRAN provide a high numerical precision with calculations of more than 10 decimals. The precision though of 2 decimals is biologically sufficient. Conventional meaning of precision is the degree to which, repeated measurements under the same constrains and conditions, produce the same results. Eight out of the nine algorithms used in this study are stochastic and one is deterministic. The deterministic has 100% precision, since for each run with identical constrains and conditions the same output is produced. Stochastic algorithms though, even if provided with the same inputs, will produce different outputs. An algorithmic precision interval would be useful and would prove the validation of the inverse problem solution system, but until convergence consistency and solution uniqueness are proven and the accuracy of the algorithms is good enough, there is no point in identifying that interval. Lastly but most importantly, precision, meaning a confidence interval, is not useful for the problem tacked. Each of the biological parameters needs to be calculated accurately. Knowing that a given estimation was made for example with 95% confidence within an interval does not provide actual confidence on the value assigned to the parameter by global optimization. On the other hand, making hypothesis testing we can determine the level of certainty of the results [46]. In this study, as aim accuracy is needed to be primarily examined and not the precision in the conventional meaning, since firstly an algorithm with sufficient accuracy needs to be identified before proceeding in such measurements.

6 Results

6.1 Aim of statistical analysis

For both the half set and the full set the procedure described in Chapter 5 involving the global optimization algorithms described in Chapter 4 with the purpose of

- Provision of an extensive comparison of global optimization algorithms capable of solving the inverse problem.
- Conclusion on whether the inverse problem converges.
- Comment of results on basis of the model reduction obtained by global sensitivity analysis.

As mentioned on Chapter 5, each algorithm was trialed for each of the 30 PE created 30 times, provided the same algorithmic unique inputs and the same termination criteria. The algorithmic common parameters were also equals, with the exception of the initial population Pops, which was computed independently and randomly for each trial of each PE and for each algorithm.

6.2 Numerical Results

It needs to be noted that all results presented in Table 4 and Table 5 are percentages. For full set the normalized accuracy per cent is:

Table 4 Full Set Numerical Results

	CRS	SCE	DE	PSO	gblSolve	SIMPSA	tdASA	SRES	MIDACO
Average J	0,004	0,016	0,010	0,014	0,022	0,017	0,025	0,014	0,012
Accuracy	18,94	20,99	24,73	30,46	23,22	29,92	27,23	25,74	31,05
N	6,13	8,88	8,40	20,31	11,48	17,10	9,92	9,85	12,58
B	20,25	19,49	26,69	31,45	18,08	29,32	25,06	26,84	30,17
pH_{ES}	9,87	13,23	13,80	25,27	15,54	20,15	16,80	15,09	20,85
$\varepsilon\,(g_{TJ})$	12,85	17,46	17,44	25,24	23,49	24,84	21,87	20,89	24,60
β_{IS}	26,29	24,43	34,23	33,78	22,09	34,22	33,02	33,64	40,83
pH_{IS}	19,95	25,80	27,17	33,34	30,28	34,77	35,18	28,16	35,84
β_{ES}	27,05	30,63	33,41	36,28	37,17	39,37	38,15	33,55	40,31
K_V	29,12	28,02	36,72	38,03	27,64	39,62	37,86	37,93	43,20

And for the half set:

Table 5 Full Set Numerical Results

	CRS	SCE	DE	PSO	gblSolve	SIMPSA	tdASA	SRES	MIDACO
Average J	0.0012	0.0050	0.0010	0.0052	0.0152	0.0295	0.0348	0.0113	0.0094
Accuracy	1,43	5,16	1,02	7,79	7,45	17,12	11,91	8,14	10,64
N	0,60	2,91	0,47	5,14	4,44	13,04	5,99	4,08	6,30
B	2,73	8,47	1,79	12,19	8,86	21,37	15,62	12,82	17,15
pH_{ES}	0,53	2,32	0,40	4,88	9,02	15,25	11,36	5,71	6,56
$\varepsilon(g_{TJ})$	1,85	6,92	1,42	8,95	7,49	18,82	14,69	9,97	12,53

These data, as a first output, allows us to observe numerically the fitting accuracy of the algorithms as well as the level of accuracy of the parameters estimation and the mean accuracy, which were defined in Chapter 5. We can identify CRS and DE as optimal algorithms for the full and the half set respectively, by the level of curve fitting accuracy, meaning they have the lowest values of *J*, as well as by the level of parameter estimation accuracy.

6.3 Results over time

For the half set we have these visualized results over time:

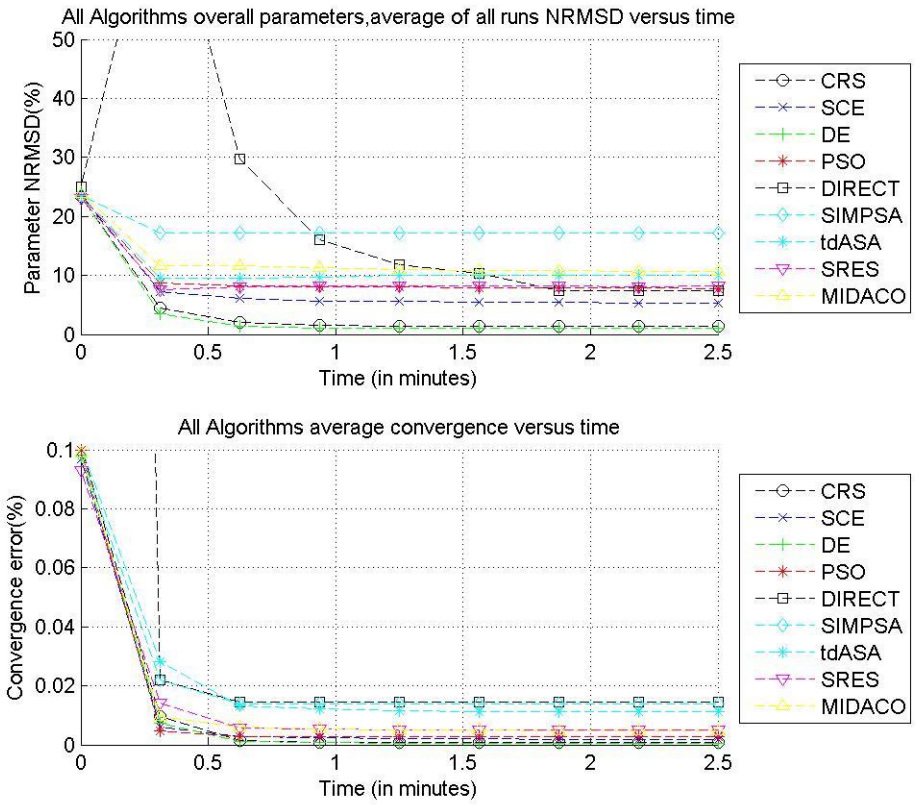

Figure 6-27 **The upper plot depicts parameters accuracy versus time for the half set The lower plot depicts curve fitting accuracy versus time for the half set**

For the full set we have these visualized results over time:

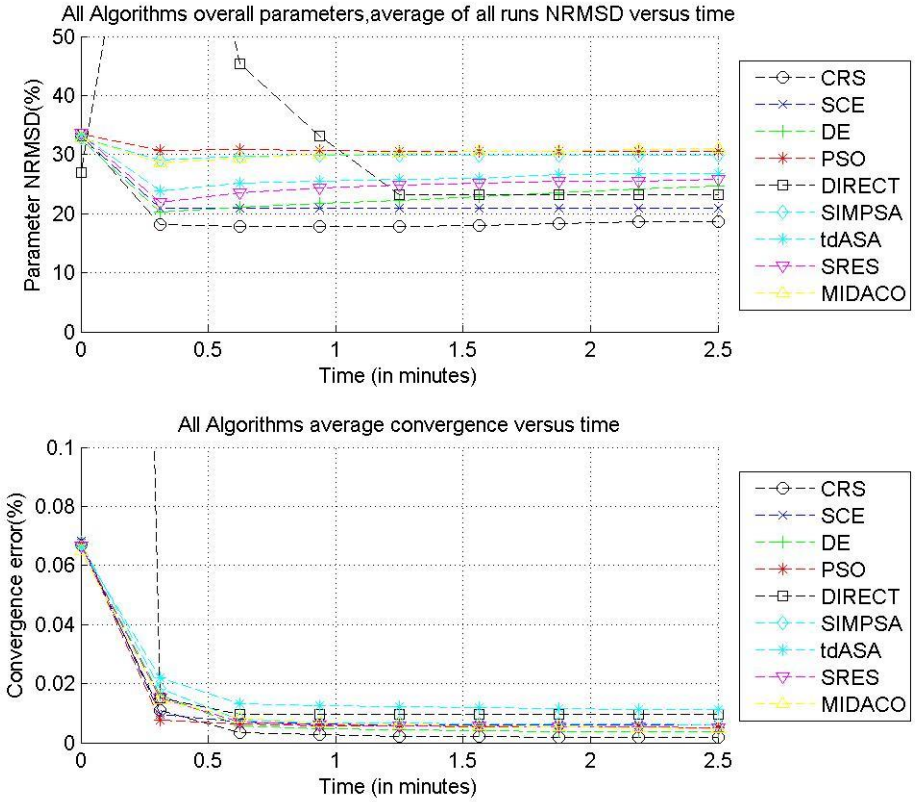

Figure 6-28 The upper plot depicts parameters accuracy versus time for the ful set
The lower plot depicts curve fitting accuracy versus time for the full set

Observing *Figure 6-1* and *Figure 6-2*, it is evident that fitting of the curves is accomplished relatively fast. A solution is produced in maximum 2.5 minutes on average. This means that after 2.5 minutes, if fitting criterion has not been met, it is more possible for the algorithm to have been entrapped in a local minimum than actually needing more time to locate the global minimum. It is also evident that, given equal time spans, when the parameter dimensionality is reduced from 8 dimensions to 4, the parameter estimation error is reduced by up to 20%. Thus a first estimation that global sensitivity analysis theoretic estimation of dimensionality reduction is beneficial for both time and accuracy of estimation of the parameters.

6.4 Histograms for algorithmic accuracy

For the half set we have the following results:

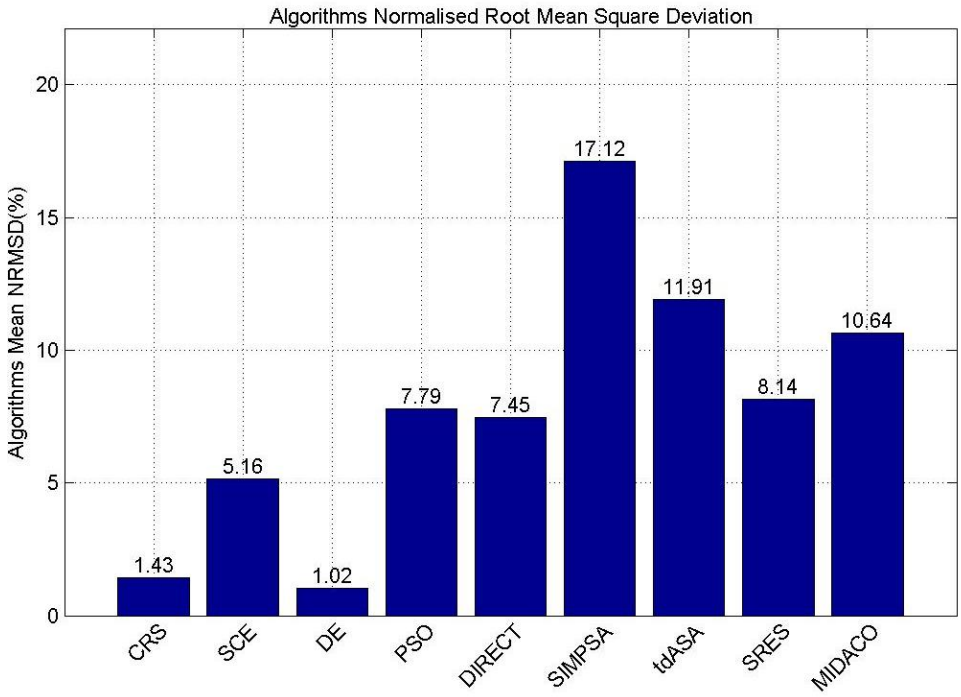

Figure 6-29 Histogram of Mean Accuracy of algorithms for half set

While for the full set we have the following results:

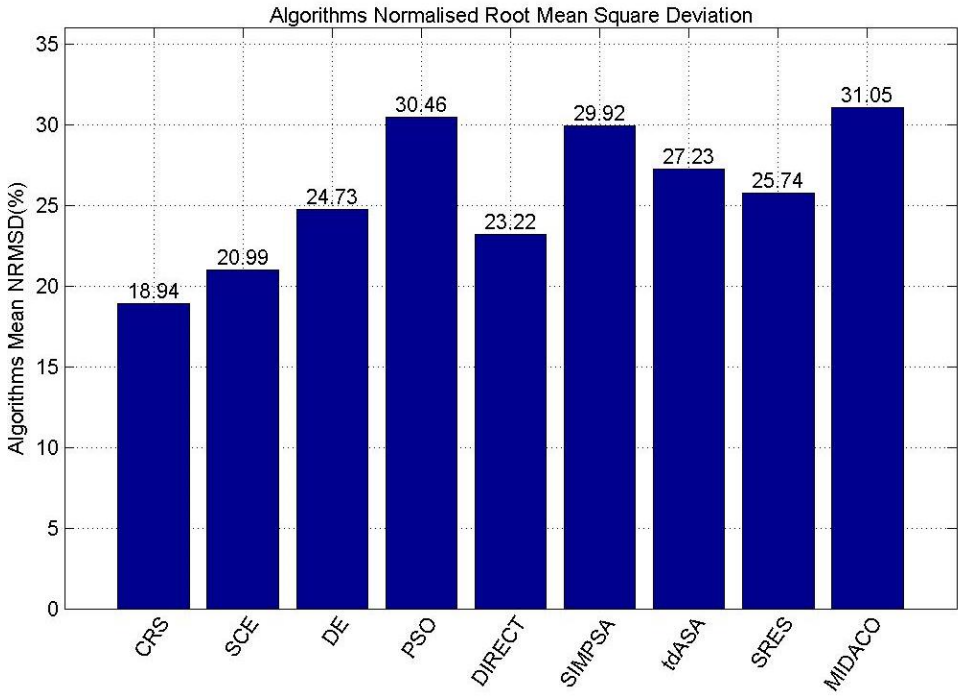

Figure 6-30 Histogram of Mean Accuracy of algorithms for full set

Observing these histograms, it is evident that the algorithms show different degrees of convergence with DE followed by CRS showing optimal performance for our inverse

problem. Although DE shows worse performance for the full set, in contrast with CRS it has the potential of reaching better accuracy given more time. Given that the full set has double the dimension, more time is needed for fitting to be done[6].

For the half set:

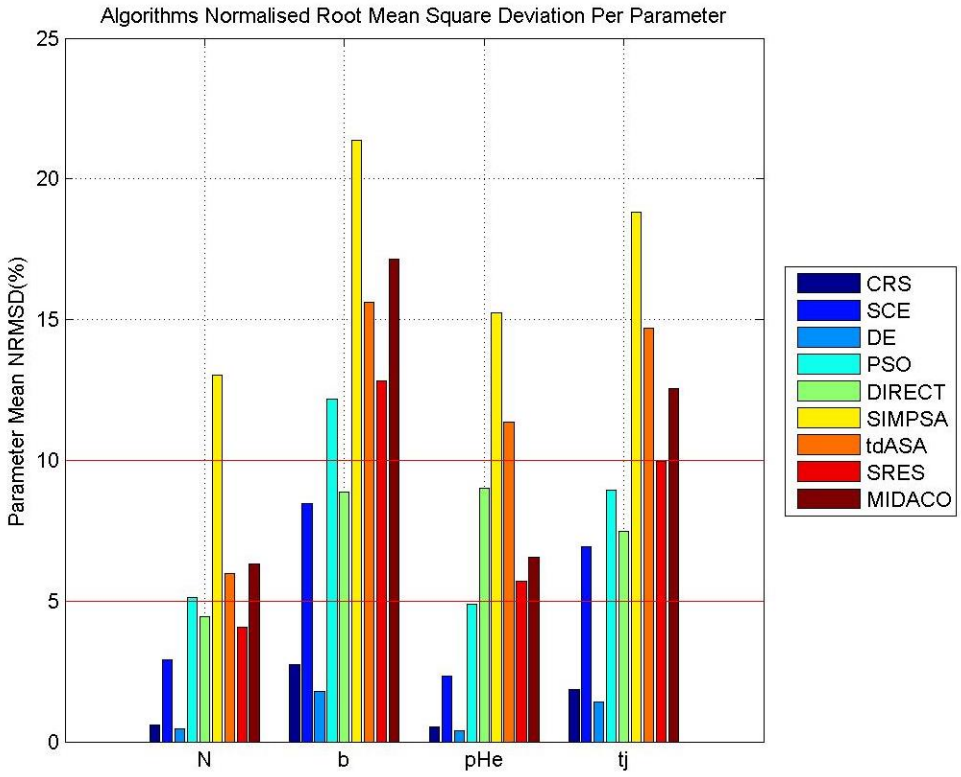

Figure 6-31 Histogram of Mean Accuracy per parameter of algorithms for half set

[6] That was experimentally confirmed with a quick unofficial trial of CRS and DE algorithms over the test bench for double the time over the full set, where CRS maintained its performance but DE showed up to 4% greater accuracy. The results are not officially included due to being run on a higher computational environment, thus losing equal footing for comparison

For the full set:

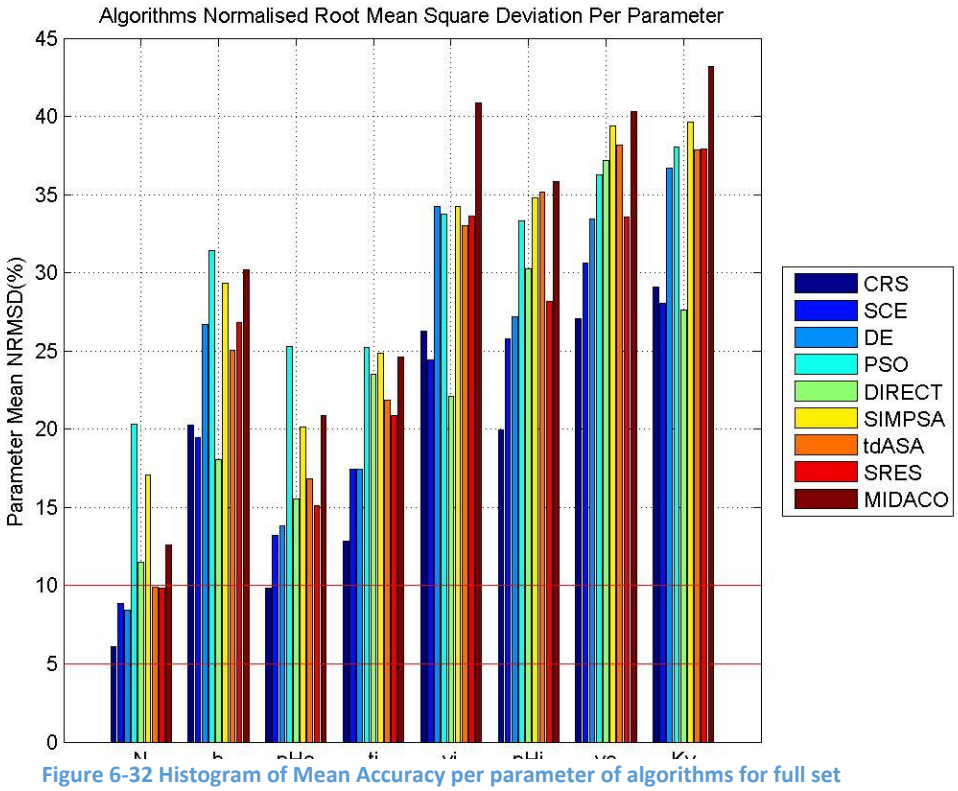

Figure 6-32 Histogram of Mean Accuracy per parameter of algorithms for full set (vi and ve are the β_{IS} and β_{ES} respectively. The difference between in names are due to missing Matlab libraries for processing Greek letters)

Observing the histograms of accuracy per parameter for each algorithm, it is evident that overall and at least when the half set is used, the problem converges adequately, since the majority of parameter estimation error are under 10% for the majority of the algorithms used in this study.

Moreover, the four parameters rejected by global sensitivity analysis (β_{IS}, pH_{IS}, β_{ES}, K_V) consistently fail to converge for all algorithms and inhibit the ability to achieve better accuracy for the parameters that consist the half set. This practically validates global sensitivity analysis theoretical estimation that the dimensionality reduction is beneficial.

6.5 Boxplots of NRMSD towards all Estimations

For the half set we have:

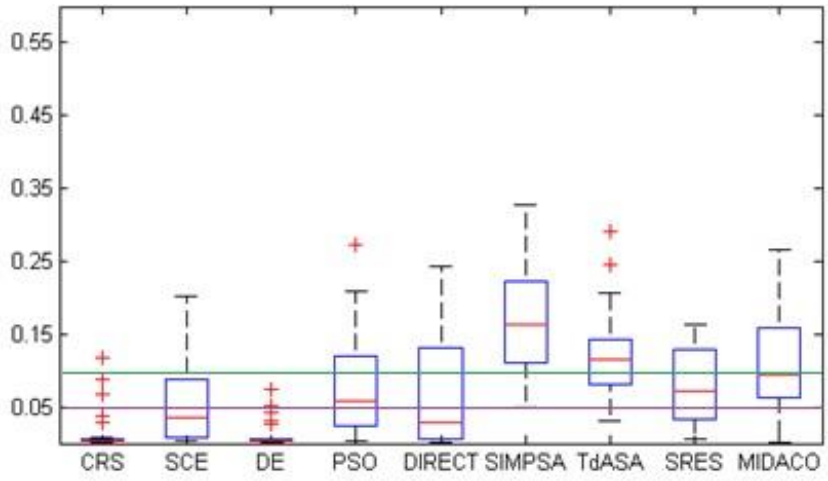

Figure 6-33 Boxplot of all estimations done by algorithms for the half set

while for the full set we have:

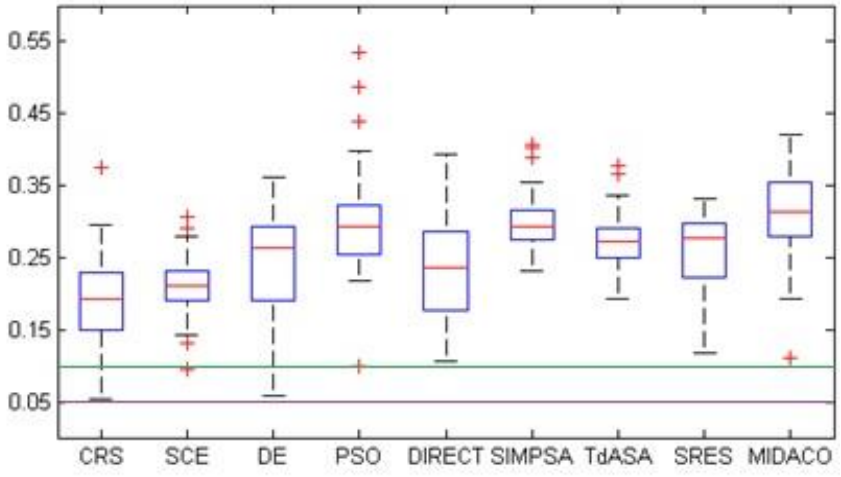

Figure 6-34 Boxplot of all estimations done by algorithms for the full set

In general, we can say that the problem converges if all of the 30 performances are under a certain threshold. (e.g. median<5 or 10%). In the boxplots the 5% threshold is depicted as a red while the 10% threshold as a green one. As shown in the boxplots, without making any assumptions for the distribution the estimations of the algorithms follow, it is evident that for the full set no such claim of convergence can be made. But as far as the half set is concerned it is evident that the median as well as most of the population of the algorithm for the majority of the algorithms converges, as the population lies under the 10% error threshold. More specifically for the half set and for the DE all of the estimations were made under that threshold, giving extra credits to the specific algorithm.

6.6 Inferring the optimal algorithm

First of all, by considering that the chosen PE curves *represent sufficiently, most of the model's output space,* the mean of the, per algorithm, accuracy μ_k represents the, on average, algorithmic accuracy:

$$\mu_k = \frac{1}{30}\sum_{PE=1}^{30} Accuracy_k^{PE} \qquad (6.1)$$

Also knowing, by the numerical data produced, which algorithm has the best degree of curve fitting, meaning the least percentage of distance between estimated curves and PEs, as well as which algorithm achieves faster fitting we can roughly rank the algorithms and infer the optimal for our inverse problem algorithm. These data are assembled in Tables 6 and 7.

For the half set:

Table 6 Accumulative Table for Algorithm ranking Metrics Measured (half set)

ALGORITHM	J (%)	ACURACCY (%)	SPEED (min)
CRS	0.0012	1.43	0.6151
SCE	0.0050	5.16	1.0298
DE	0.0010	1.02	0.5536
PSO	0.0052	7.79	0.7766
gblSolve	0.0152	7.45	*0.5273*
SIMPSA	0.0295	17.12	0.8103
tdASA	0.0348	11.91	1.6227
SRES	0.0113	8.14	0.8032
MIDACO	0.0094	10.64	1.5017

For the full set:

Table 7 Accumulative Table for Algorithm ranking Metrics Measured (full set)

ALGORITHM	J (%)	ACURACCY (%)	SPEED (min)
CRS	0,004	*18,94*	1.7332
SCE	0,016	*20,99*	2.0973
DE	0,010	*24,73*	1.7174
PSO	0,014	*30,46*	1.7326
gblSolve	0,022	*23,22*	*0.5074*
SIMPSA	0,017	*29,92*	2.0028
tdASA	0,025	*27,23*	2.2002
SRES	0,014	*25,74*	1.4269
MIDACO	0,012	*31,05*	2.4002

We can identify as optimal for the full set the CRS algorithm with greater degree of fitting and convergence within a reasonable time interval. But as optimal for the inverse problem will be chosen the optimal algorithm for the half set which we have identified as the dimensionality that the problem does converge and with sufficient curve fitting and parametric accurately. The algorithm that behaves as that is DE, which has on average the least distance between the estimated curves and PEs, the best accuracy of values of the parameters and in a time interval that competes gblSolve algorithm who as a deterministic provides fast convergence, despite being easily trapped in a local minima.

7 Conclusions and Future work

Cancer of the cervix of the uterus is a severe disease that can be proven terminal if allowed to proceed to the stage of metastasis. The need for more accurate, cheaper and faster diagnostic tools is clearly evident. This thesis aimed in taking the first significant steps of establishing a primal diagnostic tool for structural and biological parameters connected with neoplasia in the epithelium of the cervix, by using dynamic optical data, obtained by the use of DCE-OI DE, and by using an optimal global optimization algorithm in combination with a mathematical model simulating the *in vivo* diagnosis procedure that uses DCE-OI. Moreover, laying the foundations for mapping the values of the parameters and producing pseud-chromatic maps for each parameter was the ultimate goal set. For this purpose, in this study, first of all, the ability to fit mathematically obtained data to the experimentally obtained data was assessed and an accuracy that could be as high as 99.98% is reached. Moreover, DE has been identified and is being proposed as the optimal algorithm due to:

- best degree of accuracy on fitting mathematically produced curves to experimental recorded curves of Hydrogen concentration versus time,
- best degree of accuracy on identifying the values of biological and structural parameters of neoplastic cells
- high degree of performance on minimal time.

This finding is corresponding to statements throughout the literature that DE is a very good algorithm to be applied for global optimization compared to other stochastic algorithms such as the ones included in this study. More specifically, in a comparison done by Storn and Price DE was found more efficient than most SA and Genetic Algorithms. Moreover, Ali and Torn in [47] claimed that DE is more efficient than CRS algorithm. Moreover DE was found as better in parameter accuracy than PSO in [48].

On the other hand SIMPSA completely fails for both the half set and the four set due to being an inefficient algorithm for MINLP problems as stated in [36].

This efficiency of DE leads to identifying accurately the biological parameters with error in estimation as low as 1%. Moreover, it is currently achievable to have the aforementioned levels of accuracy in less than 2.5 minutes. All these of course would mean nothing if the problem was unable to converge. This ability of convergence was also identified as the majority of global optimization algorithms included in the study achieved substantial curve fitting and in a promising short time and global optimization in general provides a substantially unique problem with adequate parameter convergences at least and when the half set of four most identifiable parameters is used.

All these results come in agreement with theoretical estimations made by global sensitivity analysis where problem dimensionality was suggested. By reducing to half the dimensionality of our problem, substantial increase of both accuracy and estimation speed was achieved. Moreover, dimensionality reduction was proven consistent, as the rejected biological parameters consistently fail to converge while also inhibit greater estimation accuracy for the four most identifiable.

In the future, a similar studies manipulating more stochastic algorithms, as well as hybrid algorithms, would be beneficial, since due to the nature of the stochastic algorithms one cannot strongly claim that an algorithm is definitely better than another. An algorithm may perform better in some cases than another but can be outperformed in a different case study. Moreover, since the ultimate goal would be the creation of pseudo-chromatic maps of the parameters to be used as a fast diagnostic tool, time reduction is essential for creating a proper tool, as 2.5minutes per pixel would be a great disadvantage. For that purpose, the creation of an approximate model for our case would be beneficial, as well as downgrade of scripts to low level programming languages might optimize performance. Finally, further studies could eventually lead to real time creation of these maps by a similar system than the one used in this study.

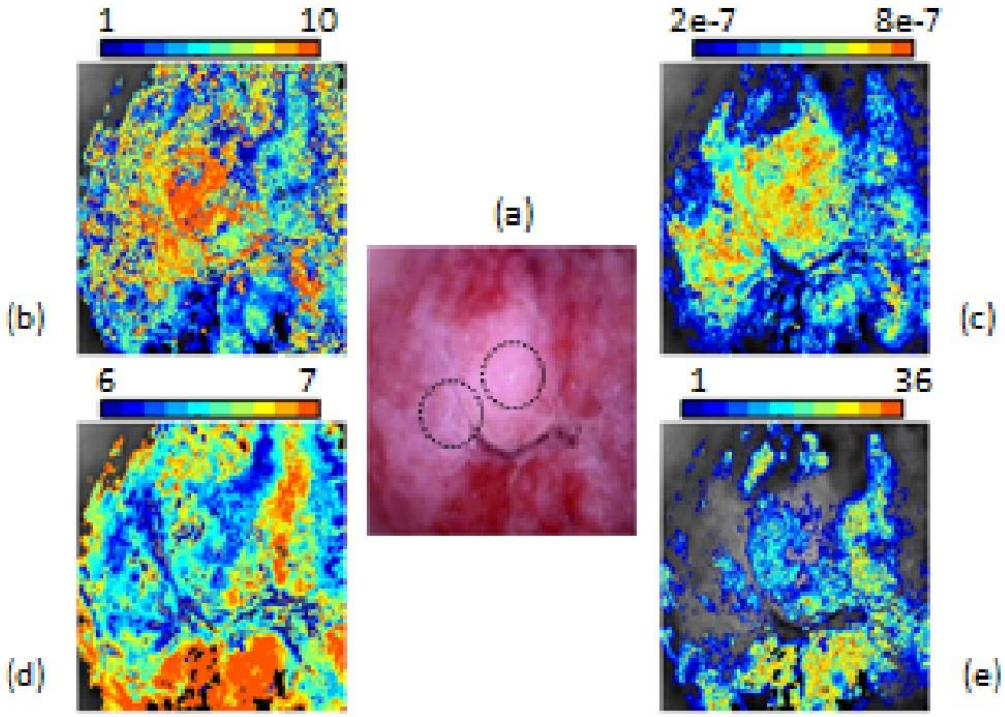

Figure 7- 35 (a) The image of a high risk cervical epithelium. The circles denote the area from where biopsies have been collected (b) - (e) Pseudo-color maps of N, b, pH_{ES}, and ε neoplasia-related parameters respectively, as they have been estimated by our model. Color-coding of the maps correspond to the various parameter value ranges.

REFERENCES

[1] E.P.Armstrong, "Prophylaxis of Cervical Cancer and Related Cervical Disease: A Review of the Cost-Effectiveness of Vaccination Against Oncogenic HPV Types". *Journal of Managed Care Pharmacy,* vol.16, no.3, pp. 217–30, Apr.2010

[2] World Health Organization, "*Fact sheet No. 297: Cancer*", Feb 2006, Retrieved 2007-12-01

[3] A.Burchell, R.Winer, S. De Sanjosé, E.Franco, "Chapter 6: Epidemiology and transmission dynamics of genital HPV infection", *Vaccine vol24 supplement 3*,ch. 6, pp. 52–61, Aug 2006

[4] L.Egendorf, "Sexually Transmitted Diseases" *Issue Series,* Greenhaven Press, New York, 2007

[5] Garcia A Hamid O, El-Khoueiry A (2006-07-06). "Cervical Cancer". *eMedicine*. WebMD. Retrieved 2007-12-02.

[6] Dolinsky, Christopher (2006-07-17). "Cervical Cancer: The Basics". *OncoLink* (Abramson Cancer Center of the University of Pennsylvania). Retrieved 2007-12-02.

[7] World Health Organization, *Comprehensive cervical cancer control: A guide to essential practice* [Online]: http://www.who.int/cancer/detection/cervical_cancer_screening/en/index.html

[8] M. Schiffman,P. E. Castle, "The promise of global cervical-cancer prevention," New England Journal of Medicine, vol. 353, pp. 2101-2104, 2005

[9] E.H. Hopman, F.J. Voorhorst, P. Kenemans, C. Meyer, T.J.M. Helmerhorst, " Observer Aggreement on interpreting Colposcopic Images of CIN", *Gynecologic Oncology,* vol.58,pp. 206-209, 1995

[10] D. Solomon, M. Schiffman, R. Tarone, E. E. Partridge, L. Kilgore, S. Hester, J. L. Walker, G. A. Johnson, A. Yadack, R. S. Guido, K. McIntyre-Seltman, R. P. Edwards, J. Gruss, N. B. Kiviat, L. Koutsky, C. Mao, J. M. Haug, D. Ferris, J. T. Cox, L. Burke, C. M. Wheeler, C. Peyton-Goodall, M. M. Manos, R. J. Kurman, D. L. Rosenthal, M. E. Sherman, M. H. Stoler, D. M. Harper, J. Rosenthal, M. Dunn, J. Quarantillo, D. Robinson, A. T. Lorincz, and L. Rich, "A randomized trial on the management of low-grade squamous intraepithelial lesion cytology interpretations," *American Journal of Obstetrics and Gynecology*, vol. 188, pp. 1393-1400, 2003.

[11] S. F. Wu, L. Meng, S. X. Wang, and D. Ma, "A comparison of four screening methods for cervical neoplasia," *International Journal of Gynecology & Obstetrics*, vol. 91, pp. 189-193, 2005

[12] G.Papoutsoglou, "Modelling of epithelial transport phenomena related with the acetowhitening optical characteristics: Potential for the *in-vivo* diagnosis of Cervical Neoplasia", M.S. thesis, ECE, Tech University of Crete, Greece, 2007

[13] Oracle ThingQuest, Education Foundation [Online]: http://library.thinkquest.org/12413/structures.html

[14] University of Ottawa, Canada, "Self Study Unit of the Basic Tissues" [Online]: http://www.courseweb.uottawa.ca/medicine-histology/english/ss_basictissues/epithelia.htm

[15] WebMD [Online]: http://women.webmd.com/picture-of-the-cervix

[16] Wikipedia, Boston University Histology Learning System quote [Online]: http://en.wikipedia.org/wiki/Cervix

[17] Eurocytology, Leonardo Da Vinci project [Online]: http://www.eurocytology.eu/static/eurocytology/eng/cervical/LP1ContentGcont.html

[18] University of Lausanne, "Swiss virtual Campus" project, [Online]: http://sepia.unil.ch/pharmacology/index.php?id=72

[19] University of Greenwich, CMS staff, "An introduction to Mathematical Modeling", [Online]: http://staffweb.cms.gre.ac.uk/~st40/Books/MathematicalModelling

[20] F. Pont, L. Duvillard, B. Verges, P. Gambert, “Development of compartmental models in stable-isotope experiments: application to lipid metabolism”, Research Support, Lab of Biochemistry of Lipoproteins, Faculty of Medicine, Dijon, France, Jun 1998

[21] G.Papoutsoglou, C. Balas, ”Estimation of Neoplasia-Related Biological Parameters through Modeling and Sensitivity Analysis of Optical Molecular Imaging Data”, Research Support, Department of Electronic and Computer Engineering, Tech University of Crete, Dec 2012.

[22] C.G.Moles, P.Mendes,J.R.Banga,“Parameter Estimation in Biochemical Pathways: A Comparison of Global Optimization Methods”,*Genome Research,* vol. 13,pp. 2467-2474, 2003

[23] C.Guus, E.Boender, H.E.Romeijn, “Stochastic methods”, *Handbook of global optimization*,pp.829-869,Kluwer Academic Publishers, Dordrecth, The Netherlands.

[24] M.Björkman, K.Holmström, “ Global Optimization Using the DIRECT Algorithm in Matlab”, *Advanced Modeling and Optimization,* vol.1, no.2, 1999

[25] D.R.Jones, C.D.Perttunen, B.E.Stuckman, ”Lipschitzian optimization without the Lipschitz constant”, *Journal of Optimization Theory and Applications,* vol.79, no.1,pp.157-181,Oct 1993

[26] M.Stamatiadou, “Global Optimization Algorithms for the defining of bio-optical parameters related to the growth of epithelial neoplasia”, Diploma Thesis, ECE, Tech University of Crete, Greece, 2010

[27] J.Tvrdik “Robust Algorithm For Estimation Of Parameters In Non-Linear Regression Models”, Int. Conference Tech. Computing, Prague 2005.

[28] J.Tvrdik,”Generalized controlled random search and competing heuristics”, *10 MENDEL 2004,International Conference on Soft Computing,* pp.228-233, University of Technology,Brno, 2004

[29] W.L.Price, “A controlled random search procedure for global optimisation”, *The Computer Journal*, vol.20, no.4, pp.367-370, Feb 1976

[30] S.Das, P.N.Sugathan, “Differential Evolution: A Survey of the State-of-the-Art”, *IEEE Transactions on Evolutionary Computation,* vol.15, no.1, pp.4-31, Feb 2011

[31] R.Storn, K.Price, “Differential Evolution - A Simple and Efficient Heuristic for Global Optimization over Continuous Spaces“, *Journal of Global Optimization*, vol.11, pp.341-359,1997

[32] Q.Y.Duan, V.K.Gupta, S.Sorooshtan, “Shuffled Complex Evolution Approach for Effective and Efficient Global Minimization”, *Journal of Optimization Thoery and Applications*, vol.76, no.3, Mar 1993

[33] T.P.Runarsson,X.Yao, “Stochastic Ranking for Constrained Evolutionary Optimization”, *IEEE Transaction on Evolutionary Computation*, vol.4 no.3, Sep 2000

[34] S.Russell, P.Norvig, “Informed Search and Exploration” ,*Artificial Intelligence A Modern Approach*, 2nd American Edition, Greek Translation, Greece, Kleidarithmos,2005 ,ch.4, sec.4.3, pp.154

[35] M.F. Cardoso,R.L. Salcedo, S.Feyo de Azevedo,” The Simplex-Simulated Annealing Approach To Continuous Non-Linear Optimization”,Comput. & Chemical Engineering,vol.20.No.9,pp.1065-1080, Jan.1996

[36] A.Corana, M.Marchesi, C.Martini, S.Ridella, “Minimizing Multimodal Functions of Continuous Variables with the “Simulated Annealing” Algorithm”, *ACM Transactions on Mathematical* Software, vol.13, no.3, 262-280, 1987

[37] M.Schlueter, J.Egea, J.R.Banga, “Extended Ant Colony Optimization for non-convex Mixed Integer Nonlinear Programming”, *Computers & Operations Research*, vol.36, no.7, pp. 2217-2229, 2009

[38] M.Schlueter, M.Gerdts, J.J. Ruckmann, “A Numerical Study of MIDACO on 100 MINLP Benchmarks”, *Optimization,*vol. 61, no. 7, pp. 873-900, 2012

[39] M.Schlueter,”Nonlinear Mixed Integer based Optimization Technique for Space Applications”,Ph.D. Dissertation, School of Mathematics, University of Birmingham, United Kingdom,2012

[40] M. Schlueter,M.Munetomo, “MIDACO User Guide”, Hokkaido University Japan,Tech.Report,2013

[41] K.E. Parsopoulos,M.N., Vrahatis,”Recent Approaches to Global Optimization Problems Through Particle Swarm Optimization”, *Natural Computing*, vol.1,no. 2-3, pp. 235-306, Jun.2002.

[42] E. Magnus ,P. Hvass, “Good Parameters for Differential Evolution”, Hvass Laboratories, Tech Rep no. HL1002, 2010.

[43] J.F. Schutte, A.A. Groenwold,”A Study of Global Optimization Using Particle Swarms”, *Journal of Global Optimization*,vol. 31,no. 1, pp. 93-108, Jan.2005.

[44] E.Aarts, J.Korst, in *Simulated Annealing and Boltzmann Machines: A Stochastic Approach to Combinatorial Optimization and Neural Computing*, Ed. New York: Wiley,1989

[45] G.Papoutsogloum,T.M.Giakoumakis,C.Balas,”Dynamic Contrast Enhanced Optical Imaging of Cervix, *in vivo*: A Paradigm for Mapping Neoplasia-Related Parameters”, 35th Ann. Int. Conf. of the IEE EMBS, Osaka, Japan, Jul 2013

[46] W.Navidi, “Hypothesis Testing”, *Statistics for Engineers and Scientists*, 3rd Edition, McGraw-Hill,ch.6, sec.Introduction, pp.396

[47] M.Ali,A.Torn,S.Viitanen, “A numerical Comparison of Some Modified Controlled Random Search Algorithms”, *Journal of Global Optimization,* vol.11, pp.377-385,1997

[48] N.D.Lagaros, D.C.Charmpis, “Efficiency and Robustness of Three Metaheuristics in the Framework of Structural Optimization”, *6th IFIP WG 12.5 Int. Conf.,* AIAI, Cyprus Larnaca, Oct 2010

Appendix

For the full set:

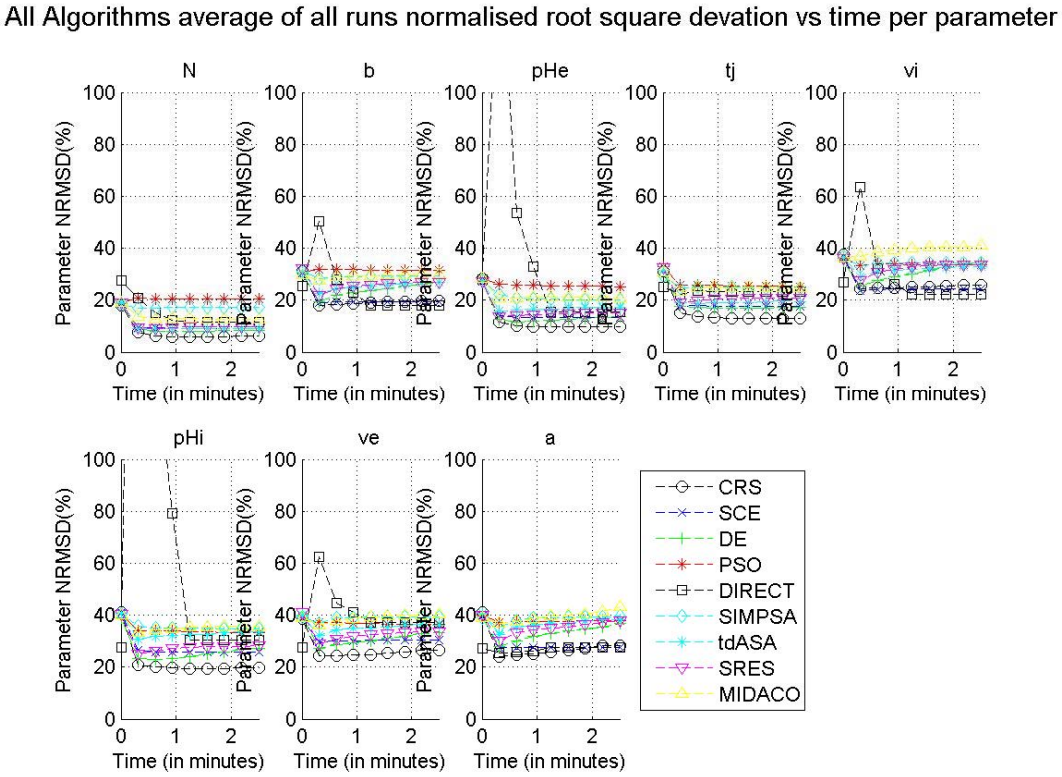

Figure 0-2 plot of accuracy per parameter versus time

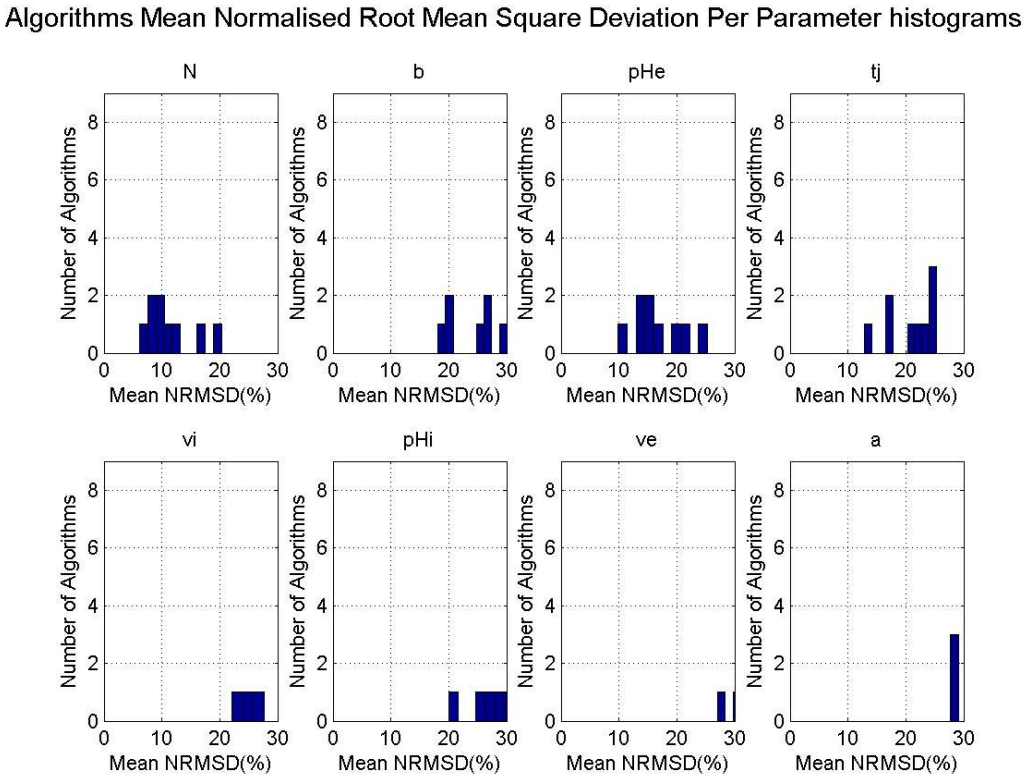

Figure 0-1 Histogram of Algorithms versus NRMSD per parameter

For the half set:

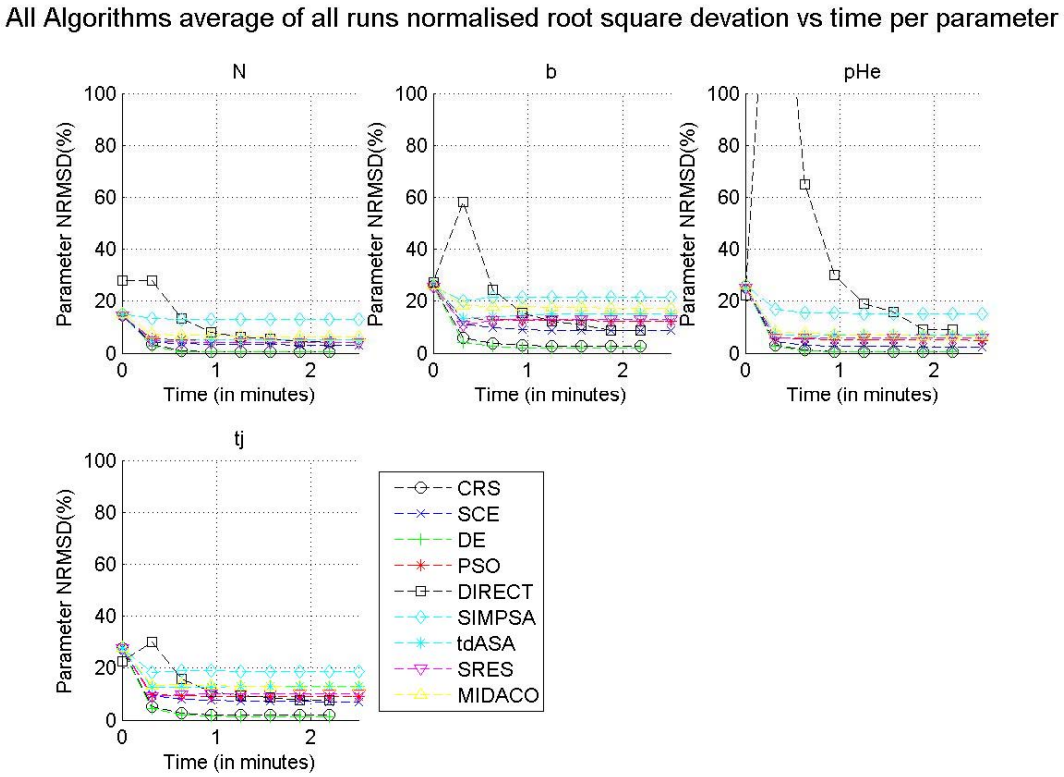

Figure 0-3 plot of accuracy per parameter versus time

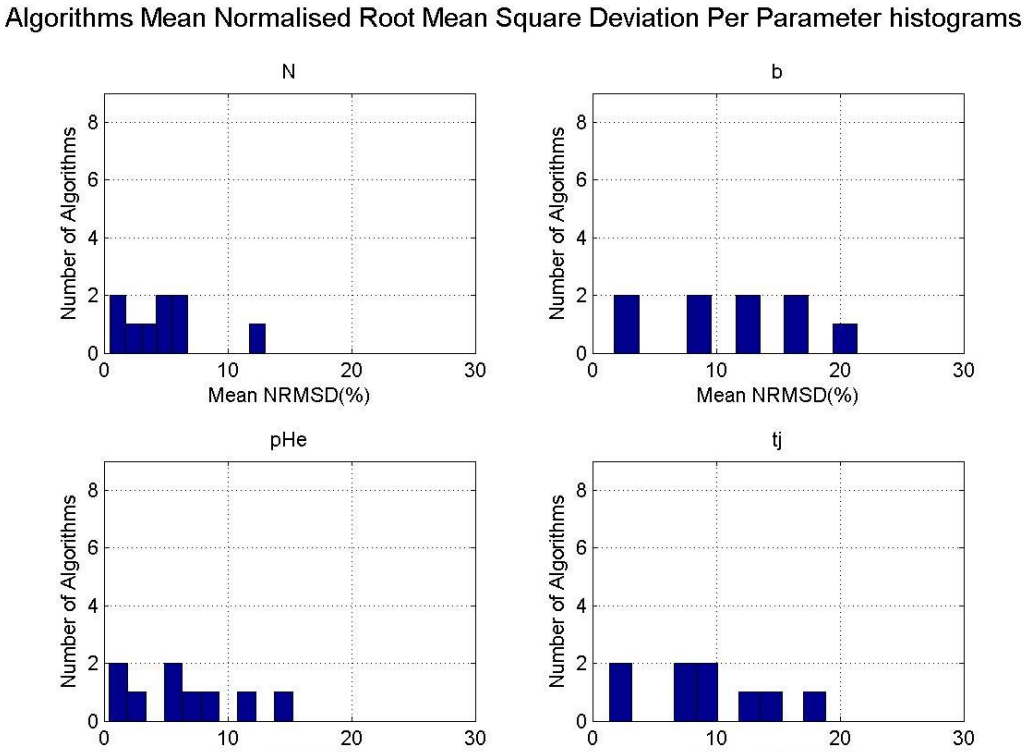

Figure 0-4 Histogram of Algorithms versus NRMSD per parameter

35th Annual International Conference of the IEEE EMBS
Osaka, Japan, 3 - 7 July, 2013

Dynamic Contrast Enhanced Optical Imaging of Cervix, *in vivo*: A Paradigm for Mapping Neoplasia-Related Parameters*

George Papoutsoglou, *Student Member*, *IEEE*, Theodoros - Marios Giakoumakis and Costas Balas, *Member, IEEE*

***Abstract*—We present a novel biophotonic method and imaging modality for estimating and mapping neoplasia-specific functional and structural parameters of the cervical precancerous epithelium. Estimations were based on experimental data obtained from dynamic contrast-enhanced optical imaging of cervix, *in vivo*. We have developed a pharmacokinetic, *in silico*, model of the optical tracer's uptake by the epithelium. We have identified that the kinetic parameters of the model correlate well with pathologic alterations in both metabolic and structural characteristics of the tissue, associated with the neoplasia progress. Global sensitivity analysis and global optimization methods were employed for identifying the key determinant set of biological parameters that dictate the model's output. Particularly, the shuffled complex evolution algorithm converged to a set of four parameters that can be estimated with an error of 7%, indicating a good accuracy and precision. These results are unique in the sense that for the first time functional and microstructural parameter maps can be estimated and displayed together, thus maximizing the diagnostic information. The quantity and the quality of this information are unattainable by other invasive and non invasive methods.**

I. Introduction

Dynamic Contrast-Enhanced (DCE) imaging is a versatile technique for the spatio-temporal recording of biomarker-induced bio-events and processes in tissues, *in vivo*, non-invasively and in real time. DCE imaging has been established as a non-surgical tool for the study of tissue perfusion kinetics, *in vivo* and has shown an impressive prognostic and predictive capacity in cancer radiology [1]. The concept of DCE is evolving rapidly and has been translated to several biomedical modalities including optical imaging. In fact, the in-vivo optical imaging aspect of DCE (DCE-OI) was developed in late nineties by C. Balas *et al*. [2], [3]. Particularly, a DCE optical imaging method and platform was developed for measuring and mapping the evanescent backscattering signals, generated during the biomarker-tissue interaction with epithelial neoplasias of the cervix, the larynx and the skin [4]. The method employs the acetic acid (AA) dilute solution 3-5% as a biomarker. In two international clinical trials, enrolling hundreds of patients DCE-OI was proved to be very efficient, demonstrating an improvement of more than 63% in diagnostic sensitivity over Papanicolaou test and colposcopy [5].

Due to the fact that DCE-OI captures the kinetics of diffusible, high-affinity labeled tracers in tissues, it, in principle, allows for the model-based estimation of biological parameters that are determining the features of the experimental data. In addition, since DCE-OI measures these data in every spatial location, it enables the mapping of the estimated parameters. To this end, we have previously reported the development of a compartmental model, which simulates the metabolic pathways that are followed by the biomarker in the epithelial tissue [6]. The biomarker uptake kinetics determine the dynamics of the biological target's optical activation and establish the link between optical and biological parameters and responses. Then, fitting the developed pharmacokinetic model to the experimental data, a set of neoplasia-related biological parameters can be estimated, comprising the solution of the inverse problem. Towards this direction, we have performed global sensitivity analysis for ranking the importance and relative estimability of the input parameters [7]. The analysis concluded that four out of nine parameters are fulfilling these criteria and can therefore be estimated using the experimental dynamic optical data as input. These parameters were found to be: the number of neoplastic layers, the size of the extracellular space, the extracellular pH and the tissue porosity.

In this paper we report a method based on global optimization for verifying whether the solution of the inverse problem (a certain set of biological parameter values) is substantially unique. Finally, we for the first time present results from the pixel-by-pixel estimation of these parameters from DCE-OI of cervical tissue, *in vivo*. Four maps have been calculated, having as pixel values the estimated parameter values. The latter are represented in the form of a pseudocolor map which is overlaid onto the clinical color image of the tissue. This enables the direct visualization of tissue locations with normal or abnormal parameter values.

II. Materials and Methods

A. Bio-Optical Background

Chemical biomarkers have been extensively used for visualizing and monitoring several bio-processes at pre-cancer and cancer stages in live cells or tissues. Optical activation of these substances depends primarily on their predefined affinity to cellular components. Still, their uptake

* This work was supported in part by: 1) the European Union (European Social Fund) and Greek National funds through the Operational Program "Education and Lifelong Learning" of the National Strategic Reference Framework–Research Funding Program: Heraclitus II–Investing in knowledge society through the European Social Fund and 2) the NSRF "cooperation" action, program "OncoSeed Diagnostics: Biology of Circulating Tumour Cells, Distant Metastasis & Development of Liquid Biopsy Methods"

C. Balas, G. Papoutsoglou and T. M. Giakoumakis are with the Department of Electronic and Computer Engineering, Technical University of Crete, Chania 73100, Greece (corresponding author to provide phone: +302821037212; fax: +302821037542; e-mail: balas@electronics.tuc.gr).

depends largely on the transport phenomena and pathways that they follow in order to reach and optically activate the target. It is therefore possible to assess valuable information regarding the functional and the structural characteristics of abnormal sites, by studying and simulating, *in silico*, the kinetics of these biomarkers. Towards this end, we have identified and modeled the transport phenomena in the case of the cervical precancerous epithelium using AA as biomarker. Particularly, the AA molecules, after topical application, reach the extracellular space (ES) of the neoplastic portion of the epithelium, where they remain considerably unionized due to the high extracellular acidity. As such, they penetrate passively through the membranes of the neoplastic cells with high selectivity. Due to the almost neutral intracellular space (IS), the intruded AA molecules are disassociated into acetate (Ac^-) and hydrogen (H^+) ions. The latter, stimulate conformational changes in the nuclear proteins. This, in turn, provokes local changes to the index of refraction and determines the macroscopically observed dynamic scattering characteristics. Next, and because the cervical epithelium is stratified, these processes are repeated in the underlying neoplastic epithelial layers. Finally, the tissue restores its original light scattering characteristics by the time the biomarker has been consumed or drained away.

B. Model Formulation and Calibration

Structurally, the cervical epithelium is a natural assemblage of well-differentiated cells which at precancer stages disorganize. Taking normal and pathologic epithelium architecture into the account, we have developed a pharmacokinetic model that encapsulates the abnormal part of the cervical epithelium and partitions it into a stack of functionally and structurally identical cells. Because during the development of neoplasia the number of abnormal cell layers constantly increases, this tissue partitioning has been designed to be flexible in size. This adaptable layered structure is delimited from its upper borders by a reservoir layer that acts as a repository that supplies the biomarker. Each of these cell layers is modeled with two compartments of interaction: the intracellular space (IS) and the extracellular space (ES) compartments. AA diffuses passively from the ES to the IS through the cell's membrane and from the upper to the lower layer(s) of the abnormal epithelium through the extracellular, porous junctions. Both transmembrane and paracellular passive fluxes are driven by concentration and potential gradients, obeying to the Fick's law and Goldman-Hodgkin-Katz flux constant field equation. The model also embodies two dynamic intrinsic processes, the AA ion buffering, occurring in both IS and ES spaces, and the active transmembrane pumping processes, which contribute in restoring the original intracellular pH (pH_{IS}) though the extrusion of H^+ ions from the IS to the ES. For more details the reader is referred to [6], [7].

Altogether, the developed model is a deterministic, non-linear, algorithm that includes a scalable system of coupled differential equations. The differential equation system that expresses material exchange between the compartments of a single neoplastic layer is the following:

$$\dot{\left[\mathrm{TA}\right]}^{i}_{\mathrm{IS}} = a^{-1}J_m^{\mathrm{AA}_i} + a^{-1}J_m^{\mathrm{Ac}^-} \quad (1)$$

$$\dot{\left[\mathrm{H}^+\right]}^{i}_{\mathrm{IS}} = -\ln 10^{\left[\mathrm{H}^+\right]^{i}_{IS}}\left(a\beta_{\mathrm{IS}}\right)^{-1}\left(q^{i}_{\mathrm{IS}}J_m^{\mathrm{AA}_i} - w^{i}_{\mathrm{IS}}J_m^{\mathrm{Ac}_i^-} - J_p^{\mathrm{H}_i^+}\right), \quad (2)$$

$$\dot{\left[\mathrm{TA}\right]}^{i}_{\mathrm{ES}} = b^{-1}J_m^{\mathrm{AA}_i} + b^{-1}J_m^{\mathrm{Ac}_i^-} + a^{-1}\varepsilon J_{\mathrm{T}}^{\mathrm{AA}_i} + a^{-1}\varepsilon J_{\mathrm{T}}^{\mathrm{Ac}_i^-}, \quad (3)$$

$$\dot{\left[\mathrm{H}^+\right]}^{i}_{\mathrm{ES}} = -\ln 10^{\left[\mathrm{H}^+\right]^{i}_{\mathrm{ES}}}\beta_{\mathrm{ES}}{}^{-1}\Big[q^{i}_{\mathrm{ES}}\left(b^{-1}J_m^{\mathrm{AA}_i} + a^{-1}pJ_{\mathrm{T}}^{\mathrm{AA}_i}\right) - w^{i}_{\mathrm{ES}}\left(b^{-1}J_m^{\mathrm{Ac}_i^-} + a^{-1}\varepsilon J_{\mathrm{T}}^{\mathrm{Ac}_i^-}\right) + b^{-1}J_p^{\mathrm{H}_i^+} + a^{-1}\varepsilon J_{\mathrm{T}}^{\mathrm{H}_i^+}\Big], \quad (4)$$

where the brackets ([…]) and the dot (·) denote the concentration time derivative, TA refers to the total AA in both ionized and unionized form, i is the i^{th} neoplastic layer (i=1,2,...,N), a and b are the linear dimensions of the IS and of the ES, where cubic and rectangular compartment geometries have been assumed, respectively, J_m describes the passive transmembrane flux between the ES and IS, β is the buffering power, q and w account for the AA's dynamic ionization constants, including its self-burning effect, ε refers to the alterations in the porosity of the tissue during neoplasia, J_p is the active proton extrusion flux that is assumed to be a piecewise linear function of pH_{IS} and pH_{ES} and J_T is the total passive paracellular flux that corresponds to the difference between the incoming and outgoing molecular paracellular fluxes between consecutive layers through the extracellular porous junctions. It should be noted here that for the reservoir layer equations (3) and (4) are abolished and for the last layer the outgoing paracellular flux is replaced by the $K_V C$ term, where K_V is the permeability at the boundary between the epithelium and the stroma and C corresponds to the concentration of either AA, Ac^- or H^+.

The value ranges of the set of neoplasia related biological parameters as they have been measured experimentally are as follows: the number of dysplastic layers, N, are in the range of 1-10; the IS and the ES linear dimensions a and b, are in the range of 10-20μm and 0.2-0.8μm, respectively; the IS and the ES buffering efficiency β_{IS}, β_{ES}, are in the range of -10 to -50mM and -10 to -30mM, respectively; the pH_{IS}, pH_{ES} values vary between 7-7.4 and 6-7, respectively; the ε parameter is in the range of 1-36 and the K_V between 10^{-6} and 10^{-7} m/s [8-13]. These value ranges comprise the input of the model when fitting of experimental data is intended. A certain combination of parameter values can best-fit the experimental data and therefore be considered, under certain circumstances, as the output of the inverse modeling.

Towards verifying the uniqueness of the inverse problem's solution we have performed consecutively three *in silico* analyses; namely, global sensitivity analysis, parameter identifiability analysis and parameter estimability analysis [7]. On the basis of theses analyses, we were able to decide which of the pertinent model parameters can potentially be estimated from available input/output data and which are impossible to assess. Specifically, we have identified a set of parameters that fulfill the following criteria: a) they are the key determinants of the line-shape of the model's output that fits the experimental dynamic optical data and b) they display no collinearities and minimum interdependency with each other. The initial nine input parameters of the model have been reduced to four by discarding parameter K_V as displaying null sensitivity function and the parameters β_{IS},

β_{ES}, and pH_{IS}, as not fulfilling the combined non-unity correlation coefficient, displaying also low estimability ratio and sensitivity indices. Additionally, the IS linear dimension parameter (a) did not fulfill the collinearity criterion. On the basis of both sensitivity and estimability analyses we have identified that the key determinants (in descending ranking order) are: the number of neoplastic layers (N), the size of the ES (b), the extracellular pH (pH_{ES}) and the tissue's porosity (ε).

C. Solving the Inverse Problem for Parameter Estimation

Even though the implementation of these three analyses enhances the well-posedness of our parameter estimation problem, it does not prove a deterministic relation between the solution and the parameter values. We have identified global optimization methods as the most efficient tool for verifying whether our method has the capacity of providing a substantially unique parameter value combination, when a certain experimental curve is fitted [14]. The first step of the analysis involved the generation of "pseudoexperimental" (PEX) data by collecting the model responses to a known range of values of all four parameters. Next, the PEX curves were fitted until an acceptable level of goodness of fit is reached. At that point a new set of parameters is collected and the procedure is repeated 54 times. Finally, the accuracy and reproducibility of model predicted parameter values was accessed by comparing them with the known PEX values. For implementing this approach we have preliminary employed and tested a series of global estimation techniques that randomly search to converge to the global extrema under a recursive, evolutionary strategy [14]. These methods benefit from the fact that they are easy to implement and not critically dependent on a priori information about the objective function. Under this framework, constrained, direct search, point-to-point and population based, global optimization algorithms such as the simulated annealing, controlled random search, shuffled complex evolution, genetic algorithm and differential evolution, have been comparatively evaluated with the purpose of identifying the best performing algorithm in estimating parameter values in the vicinity of the PEX curve input values, with adequate reproducibility. The normalized root mean squared deviation (NRMSD) was used as convergence/reproducibility metric.

D. Experimental Procedure

Experiment data were obtained from women referred to colposcopy after having an abnormal Pap-test. The DCE-OI head was adapted to a colposcope and a set of 30 images were collected from each case before and after applying AA. The reader can find more details on the image acquisition procedure in [15]. Diffuse reflectance (DR) vs. time curves were calculated for every image pixel, with reflectance values measured at 540 nm (center wavelength), as in this spectral band the signal-to-noise-ratio is maximized. We have selected a case with (biopsy confirmed) high grade cervical neoplasia. From the acquired, in time sequence, image set we have derived 2 million of DR vs. time curves, each corresponding to a single pixel. These curves are one-by-one best fitted and the values of the four parameters are estimated. These four values comprise the pixel values of four maps at the same spatial coordinates. The parameter value-ranges are represented with the aid of a pseudocolor scale and the resulting four pseudocolor maps are overlaid onto the colposcopic image of the tissue. This will, for the first time allow, the clinicians to observe and to localize microstructural and functional alterations, during their routine clinical (macroscopic) examination of the cervix.

III. Results and Discussion

We have found that the best performing algorithm is the shuffled complex evolution (SCE), which converges to solutions of the least NRMSD. The analysis of the factors that may explain the observed differences in the performances between different algorithms goes beyond the scope of this report. For the purposes of current analysis we adopt the SCE algorithm, which gave the results depicted in table I. The results refer to a set of 9 repetitive parameter estimations performed for each PEX signal. It is clear that the chances to convergence to a unique set of parameter values are considerably high, while they vary slightly over the range of the CIN grades. On average, the deviation of the predicted values from the reference ones has been found to be 7% suggesting a high degree of convergence of an almost unique set of parameters' for a given experimental curve. This finding advocates that the estimation of functional and structural parameters can be performed with adequate precision and accuracy.

On the basis on this finding, we claim that the biological parameters that can be estimated through this method from the DCE-OI and the derived DR vs. time curves are realistic and reflect the actual status of the structure and functionality of the tissue. Figure 1(a) shows a DCE-OI image corresponding to a high-grade cervical epithelium (CIN II/III). The circles on this image indicate points from which the biopsy samples were obtained. Figures 1(b)-(e) illustrate the four maps expressing the values ranges and the spatial distribution of the four parameters, calculated for every image pixel. More specifically, fig. 1(b) depicts the spatial distribution of the structural parameter, which expresses the number of neoplastic epithelial layers. As discussed previously, it has been established that the number of neoplastic layers are increasing with the neoplasia growth [8]. By comparing figs. 1(a) and 1(b) it becomes clear that the layer number parameter takes the maximum values (8-10) at the points where the biopsies had been taken, and histology results suggested high occupation of the epithelium by neoplastic layers. This can be reasonably considered as a confirmation of the validity of our results. Fig. 1(c) depicts the spatial distribution of another key structural parameter, which is also assessed histologically as having high predictive value. Parameter (b) expresses the size of the

TABLE I. The precision of the SCE algorithm

Parameter	NRMSD			
	CIN I	CIN II	CIN III	Median
N	9%	9%	4%	9%
b	16%	3%	5%	5%
pH_{ES}	2%	8%	5%	5%
ε	13%	7%	7%	7%

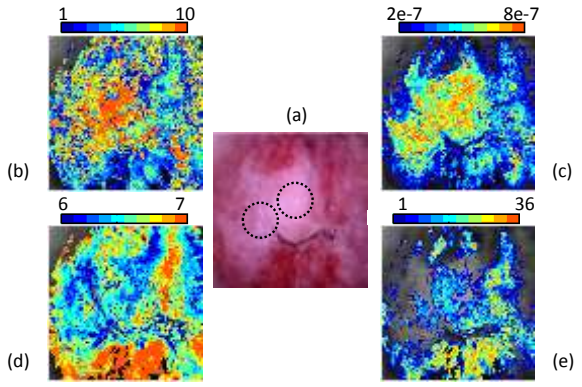

Figure 1. (a) The image of a high risk cervical epithelium. The circles denote the areas from where biopsies have been collected. (b)-(e) Pseudocolor maps of N, b, pH_{ES} and ε neoplasia-related parameters respectivelly, as they have been estimated by our model. Color-coding of the maps corespond to various parameter values.

extracellular space, which is known to increase with the neoplasia progress [8]. As it can be seen in the map of parameter (b), large extracellular spaces exist in the vicinity of the biopsy confirmed high grade points. Additionally, high b-parameter areas are co-localized with the high N-parameter areas, something that can be considered as a verification of the consistency of our findings with the actual biology of neoplasia growth. As it can be seen in fig 1b the number of dysplastic layers is fully consistent with the histological classification and are laying within the nominal value-ranges found in the literature. It is therefore evident that the method presented in this paper may comprise a non-invasive a novel optical biopsy method. Principally, the fact that our approach is based on live tissue imaging makes the assessment of functional characteristics possible, in contrast to histology, which uses dead tissue samples.

Referring now to the functional parameters, our consistency claim applies also to the findings illustrated in fig. 1(d) where areas with high, close to normal, pH_{ES} values are color-coded with red and areas with low pH_{ES}, values with blue. It is distinctly shown that lower pH_{ES} are co-located with high areas with high N and b, depicting the lower acidity of the extracellular space, which is in full agreement with the finding of other studies [11-13]. Finally, fig. 1(e) shows the mapping of the permittivity of the tissue to the biomarker. In general, CIN carcinogenesis disrupts the state of the tissue adhesion structures, which has been associated with increased tissue permeability [16]. This leads to the loosening of these particular junctions, transforming the tissue from tight to leaky increasing the possibility of metastasis. Particularly, according to the "acid-mediated tumor invasion model", the H^+ flow to peritumoral normal tissue provokes normal cell necrosis or apoptosis and extracellular matrix degradation [11]. Because, the tumor cells are capable of resisting to the toxicity induced from this flow, they are able to invade the damaged normal tissue. This allows them to spread, and eventually form invasive cancers. The aforementioned finding suggests strongly that our method can provide a better insight to the neoplasia growth and tumor metastasis.

IV. Conclusion

This paper describes a novel biophotonic method and imaging modality for estimating and mapping a set of neoplasia-related biological parameters, from dynamic optical data (DCE-OI), *in vivo*. Global optimization showed that the estimations of our method are of adequate accuracy and precision. It was also shown that the estimated, in two millions of pixels, values of the four parameters are quite consistent with information provided in the literature. Our findings suggest strongly that our method can improve our understanding of the neoplasia development mechanisms and of tumor growth and metastasis physiology. Corollary, it may become a valuable diagnostic tool that will also facilitate the development and evaluation of new cancer therapies.

References

[1] C. Yue, "The Promise of Dynamic Contrast-Enhanced Imaging in Radiation Therapy," *Sem. Rad. Onc.*, vol. 2, no. 21, pp. 147–156, 2011.

[2] C. Balas, "Methods for characterizing tissues," WO 2008/001037, U.S. Patent P91785US00, 2011.

[3] C. Balas, *et al.*, "In vivo detection and staging of epithelial dysplasias and malignancies based on the quantitative assessment of acetic acid-tissue interaction kinetics," *Jour. Photoch. Photob. B-Biol.*, vol. 53, no. 1–3, pp. 153–157, 1999.

[4] C. Balas, A. Dimoka, I. Orfanudaki and E. Koumantakis, "*In vivo* assessment of acetic acid–cervical tissue interaction using quantitative imaging of back-scattered light: its potential use for the *in vivo* cervical cancer detection grading and mapping," *SPIE-Optical Biopsies and Microscopic Techniques*, vol. 3568, pp. 31-37, 1999.

[5] W. Soutter, *et al*., "Dynamic spectral imaging: improving colposcopy," *Clin. Cancer Res.*, vol. 15, no. 5, pp. 1814–1820, 2009.

[6] C. Balas, G. Papoutsoglou and A. Potirakis, "*In vivo* molecular imaging of cervical neoplasia using acetic acid as biomarker," *IEEE Jour. Sel. Top. Quant. Elect.,* vol. 14, no. 1, pp. 29-42, Jan-Feb, 2008.

[7] G. Papoutsoglou and C. Balas, "Estimation of Neoplasia-Related Biological Parameters through Modeling and Sensitivity Analysis of Optical Molecular Imaging Data", *IEEE Trans Biom Eng*, to be published.

[8] D. Walker *et al.*, "A study of the morphological parameters of cervical squamous epithelium,"*Physiol. Meas.,* vol. 24 pp. 1–15, 2003.

[9] R. Jain,"Transport of molecules across tumor vasculature, " *Cancer Met. Rev.*, vol. 6, pp. 559-593, 1986

[10] P. Swietach, R. D. Vaughan-Jones and A. L. Harris, "Regulation of tumor pH and the role of carbonic anhydrase 9," *Cancer Met. Rev.*, vol. 26, pp 299-310, 2007

[11] P. A. Schornack and R. J. Gillies, "Contributions of cell metabolism and H^+ diffusion to the acidic pH of tumors," *Neoplasia*, vol. 5, no. 2, pp 135-145, 2003.

[12] M. Boyer, M. Barnard, D. Hedley and I. Tannock, "Regulation of intracellular pH in subpopulations of cells derived from spheroids and solid tumours," *Br. Jour. Cancer.*, vol. 68, no. 5, pp 890-897, 1993.

[13] A. Avdeef, "Leakiness and size exclusion of paracellular channels in cultured epithelial cell monolayers-interlaboratory comparison.," *Pharm. Res.*, vol. 27, no. 3, pp. 480–9, Mar. 2010.

[14] G. Papoutsoglou, M. Stamatiadou and C. Balas, "In silico Modeling and Global Optimization of Dynamic Bio-optical Processes for Probing, in vivo, Biological Features of Neoplasia," *in 2012 Conf. Proc. iCBEB Int. Conf.,* pp. 332-335, 28-30 May 2012

[15] C. Balas, "A novel optical imaging method for the early detection, quantitative grading, and mapping of cancerous and precancerous lesions of cervix," *IEEE Trans Biomed Eng,* vol. 48, no. 1, pp. 96-104, Jan. 2001.

[16] G. Sobel, *et al*., "Increased expression of claudins in cervical squamous intraepithelial neoplasia and invasive carcinoma.," *Hum. Pathol.*, vol. 36, no. 2, pp. 162–9, Feb. 2005.